A STUDY OF SWITCHGRASS PYROLYSIS: PRODUCT VARIABILITY AND REACTION KINETICS

By

Jonathan Matthew Bovee

A THESIS

Submitted to
Michigan State University
in partial fulfillment of the requirements
for the degree of

Biosystems Engineering – Master of Science

2014

ProQuest LLC.
789 East Eisenhower Parkway
P.O. Box 1346
Ann Arbor, MI 48106 - 1346

ABSTRACT

A STUDY OF SWITCHGRASS PYROLYSIS: PRODUCT VARIABILITY AND REACTION KINETICS

By

Jonathan Matthew Bovee

Samples of the same cultivar of cave-in-rock switchgrass were harvested from plots in Frankenmuth, Roger City, Cass County, and Grand Valley, Michigan. It was determined that variation exists, between locations, among the pyrolytic compounds which can lead to variability in bio-oil and increased processing costs at bio-refineries to make hydrocarbon fuels. Washed and extractives-free switchgrass samples, which contain a lower alkali and alkaline earth metals content than untreated samples, were shown to produce lower amounts of acids, esters, furans, ketones, phenolics, and saccharides and also larger amounts of aldehydes upon pyrolysis. Although the minerals catalyzed pyrolytic reactions, there was no evidence indicating their effect on reducing the production of anhydrosugars, specifically levoglucosan. To further link minerals present in the biomass to a catalytic pathway, mathematic models were employed to determine the kinetic parameters of the switchgrass. While the calculated activation energies of switchgrass, using the FWO and KAS methods, were 227.7 and 217.8 kJ mol^{-1}, correspondingly, it was concluded that the activation energies for the switchgrass hemicellulose and cellulose peaks were 115.5 and 158.2 kJ mol^{-1}, respectively, using a modified model-fitting method. The minerals that effect the production of small molecules and levoglucosan also have an observable catalytic effect on switchgrass reaction rate, which may be quantifiable through the use of reaction kinetics so as to determine activation energy.

ACKNOWLEDGEMENTS

I would like to thank my family for all of their support throughout my endeavors. I would also like to personally thank Dr. Bradley Marks, Dr. James Steffe, Dr. Ajit Srivastava, and especially my advisor, Dr. Christopher Saffron. This was a wonderful opportunity and I couldn't be happier that I was given a chance to become part of such an exceptional group of individuals. An immense thanks to Dr. David Hodge and Dr. James Jackson, of my committee, who have been crucial to my limited background in chemistry and have also served as a catalyst in my renewed interest. Dr. Kurt Thelen provided intellectual support on the feedstock involved and also provided raw materials needed for experiments, without either this research would be lost. I would like to thank my friends at the agronomy farm, Bill Widdicombe and Brian Graff, for their help with biomass reconstitution, especially during the absence of time, this is greatly appreciated. Distinct gratitude is also felt toward Dr. Shantanu Kelkar for all of his vast insight in the laboratory, especially with the GC/MS. This research would have not been possible without the help from my partners at the North-Eastern Sun Grant Initiative, Michigan State University AgBio Research, and the Great Lakes Bio-Energy Research Center. Thank you, Dr. Zhenglong Li, Dr. Somnath Bhattacharjee, Chai Li, Mahlet Garedew, Rachael Sak, Kristine VanWinkle, Nichole Erickson, and Kristine Henn for being such an awesome and supportive group to work with. I hope that Barb Delong and Cheryl Feldkamp accept a special thank you for always helping me get where I need to be. And to all of my professors and friends, please accept a towering thank you for permitting me to learn from you.

TABLE OF CONTENTS

LIST OF TABLES

LIST OF FIGURES

INTRODUCTION

INTRODUCTION

Peak oil skepticism has sparked an increasing interest in alternative fuel methods that are carbon neutral and have the potential to offset America's dependence on both foreign and national oil supplies. As a result of this growing concern, the Energy Independence and Security Act (EISA) of 2007 has provided revised Renewable Fuels Standards (RFS), which mandate the use of 36 billion gallons per year (BGY) of renewable fuels by the year 2022 [4]. Some of the renewable fuels sanctioned by the RFS to fulfill the forthcoming objective are 1 BGY of biomass-based biodiesel, 15 BGY of conventional biofuels, and 16 BGY of cellulosic biofuels [4]. The *U.S. Billion-Ton Update (BTS): Biomass Supply for a Bioenergy and Bioproducts Industry* (2011) is a revised study organized to determine the feasibility of producing one billion dry tons of sustainable biomass per year, with the purpose of displacing at least 30% of the nation's petroleum utilization [4]. In 2009, it was estimated that petroleum accounted for approximately 37% of the total primary energy consumption in the United States [4]. The U.S. Energy Information Administration (EIA) has reported that only 40% of petroleum utilized in 2012 was imported product [5]. Therefore, assuming an equivalent amount of petroleum is used for energy consumption during 2012, and one cannot distinguish between foreign and native oil, then approximately 15% of the total primary energy consumption can be attributed to petroleum imports.

First generation feedstocks currently used for bio-energy production typically include sugars, such as sugar cane, and starches, such as corn and wheat. Starches can be fermented to produced ethanol, which can be a used in gasoline blending or to produce E85, which is utilized as a substitute for transportation fuel. However, a dilemma exists when using a first generation

feedstock, such as corn, for the production of conventional biofuels as to the quantity of feedstock that can be consumed for energy production, without negatively influencing food supplies. Subsequently, a need has arisen for a sustainable second generation feedstock that does not conflict with food reserves, and that also provides efficient energy conversion characteristics. Although sugars and starches are typically fermented to form useful alcohols, such as ethanol, second generation feedstocks can also be converted to bio-oil and higher end chemicals through thermochemical conversion techniques. Even though second generation feedstocks range from herbaceous to woody biomass types, extensive research has been dedicated to switchgrass, *Panicum virgatum*, as a viable feedstock for thermochemical conversion via fast pyrolysis [6]. Pyrolysis is the thermochemical breakdown of organic material in an oxygen-absent environment, and in many experimental cases nitrogen or helium is used as the purge and carrier gas. Fast pyrolysis is typically carried out between 400 – 600 $^{\circ}$C with the feedstock having an optimal reactor residence time on the order of seconds. The products of fast pyrolysis consist of a liquid bio-oil portion, a solid bio-char portion, and non-condensable gas portion.

There have been studies committed to determining the feasibility of switchgrass as a second generation feedstock [7], [8], [9], [10], [11], [12], [13], and McLaughlin et al. have reported a reduction in overall switchgrass production costs by 25% with an increased crop yield of 50%, while using key protocols [14]. Some of the protocols crucial to optimizing switchgrass production as an energy feedstock are: (1) the selection of the proper switchgrass cultivar for bio-energy production; (2) the reduction of fertilizer and water usage during cultivation and (3) choosing the proper harvesting practices [9], [14]. However, since different

switchgrass cultivars produce chemically diverse bio-oils, it is imperative to understand the pyrolytic products prior to selecting an optimal cultivar. The objectives of this study are to 1) investigate the influences that variation in switchgrass cultivars and inorganic material have on pyrolytic products, and 2) to determine a working kinetic model which can be used to better understand product variability among switchgrass grown at different locations.

Inorganic materials have been shown to play a role in the production of small molecules and furan derivatives during fast pyrolysis through alkali catalyzed glucose degradation, which leads to a ring scission, instead of depolymerization, of cellulose chains during pyrolysis [15], [16], [17], [18], [19]. It follows that deviations within the inorganic content in the same cultivar of biomass may likely yield inconsistent pyrolytic compounds. On a broad scale, variation in pyrolytic compounds can lead to irregularities within bio-oil and increase the cost of upgrading at centralized bio-refineries. Therefore, if the source of the disparity between pyrolytic compounds is established and eliminated, it would be advantageous in order to generate a uniform bio-oil.

Alkali and alkaline earth metals have been shown to have a catalytic effect on the pyrolysis of biomass by decreasing the onset reaction temperature [18], [20], [21]. Since peak reaction temperature is also related activation energy [22], a decrease in peak reaction temperature should yield a corresponding decrease in activation energy. So, switchgrass with a lower inorganic content may produce pyrolytic compounds that are less variable, but may contain higher activation energy than switchgrass with a greater mineral content. Consequently, a working kinetic model may appropriately explain the differences among activation energy given switchgrass with diverse alkali and alkaline earth metals content.

CHAPTER 1

LITERATURE REVIEW

1.1 Biomass Composition and Pyrolysis Products

Cellulose is a homopolymer of β-(1-4) glycosidic linked D-glucose units (figure 1) and is the most abundant renewable organic material on Earth [23], [24]. Cellulose contains a non-reducing end, where cellulose polymerization begins, that contains glycosidic bonds and no free bonding positions; it also contains a reducing end, where polymerization continues or ends, that contains a free anomeric end on the 1-C position [23], [24]. Hydrogen bonding occurs within chains and between chains of cellulose to form an insoluble, stable, and crystalline group of cellulose chains known as *microfibrils*. The heat addition via fast pyrolysis supplies energy required to break the glycosidic bonds between cellobiose units (depolymerization) to create monomeric glucose units. This is one of two parallel reaction pathways during the fast pyrolysis of cellulose, in which the other is fragmentation, or ring scission [25]. The depolymerization of cellulose during pyrolysis results in the principal production of anhydrosugars and furans [26], [27], [28]. Among the anhydrosugars, levoglucosan is a six carbon sugar that is not only prominent, but also produced in copious amounts compared to other pyrolytic compounds. Notable furans produced during cellulose pyrolysis include furfural and hydroxymethylfurfural [25], [28], [29]. The fragmentation process of cellulose pyrolysis results in the production of linear compounds of esters, carbonyls, and alcohols [25]. Some of the significant compounds produced as a result of ring scission include acetol, acetone, glycoaldehyde, and acetic acid [28], [29].

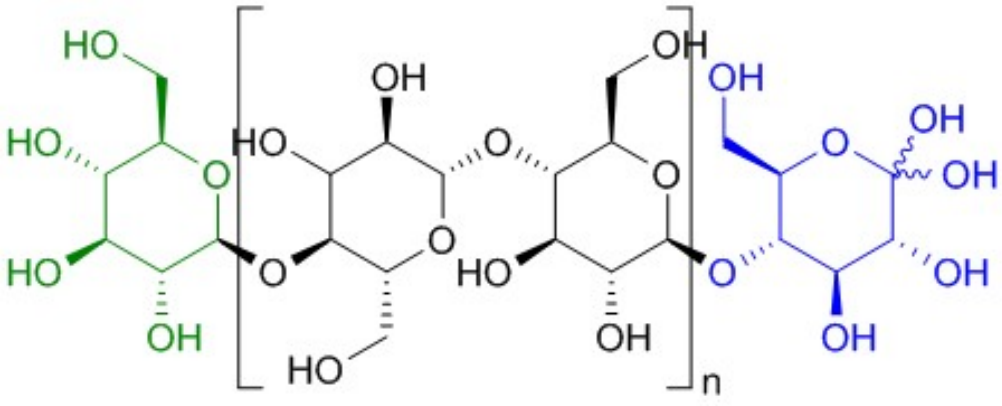

Figure 1. Representation of repeating cellobiose unit, where *n* is any integer, that constitutes a cellulose chain. The reducing end of the cellulose chain (blue) contains a free anomeric carbon; whereas, the non-reducing end (green) has glycosidic bonds instead. For interpretation of the references to color in this and all other figures, the reader is referred to the electronic version of this thesis.

Cellulose microfibrils are held together within the primary cell wall by pectins and cross-linking glycans (hemicelluloses). Since hemicelluloses can differ based on their side chain constituents or the distribution of their glycosidic bonds, they are classified into one of four structurally distinct groups, which are xylans, mannans, xyloglucans, and mixed-linkage β-glucans [30]. Switchgrass hemicellulose chains (figure 2) are polysaccharides with a backbone of β-(1-4) linked D-xylose units with L-arabinose substitutions at either, or at both, the two or three carbon positions [30], [31], [32]. Similar to cellulose, cross-linking glycans undergo both depolymerization and ring scission during pyrolysis and produce comparable compounds to cellulose, such as furans, cycloalkanes, acids, carbonyls, alcohols, and aldehydes [25], [28], [29]. However, since xylan units are only five carbon sugars they cannot form the six carbon anhydrosugars that glucose monomers form during pyrolysis. In this respect, levoglucosan and other six carbon anhydrosugars are products that are specific to cellulose pyrolysis [29].

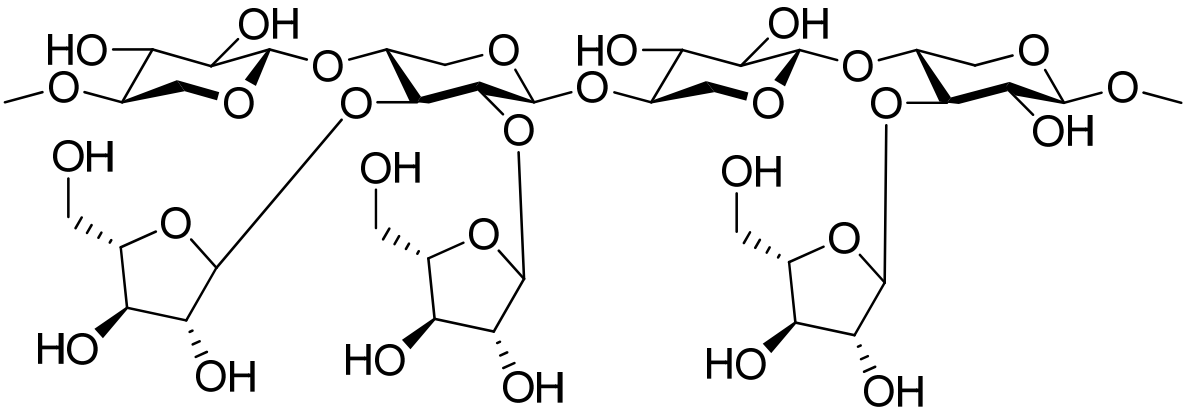

Figure 2. Switchgrass hemicellulose chain. β-(1-4) linked xylan units with L-arabinose substitutions.

Lignin is a polymer composed of monolignol units (figure 3) and their biosynthetic intermediates; however, unlike cellulose and hemicellulose, there has yet to be an observed pattern of a repeating structure. Beginning with phenylalanine, lignin is synthesized through a known biosynthetic pathway via various enzymes, and ends with the polymerization of either *p*-coumaryl alcohol, coniferyl alcohol, or sinapyl alcohol units depending on biomass species [1], [2]. Syringyl lignin, or S-lignin, that is polymerized from sinapyl alcohol is limited to angiosperms; however, lignins polymerized from *p*-coumaryl and coniferyl alcohol can be found in both angiosperms and gymnosperms [1], [2]. The products of lignin pyrolysis are mainly phenolic compounds formed during demethylation and akylation of lignin monomeric units (figure 4) [3].

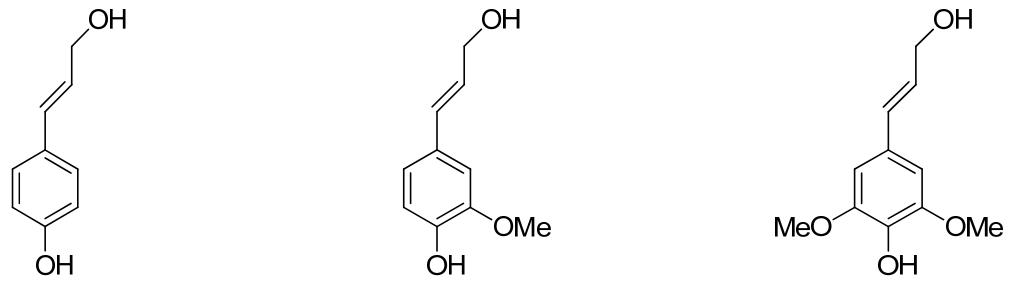

p-coumaryl alcohol (H-lignin) coniferyl alcohol (S-lignin) sinapyl alcohol (S-lignin)

Figure 3. Monolignols produced via biosynthetic pathway [1], [2].

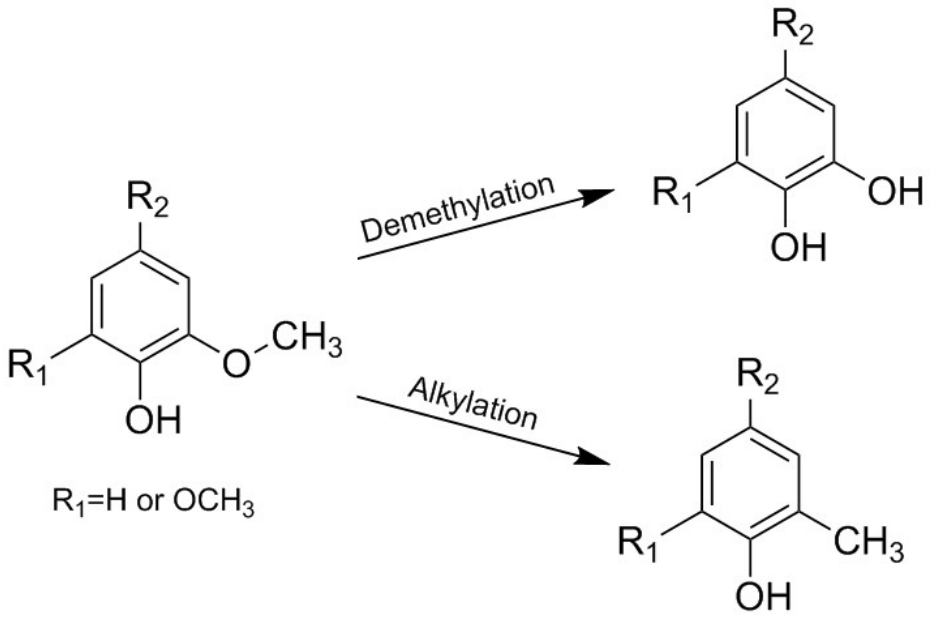

Figure 4. Proposed reaction pathways for the pyrolysis of lignin monomeric unit [3].

Although there is much to be gained in the pursuit of thermochemical conversion of biomass to liquid fuels, the resulting conglomerate of pyrolysis products can generate a bio-oil that is: (1) unstable due to secondary reactions, (2) corrosive due to the production of acids, such as formic and acetic acid, (3) highly viscous, (4) highly oxygenated compared to current hydrocarbons used as transportation fuel, (5) high in water content and (6) low in heating value [33], [34], [35].

1.2 Effect of Alkali and Alkaline Earth Metals on Pyrolysis Products

In previous studies it has been theorized that in the absence of alkali and alkaline earth metals, the mechanism of cellulose pyrolysis favors the production of anhydrosugars, such as levoglucosan, via cleavage of β-O-4 linkages (figure 5) [36], [37], [38].

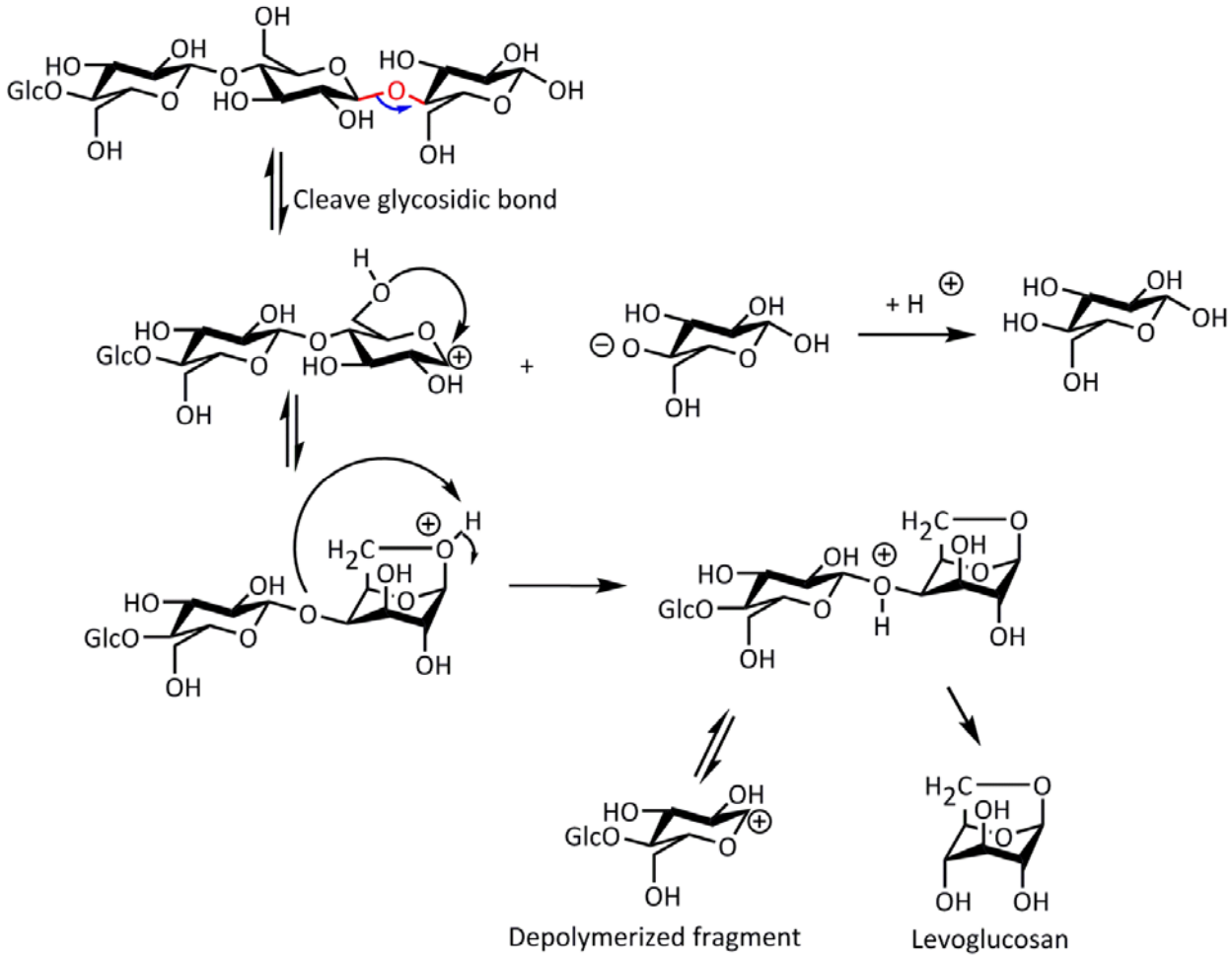

Figure 5. Theorized mechanism for cellulose degradation during pyrolysis to form levoglucosan. Adapted from Evans et al. (1987) with help from Dr. Somnath Bhattacharjee.

Since the compounds formed during pyrolysis will be dependent upon the composition of the biomass, it stands to reason that metals present in the biomass during pyrolysis may play an important role on the production of specific compounds. In fact, many studies have

concluded an influence of alkali and alkaline metals, especially potassium and sodium, on the production of pyrolytic compounds. As a result, a theorized mechanism has been proposed for the pyrolysis of cellulose in the presence of alkali and alkaline earth metals that favors the production of furans and smaller compounds instead of levoglucosan (figure 6) [36], [37].

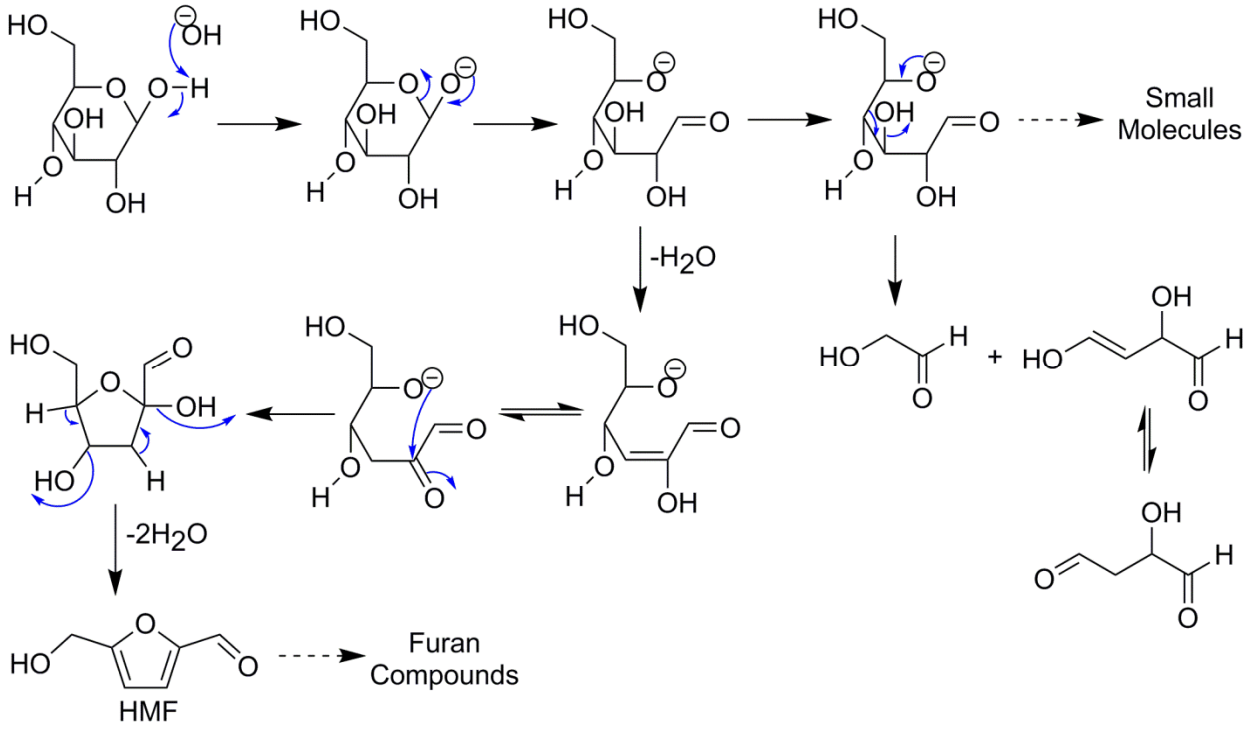

Figure 6. Theorized mechanism for glucose degradation during pyrolysis with alkali-metal-catalyzed pathways. Adapted from Huber et al. (2006) with help from Dr. Somnath Bhattacharjee.

One of the main reasons the aforementioned pathways are still under debate, even after 20 years, is that the low and varying inherent concentrations of metals found in biomass can lead to difficulties in experimental models and statistical analysis. The total alkali and alkaline earth metals (AAEM) content in biomass samples is typically less than 3% w.t. in most Northwestern grass species, and differentiation between metal concentrations for a single sample is nearly impossible. Instead of attempting an experimental approach that requires

varying the inherent concentration of metals for a single sample, many researchers have essentially “cleaned” biomass samples via washing techniques (usually water or acid washing) and subsequently doped samples with known metal concentrations [15], [19], [21], [39], [40].

A downside to acid washing procedures used to clean biomass is the invasive nature on the crystalline structure of cellulose. An acid wash of only 3% HCl on ash-free microcrystalline cellulose has been shown to result in an amorphous cellulose product with a degree of polymerization of less than half the original value [41]. Acid hydrolysis may also occur during acid washing procedures – breaking cellulose chains into glucose monomers. This creates a problem when trying to accurately predict the catalytic effects that metal salts play on crystalline cellulose, as opposed to amorphous cellulose or d-glucose monomers. After acid washing with HCl, H_2SO_4, and H_3PO_4, Wang et al. (2007) observed a decrease in levoglucosan production from the pyrolysis of cellulose filter paper. However, Kim et al. (2011) have shown an increase in the production of levoglucosan after the acid washing of “wax-free” poplar [18]. Wax-free, or extractives-free, poplar samples were created by performing a 7 hour extraction using a 1:2 v/v ethanol and benzene mixture. These conflicting results raise a question of what role the extractives play in the pyrolysis of holocellulose. And since it is unclear whether amorphous cellulose clearly produces a lower quantity of levoglucosan compared to microcrystalline cellulose, even in the absence of metal salts, differentiation between the cause of low levoglucosan production from the pyrolysis of demineralized (acid washed) cellulose doped with inorganic salts proves difficult.

Fahmi et al. (2007) investigated the effects of alkali and alkaline earth metals on the pyrolysis products of switchgrass using only water washing techniques [21]. They concluded

that washing switchgrass in de-ionized water at 60°C for 2 hours decreased potassium and sodium content by 90 and 81%, respectively. Using the same washing procedure for *Festuca mairei*, they also reported a 900% increase in levoglucosan production via fast pyrolysis. Water washing techniques used to remove minerals from biomass samples can prove just as effective as acid washing, while minimizing hemicellulose hydrolysis and maintaining the degree of polymerization of cellulose.

A non-invasive washing technique that does not disrupt cellulose crystallinity may play an important role in better simulating cellulose degradation during pyrolysis. However, demineralizing biomass samples cannot completely remove metal ions and the biomass may still contain chelated species of alkali and alkaline earth metals within the cellulose polymer [19]. Ultimately, even though there has been evidence linking AAEM content to small molecule production and decreased levoglucosan production during pyrolysis, more research is needed to provide a clearer picture of the extent of these effects and whether or not AAEM content can solely be linked to specific product distributions.

1.3 Kinetic Modeling for Pyrolysis of Biomass

The metals present in biomass samples do more than just play a critical role in the production of small molecules during cellulose pyrolysis, they also catalyze pyrolytic reactions which result in lower reaction onset temperatures and activation energies [19], [42]. The reaction onset temperature can be defined as the temperature at which the derivative of the reaction rate begins to vary significantly from zero. Thus, the reaction onset temperature indicates the beginning of pyrolysis, with lower onset temperatures signifying catalysis.

There has been extensive research dedicated to the kinetic modeling of fast pyrolysis and the effects that inorganics have on pyrolysis products [19], [22], [42], [43], [44], [45], [46], [47], [48], [49], [50], [51]. Most kinetic studies performed involve thermogravimetric analysis with an end goal of determining the activation, or apparent activation, energy and pre-exponential factor described in a rate equation (Eq. 1.1) that best fits biomass degradation under pyrolytic conditions.

$$\frac{d\alpha}{dt} = Aexp\left[\frac{-E_a}{RT}\right] f(\alpha) \quad 1.1$$

The left hand side differential represents the change in α, the conversion fraction, with respect to time, while A, E_a, R, T, and *f(α)* represent the pre-exponential factor (s^{-1}), the activation energy (kJ mol^{-1}), the universal gas constant (kJ K^{-1} mol^{-1}), the absolute temperature (K), and the conversion function, respectively. The conversion function may change depending on the reaction; however, it is always contingent upon the conversion fraction, α, which is defined by Eq. 1.2.

$$\alpha = \frac{m_i - m}{m_i - m_f} \quad 1.2$$

Where m_i, m_f, and m are the initial mass, final mass, and temperature-dependent mass of the biomass sample, respectively. Since pyrolytic reaction pathways are complicated and research is still underway in the field of reaction kinetics, researchers usually make assumptions in order to simplify the reaction rate equation. Although chemical reactions should typically govern what conversion functions one should use when estimating kinetic parameters, the conversion function is often simplified into a first-order function shown by Eq. 1.3.

$$f(\alpha) = 1 - \alpha \quad (1.3)$$

A differential thermogravimetric (DTG) profile of cellulose decomposition under pyrolytic conditions will show a single, and usually sharp, peak anywhere from 300 – 400 °C. Since a single DTG peak is a suitable representation of a single step reaction, kinetic studies performed using pure forms of cellulose are typically done so with the assumption the reaction is 1st order [22], [43], [51]. Although kinetic parameters will usually differ depending on the method employed to determine them, it is generally accepted that the activation energy of cellulose is between 200 – 250 kJ mol^{-1} [22], [43], [52], [53]. This is supported through Antal et al. (1998) who used a best-fit method and determined an activation energy for microcrystalline cellulose (Avicel PH-105) ranging from 234 – 244 kJ mol^{-1} at heating rates of 1 and 65 °C min^{-1}, respectively [43]. On the other hand, Cabrales and Abidi (2010) employed a model-free method and determined an activation energy for cellulose at a much lower value of 164 kJ mol^{-1} [51]. The type of cellulose used during experimental studies and the methods utilized to establish kinetic parameters can play a role in the discrepancy of the activation energy and should not be overlooked during thermogravimetric analysis.

The path that most researchers have taken to determine kinetic parameters for raw biomass involves the initial determination of parameters for the individual constituents of the biomass, such as cellulose, hemicellulose, and lignin [45], [54]. The idea is that simpler rate equations can be developed for the biomass components and ultimately fit together to describe the more complex reactions of the raw biomass. Yaman et al. (2010) investigated the

DTG profiles of the holocellulose (combination of hemicellulose and cellulose portion of biomass) and lignin portions of extractives-free hazelnut shells [45]. Their study involved the use of differential scanning calorimetry (DSC) and the Borchardt-Daniels' kinetic model to determine activation energies. Yoon et al. (2011) used a summative kinetic model (similar to equation 1.1) to determine activation energies and pre-exponential factors for commercially produced cellulose, hemicellulose, and lignin and compared them to the kinetic parameters obtained from selected conifers. Although it seems logical to determine the parameters for each portion of biomass and subsequently determine the manner in which they relate to the actual biomass; the downside to this approach is that by using commercially purchased cellulose, hemicellulose, or lignin samples for thermogravimetric experiments, it will be difficult for one to precisely predict how an actual biomass sample will react. To harness the power of this logical approach, the constituents of the biomass under consideration would first have to be extracted with minimal structural or chemical interference to the biomass. Steam explosion, liquid hot water, and acid pretreatment are effective at removing the hemicellulose fraction from biomass, but can also disturb methyl groups between phenols reducing lignin content [55], [56]. Alternatively, ammonia fiber expansion (AFEX) and organosolv pretreatments are more successful at retaining the lignin fraction with partial dissolution of hemicellulose [57], [58], [59], [60]. Furthermore, some pretreatments, such as acid and AFEX, can disrupt the cell wall structure by decrystallizing cellulose microfibrils, while the organosolv process does not [61], [62]. By utilizing the correct pretreatment methods, it may be possible to perform thermogravimetric analysis with minimal structural and chemical interference to the individual

biomass constituents. Such techniques may prove more accurate in determining kinetic parameters of specific biomass species than by using commercially purchased samples.

CHAPTER 2

VARIATION IN PYROLYSIS PRODUCTS OF SWITCHGRASS GROWN AT DIFFERENT LOCATIONS

2.1 Introduction

A single cultivar of cave-in-rock switchgrass harvested from various latitudinal plots in Michigan, cultivated using equivalent practices, is hypothesized to contain similar amounts of organic materials. However, the inorganic content of the switchgrass is theorized to be variable, given the varying nature of the soil properties between latitudes. Furthermore, it is predicted that the switchgrass samples will yield similar pyrolytic compounds, providing they contain a comparable organic material content. However, if variation exists among pyrolytic compounds it may be attributed to the alkali and alkaline earth metals content within the switchgrass samples. Moreover, inconsistent pyrolytic compounds can lead to inhomogeneous bio-oil and expand the cost of upgrading to hydrocarbon fuels at centralized bio-refineries. Consequently, the objective of this section is to investigate the influences that variation in switchgrass cultivars and inorganic material have on pyrolytic products.

2.2 Materials and Methods

2.2.1 Feedstock Analysis

The same species of switchgrass (*Panicum virgatum L.*) was harvested from plots in Frankenmuth, Roger City, Cass County, and Grand Valley Michigan (figure 7) by the Department of Crop and Soil Sciences of Michigan State University. All plots were fertilized with approximately 95 lbs acre^{-1} of nitrogen. All biomass was dried at room temperature and milled to a particle size less than 0.5 mm using a Wiley Mill (Standard Model No. 3, Arthur H. Thomas, Philidelphia, PA). Analysis of both the organic and inorganic matter of the biomass was performed at Dairyone Labs (Ithaca, NY) and is described in the following text. Organic matter,

which includes acid detergent fiber (ADF), neutral detergent fiber (NDF), and acid detergent lignin (ADL) was established using ANKOM Technology Methods 5, 6, and 9, respectively. Cellulose content was determined by calculating the difference between ADF and ADL and hemicellulose content was determined by computing the difference between NDF and ADF [63]. Individual inorganic minerals, such as calcium, phosphorus, magnesium, potassium, sodium, and iron were determined through microwave digestion followed by inductively couple plasma – radial spectrometry, while complete ash content was assessed applying NREL's procedure for the *Determination of Ash in Biomass* [64]. The chloride concentration of the switchgrass was measured by means of a nitric acid extraction, followed by potentiometric titration with silver nitrate using a silver electrode.

2.2.2 Soil Analysis

All soil samples were analyzed at the Michigan State University Soil and Plant Nutrient Lab using *Recommended Chemical Soil Test Procedures for the North Central Region* [65]. The pH of all soil samples were measured potentiometrically using a mixture of deionized water and soil with a 1:1 mass ratio. The percentage of phosphorus in the soil was determined using a Bray P1 extraction, in which the extractant consisted of 0.25 M HCl in 0.03 M NH_4F. The percent of potassium, magnesium, and calcium present in the soil was determined by extraction, using a solution of 1 M NH_4OAc at pH 7.0, followed by atomic adsorption spectrometry. The estimates of exchangeable cations and total cation exchange capacity were determined using equations provided by the *Recommended Chemical Soil Test Procedures for the North Central Region* [65].

2.2.3 Washing Procedures

Approximately 10 g of biomass were washed using 500 mL of deionized water at 60 °C for 2 hours [66]. After the washing procedure the biomass was rinsed in excess of deionized water and filtered using cellulose filter paper and a Buchner funnel. Following filtration the samples were oven dried at 40 °C for 24 hours. Dry samples were stored in glass vials at room temperature for future analysis. Samples prepared in this manner are referred to as "washed" samples.

Extractives were removed from all biomass following protocols outlined in the *Determination of Extractives in Biomass* [67]. First, a cellulose extraction thimble was filled with 2 – 10 g of a biomass sample and placed in the Soxhlet apparatus. Approximately 190 mL of deionized water was added to a 500 mL round bottom boiling flask and set to reflux for 24 hours. Following reflux, the boiling flask was cleaned and dried. The second reagent used was 190 mL of 200-proof ethanol and it was set to reflux for 24 hours. Once the ethanol extraction was complete, the biomass was washed using cellulose filter paper in a Buchner funnel with 100 mL of deionized water and dried at 40 °C for 24 hours. The dry samples were kept in glass vials at room temperature for future analysis. Samples prepared in this manner are referred to as "extractives-free" samples.

2.2.4 Py-GC/MS

Pyrolysis of all biomass samples was conducted using a CDS Pyroprobe 5250 (CDS Analytical Inc, Oxford, PA) connected to a Shimadzu QP-5050A gas chromatograph – mass spectrometer (Shimadzu Corp, Columbia, MD). Approximately one half milligrams of biomass

were packed into quartz tubes between quartz wool and a quartz filler rod. Samples from each location were run in triplicate. Helium was used as a carrier gas at a flow rate of 1 mL min^{-1} and the pyroprobe was heated to approximately 600 °C at a rate of 1000 °C min^{-1} with a six second hold. Pyrolysis vapors were carried into a Restek 1701 column (Restek, Bellefonte, PA) 60 meters in length, 0.25 millimeters in diameter, together with a film thickness of 25 µm. The GC column used a split ratio of 1:100 with a gas flow rate of 1 cm s^{-1}. After holding the GC oven at 40 °C for one minute, the temperature was increased to 270 °C at a rate of 8 °C min^{-1}. Both the detector and injector temperature were set to approximately 280 °C. The mass spectra of the samples were determined using an ionization mode for a mass to charge ratio (*m/z*) of 28 to 400. Compounds were identified by comparing the mass spectra of peaks to standard spectra found in the NIST (National Institute of Standards and Technology) database. Four point calibration curves were determined using external standards of pure compounds (Sigma-Aldrich Co., St. Louis, MO) in acetonitrile to confirm peak identities. Compounds that were unidentifiable by comparison to both the NIST database and pure external standards were checked against mass spectra given in *Pyrolysis-GC-MS Characterization of Forage Materials* [68]. All statistical analysis performed on identified compounds was done so using the average and normalized peak percent area of the mass spectra.

2.2.5 Thermogravimetric Analysis (TGA)

Thermogravimetric analysis was performed on all samples using a Mettler-Toledo TGA/DSC1 (CH-8603 model, Mettler-Toledo, Schwerzenbach, Switzerland) to plot weight loss as

a function of temperature. Experiments were performed using approximately 5 mg of sample in 70 µL aluminum-oxide crucibles (Mettler-Toledo, Schwerzenback, Switzerland) with two replicates per sample. Nitrogen was used as the experiment gas and was continually purged through the furnace at a flow rate of 20 mL min^{-1}. After samples were initially purged with nitrogen for 10 minutes at 30 °C inside the furnace, a heating rate of 10 °C min^{-1} was used to heat the sample to 800 °C. The sample mass was measured every second using an MX1/XP1 microbalance and recorded using STARe Software Version 10.00d (Mettler-Toledo, Schwerzenback, Switzerland). The thermogravimetric (TG), conversion fraction (α), and first-derivative thermogravimetric (DTG) data were extracted from the STARe software before further analysis.

2.2.6 Statistical Analysis

Mean differences were calculated using SAS Enterprise Guide Version 4.2 (SAS Institute Inc., Cary, NC). Remaining statistical analysis, as well as the creation of tables and graphs were done so using Microsoft© Excel© 2010 Version 14.0 (32-bit).

2.3 Results and Discussion

The soil properties were determined from the plots located in Frankenmuth, Roger City, Cass County, and Grand Valley and are shown in table 1. It is shown that the Grand Valley soil contained, comparatively, the largest amount of potassium, magnesium, and calcium, as well as the highest cation-exchange capacity (CEC). With a value of 14.8 meq $100g^{-1}$ (table 1), the CEC of the Grand Valley soil is approximately one and half times greater than all other soils. The cation exchange capacity is defined as the largest quantity of cations the soil is able to hold and

available for exchange with the soil solution. Therefore, the amount of minerals present in the soil correlate with the CEC value. Since the Grand Valley soil has a much higher CEC value, comparatively, it also has a higher content of potassium, magnesium and calcium, comparatively. The amount of potassium, magnesium and calcium found in the Grand Valley soil are 255.5, 407.5, and 2033.5, respectively (table 1). Switchgrass composition revealed that the cellulose content of all switchgrass samples was in a relatively narrow range (34.9 – 36.2 %) excluding Cass County, which had a comparatively higher value of 42.4 % (table 2). Cass County also had the lowest total percent of alkali and alkaline earth metals (AAEM) and the lowest ash content, which are 0.79 and 3.53%, respectively. Given that the presence of inorganics in biomass are shown to catalyze pyrolytic reactions [15], [16], [18], [19], [66], it would be expected that Cass County switchgrass would have the highest onset temperatures for pyrolysis compared to the other three samples.

Comparison of untreated, extractives-free, and washed switchgrass (figure 8) revealed that both the washed and extractives-free biomass had considerably less alkali and alkaline earth metals present in the biomass samples. There was a 50 – 60 % drop in the total percent AAEM content after both treatment procedures for Frankenmuth, Roger City, and Grand Valley switchgrass samples. However, the total percent AAEM content only dropped 32.4% and 38.3% for washed and extractives-free Cass County switchgrass, respectively. The comparatively minor drop in the total percent AAEM content for Cass County switchgrass could be contributed to its low initial AAEM content.

Py-GC/MS revealed 44 principal compounds produced during the pyrolysis of the switchgrass samples over all locations, which were classified into 7 main groups (table 3). The

peak areas of these major compounds were normalized and peak data is reported as percent of total peak area. Figure 9 shows a stack plot of representative pyrograms for untreated switchgrass samples from Frankenmuth, Roger City, Cass County, and Grand Valley. The chromatograms show a clear variation between the production of acetol, hydroxymethylfurfural (HMF), and levoglucosan over switchgrass location. However, since it was difficult to observe variances between compounds solely from the visualization of the chromatograms, additional analysis was required. Statistical analysis was necessary in order to further investigate the differences between pyrolysis compounds between switchgrass locations, therefore, a one-way analysis of variance (ANOVA) was performed using Tukey's honest significance test (HSD) in order to determine possible mean differences between groups of compounds (figure 10). The reaction mechanism described in figure 6 for glucose degradation in the presence of alkali-metals suggests samples with high AAEM contents should favor the production of lower molecular weight compounds and furans over levoglucosan. Since Cass County switchgrass had the highest cellulose content (42.4%) and the lowest AAEM content (0.79%), it might be expected that it would favor the production of levoglucosan over acetic acid, acetol, and furans. Surprisingly, Grand Valley switchgrass, not Cass County, produced the highest quantity of saccharides (levoglucosan and 3,4-anhydro-d-galactosan) even though its cellulose content was comparable to Frankenmuth and Roger City, and even though Grand Valley switchgrass has a fairly modest AAEM content (1.22%). Since both washing techniques reduced the total AAEM content of all switchgrass samples, variances in pyrolytic compounds between washing techniques were further investigated. A one-way ANOVA was performed using a Bonferroni correction to explore mean differences among acids,

aldehydes, esters, furans, ketones, phenolics, and saccharides produced for untreated, washed, and extractives-free switchgrass (figure 11). Samples with a higher AAEM content appear to produced larger quantities of acids, while those with lower a lower AAEM content produced lesser acids with an increased production of aldehydes. Although the aforementioned reaction mechanism would favor the production of six carbon sugars, instead of smaller molecules, in the presence of minerals, it appears there may be another competing reaction during levoglucosan formation in which aldehydes are formed. To support this theory, there were no observable mean differences between treatments for the production of saccharides (Figure 11), which is counterintuitive to the mechanism proposed in Figure 6. This suggests that the total AAEM content of the biomass sample is not the only factor associated with the production of smaller molecules and furans during pyrolysis.

Thermogravimetric analysis was performed and the switchgrass cellulose and hemicellulose peak behavior was observed during pyrolysis. The thermogravimetric curves (TG curve) and first derivative of the conversion fraction curves (DTG curve) were plotted as a function of temperature over all treatments for each switchgrass sample (Figure 12). The conversion fraction, designated as α, can be defined as the degree to which the pyrolysis reaction has proceeded and is defined by equation 2.1.

$$\alpha = \frac{m_i - m}{m_i - m_f} \qquad 2.1$$

The initial, final, and time-dependent mass of the sample are represented by m_i, m_f, and m, respectively. Since alkali and alkaline earth metals can have a catalytic effect on the pyrolysis of samples, it would be expected that switchgrass samples with a higher AAEM content would

start degradation at an earlier temperature. The DTG curves for all switchgrass samples indicated that sample degradation began at lower temperatures for untreated samples versus washed and extractives-free samples (Figure 12). This suggests a possible connection between the metals present in the biomass, the onset temperature of cellulose and hemicellulose degradation, and the maximum rates of reaction. The peak reaction rate temperature of cellulose degradation was diverse for all samples (Figure 13) and it can be seen in all cases, except for Cass County, that the untreated switchgrass has a lower cellulose peak temperature. Therefore, the maximum rate of cellulose degradation for untreated switchgrass, or switchgrass with a comparatively higher AAEM content, occurs at a lower temperature than treated switchgrass, which indicates a slight catalysis of the cellulose portion of the sample. Although the DTG curves explicitly show this phenomenon, results from Py-GC/MS indicate no decrease in the production of saccharides (particularly levoglucosan) from an increased AAEM content, even though there is a dramatic (around 10%) difference in the amount of acid production between untreated and treated switchgrass.

2.4 Conclusions

It has been observed that the Cass County switchgrass contained the lowest AAEM content among the grass samples. In theory, a low AAEM content would favor a depolymerization reaction mechanism, leading to increased anhydrosugars production, instead of ring scission during fast pyrolysis. However, the Grand Valley switchgrass samples, which contained only a comparatively moderate AAEM content, produced the largest fraction of saccharides and the smallest fraction of acids during pyrolysis. It was also shown that both washed and extractives-free switchgrass contain substantially lesser amounts of alkali and

alkaline earth metals than untreated switchgrass samples. The most notable variation in pyrolytic products between treated and untreated samples was the decrease in acid production and the increase in aldehyde formation for washed and extractive-free switchgrass samples. Although there were no observable differences in saccharide production among treated and untreated switchgrass samples, it is possible a competing reaction exists for the formation of aldehydes which hinders the production of levoglucosan. The thermogravimetric data for treated and untreated samples indicate a general trend that samples with high AAEM contents tend to have lower cellulose peak reaction temperatures, which also supports the theory that metals present in the biomass samples can catalyze pyrolytic reactions.

CHAPTER 3

PYROLYSIS KINETICS OF MICROCRYSTALLINE CELLULOSE AND SWITCHGRASS

3.1 Introduction

The presence of alkali and alkaline earth metals within switchgrass samples have been shown to affect the variability among pyrolytic products of a single cultivar harvested from varying latitudes in Michigan. An increase in the production of acids, furans, ketones, and other small molecules for untreated switchgrass samples indicate a reaction mechanism which favors ring scission during pyrolysis. It is theorized that minerals, which catalyze these pyrolytic reactions, can also lower the reaction onset temperature of switchgrass samples and reduce activation energy. Decreasing the activation energy, or the minimum energy required for pyrolysis to occur, can lead to reduction in costs required to power large scale reactors. Therefore, it is beneficial to determine a working kinetic model which can be used to better understand product variability among switchgrass grown at different locations.

3.2 Materials and Methods

Avicel (PH 101) was obtained from Sigma-Aldrich and used during all cellulose experiments. Switchgrass was obtained from the Crop and Soil Science Research Farm on the Michigan State University campus. The switchgrass samples were dried to less than 10% moisture content at room temperature and milled to a particle size of less than 0.5 mm (US Mesh #35) using a Wiley Mill (Standard Model No.3, Arthur H. Thomas, Philadelphia, PA). Ash values for switchgrass were determined using the NREL/TP-510-42622 procedure for ash determination in biomass [64]. Ash values for Avicel PH-101 were determined by a *Residue on Ignition/Sulfated Ash* test and provided from Sigma-Aldrich.

A Mettler-Toledo TGA/DSC1 (CH-8603 model, Mettler-Toledo, Schwerzenbach, Switzerland) was used to simulate fast pyrolysis and plot biomass weight loss as a function of time and temperature. Experiments were performed using approximately 5 mg of sample in 70 µL aluminum-oxide crucibles (Mettler-Toledo, Schwerzenback, Switzerland) with two replicates per sample. A constant nitrogen flow rate of 20 mL min^{-1} was used during all experiments to keep the experimental atmosphere inert. The furnace was purged with nitrogen for 10 minutes at the beginning of each experiment. After the nitrogen purge, samples were heated from room temperature to 105 °C at a constant heating rate of 5, 10, 15, 20, 25, 30, 35, 40, and 50 °C min^{-1} and held at 105 °C for 15 minutes to eliminate excess moisture from the biomass samples. Directly after the drying phase of the experiment, samples were heating to 650 °C using the same heating rate. The sample mass was measured every second using an MX1/XP1 microbalance and recorded using STARe Software Version 10.00d (Mettler-Toledo, Schwerzenback, Switzerland). The thermogravimetric (TG), conversion fraction (α), and first-derivative thermogravimetric (DTG) data was extracted from the STARe software before further analysis.

For the model-fitting method used, a least-squares fit was determined using the solver add-on in Microsoft Excel 2010 (Microsoft Corp., Redmond, WA). All parameters for the Kissinger-Akahira-Sunose and the Flynn-Wall-Ozawa method were determined using the author's custom programs in Matlab R2010a (Mathworks Inc., Natick, MA). All graphs and tables were created using Microsoft Excel 2010.

3.3 Theory

Determining what cultivars will result in high bio-oil yields during fast pyrolysis is not only related to biomass composition, but also to the manner of the degradation. In order to optimize pyrolysis reactors for high bio-oil yields, it is important to ascertain the point at which one can spend the least amount of energy to obtain the maximum amount of product. Exceeding the minimum energy required to perform pyrolysis on a feedstock will result in increased operational costs and, subsequently, increased bio-oil costs. Kinetic studies that can determine the activation energy, or the lowest energy needed to perform pyrolysis, become useful for reducing any excess energy inputs to reactors. The rate constant determined from kinetic studies will also help increase reactor efficiency and bio-oil yield. Additionally, reaction rate coefficients are desired in order to size pyrolysis reactors prior to formulating the process economics. Since it is difficult to perform kinetic studies inside a large scale pyrolysis reactor, thermogravimetric analysis can be used to simulate biomass pyrolysis on a small scale. However, it is vital to determine whether or not a small scale simulation is comparable before any extensive studies are performed for individual feedstocks.

Often, in order to correctly simulate biomass degradation during pyrolysis, a kinetic model is needed that takes into account two of the major constituents, cellulose and hemicellulose. However, if biomass containing large cellulose content is pyrolyzed, then kinetics can usually be approximated as first order – neglecting any effects from hemicellulose, lignin, or extractives. Besides the issues associated with the amount of energy needed for pyrolyzing each biomass component, activation energies and exponential constants often differ depending on the method used to obtain them. Methods used to determine kinetic

parameters are typically categorized into either model-fitting or model-free. Model-fitting kinetics assumes a constant reaction mechanism (not altering with time or temperature) and is used to estimate single values for the activation energy and the pre-exponential factor. Model-free kinetics, however, assumes a varying reaction mechanism, which leads to multiple activation energy and pre-exponential factor values throughout the reaction depending on the fractional conversion state. The first method investigated in this study was a model-fitting method, in which single values were approximated for the activation energy and the pre-exponential factor using theoretical equations and subsequently estimated based on a least squares fit to experimental data. This method was used by Huang et al. [22] to estimate kinetic parameters for cellulose filter paper, xylan, alkali lignin, as well as other raw biomass types such as rice husk, corn leaves, and sugarcane. Equation 3.1 shows the general form of the reaction rate used for pyrolysis of biomass.

$$\frac{d\alpha}{dt} = kf(\alpha) \tag{3.1}$$

The generalized reaction rate equation indicates that the rate of change of the conversion fraction during pyrolysis is dependent on a rate constant, represented by *k*, and a function of the conversion fraction, represented by *f(α)*. The rate constant is temperature dependent and given by the Arrhenius equation (equation 3.2), while *f(α)* is dependent on the solid state model under consideration. For nth order reactions, *f(α)* can be described by equation 3.3.

$$k = A \cdot Exp\left[\frac{-E_a}{RT}\right] \tag{3.2}$$

$$f(\alpha) = (1-\alpha)^n \tag{3.3}$$

From equation 3.2, A, E_a, R, and T represent the pre-exponential factor (s^{-1}), the activation energy (kJ mol^{-1}), the universal gas constant (kJ mol^{-1} K^{-1}), and the absolute temperature (K). The function of the conversion fraction can also be expressed in multiple forms, such as power laws, but the form shown in equation 3.3 is the most commonly used in kinetic studies related to pyrolysis. Substituting equation 3.2 and 3.3 into the initial rate equation and using a heating rate, β, which is equal to the change in temperature divided by the change in time (dT/dt), gives:

$$\beta \frac{d\alpha}{dT} = A \cdot Exp\left[\frac{-E_a}{RT}\right](1-\alpha)^n \tag{3.4}$$

Equation 3.4 can be rearranged in order to integrate both sides, which yields:

$$\int_0^{\alpha} \frac{d\alpha}{(1-\alpha)^n} = \frac{A}{\beta}\int_0^{T} Exp\left[\frac{-E_a}{RT}\right] dT \tag{3.5}$$

The integral on the left hand side (LHS) of equation 3.5 gives:

$$\int_0^{\alpha} \frac{d\alpha}{(1-\alpha)^n} = \frac{(1-\alpha)^{1-n} - 1}{(n-1)} \tag{3.6}$$

The integral on the right hand side (RHS) of equation 3.5 gives:

$$\frac{A}{\beta}\int_0^{T} Exp\left[\frac{-E_a}{RT}\right] dT = \frac{A}{\beta}\left(Exp\left[\frac{-E_a}{RT}\right]T - \frac{E_a}{R}\gamma\right) \tag{3.7}$$

Although the solution to the LHS of equation 3.5 is straightforward, there have been many variations on the solution to the RHS of equation 3.5. To obtain a single value for the activation energy and pre-exponential factor of a homogeneous solid, or biomass, the term γ can be solved using the Euler Gamma function and approximated as a series solution. This

method has been employed in studies from Kissinger (1957) and Huang et al. (2011) [22], [69]. Expanding the series to five terms yields equation 3.8:

$$\gamma = -\frac{1}{2}Exp\left[\frac{-E_a}{RT}\right]\left(Exp\left[\frac{E_a}{RT}\right]\left(Ln\left[\frac{-E_a}{R}\right] - Ln\left[\frac{E_a}{R}\right] - Ln\left[\frac{-R}{E_a}\right] + Ln\left[\frac{R}{E_a}\right]\right) + \left(\frac{-2RT}{E_a} + \frac{2R^2T^2}{E_a^2} - \frac{4R^3T^3}{E_a^3} + \frac{12R^4T^4}{E_a^4} - \frac{48R^5T^5}{E_a^5} + 0T^6\right)\right) \quad 3.8$$

The log terms from the series cancel to zero and some higher order terms can be assumed to approach zero, since the magnitude of the activation energy for cellulose could potentially be 600 - 700 times greater than that of the absolute temperature. Assuming only the first two higher order terms are important, then equation 3.7 becomes:

$$\frac{A}{\beta}\int_0^T Exp\left[\frac{-E_a}{RT}\right]dT = \frac{A}{\beta}\left(Exp\left[\frac{-E_a}{RT}\right]T - \frac{E_a}{R}\left(Exp\left[\frac{-E_a}{RT}\right]\left(\frac{RT}{E_a}\right)\left(1 - \frac{RT}{E_a}\right)\right)\right) \quad 3.9$$

Simplification of equation 3.9 gives a “less messy” version of the integral of the RHS of equation 3.5 and can be written as:

$$\frac{A}{\beta}\int_0^T Exp\left[\frac{-E_a}{RT}\right]dT = \frac{ART^2}{\beta E_a}Exp\left[\frac{-E_a}{RT}\right] = \frac{kRT^2}{\beta E_a} \quad 3.10$$

Equation 3.6 and 3.10 can be equated and re-written as:

$$\frac{(1-\alpha)^{1-n}-1}{(n-1)} = \frac{kRT^2}{\beta E_a} \quad 3.11$$

By definition, the maximum value of the reaction rate occurs when its derivative reaches a value of zero. Thus, differentiation of equation 3.4 with respect to temperature will equal

zero at the maximum reaction rate. The temperature (T_m) at which the maximum reaction rate occurs can also be found using this method.

$$\frac{d}{dT}\left(\frac{d\alpha}{dT}\right) = \frac{d}{dT}\left(\frac{A}{\beta}\cdot Exp\left[\frac{-E_a}{RT}\right](1-\alpha[T])^n\right)$$

$$\frac{d}{dT}\left(\frac{d\alpha}{dT}\right) = \frac{A\cdot E_a\cdot Exp\left(\frac{-E_a}{RT}\right)}{RT^2\beta} - \frac{A\cdot Exp\left(\frac{-E_a}{RT}\right)n(1-\alpha)^n - 1\frac{d\alpha}{dT}}{\beta} \quad 3.12$$

$$\frac{d}{dT}\left(\frac{d\alpha}{dT}\right) = \frac{E_a}{RT^2} - \frac{A\cdot Exp\left(\frac{-E_a}{RT}\right)n(1-\alpha)^n - 1}{\beta} \quad 3.13$$

Therefore, setting equation 3.13 equal to zero gives:

$$\frac{E_a}{RT^2} - \frac{A\cdot Exp\left(\frac{-E_a}{RT}\right)n(1-\alpha)^n - 1}{\beta} = 0 \quad 3.14$$

$$\frac{E_a\beta}{RT_m^2} = An(1-\alpha_m)^n - 1 Exp\left[\frac{-E_a}{RT_m}\right] = k_m n(1-\alpha_m)^n - 1 \quad 3.15$$

The *m* subscript corresponds to the temperature value at the maximum reaction rate. Since the conversion fraction and the rate constant are functions of temperature, they are labeled corresponding to their values at T_m. Substituting equation 3.11 into equation 3.15 gives:

$$\frac{E_a\beta}{k_m RT_m^2} = \frac{(n-1)}{(1-\alpha_m)^1 - n - 1} = n(1-\alpha_m)^n - 1 \quad 3.16$$

Subsequently, solving equation 3.16 for the maximum conversion fraction yields:

$$(1-\alpha_m) = n^{1/1-n} \quad 3.17$$

Solving equation 3.16 for the activation energy gives:

$$E_a = \left[\frac{k_m}{\beta}\right] RT_m^2 n(1-\alpha_m)^{n-1} = \left[\left(\frac{d\alpha}{dT}\right)_m (1-\alpha_m)^{-n}\right] RT_m^2 n(1-\alpha_m)^{n-1}$$

$$E_a = \left(\frac{d\alpha}{dT}\right)_m RT_m^2 n(1-\alpha_m)^{-1} \quad 3.18$$

Substituting equation 3.17 into equation 3.18 and simplifying gives an expression (equation 3.19) for calculating the activation energy by only knowing the reaction order, the universal gas constant, the maximum temperature, and the maximum reaction rate.

$$E_a = \left(\frac{d\alpha}{dT}\right)_m RT_m^2 \left(n^{n/n-1}\right) \quad 3.19$$

In order to find the pre-exponential factor, equation 3.19 and equation 3.17 can be substituted into equation 3.16.

$$\frac{E_a \beta}{n(1-\alpha_m)^{n-1} RT_m^2} = k_m$$

$$\left(\frac{d\alpha}{dT}\right)_m RT_m^2 n^{n/(n-1)} \frac{\beta}{n(1-\alpha_m)^{n-1} RT_m^2}$$

$$= A \cdot Exp\left[\frac{-1}{RT_m}\left(\left(\frac{d\alpha}{dT}\right)_m RT_m^2 n^{n/(n-1)}\right)\right] \quad 3.20$$

$$A = n^{n/(n-1)} \beta \left(\frac{d\alpha}{dT}\right)_m Exp\left[n^{n/(n-1)} \left(\frac{d\alpha}{dT}\right)_m T_m\right]$$

Equations 3.19 and 3.20 are used to calculate the activation energy and pre-exponential factor in cases where the reaction order is greater than unity. In the case that the reaction order is unity, it can be seen that:

$$\lim_{n \to 1} n^{n/n-1} = e \quad 3.21$$

So in the case of a first order reaction, the activation energy becomes:

$$E_a = \left(\frac{d\alpha}{dT}\right)_m eRT_m^2 \quad 3.22$$

And the pre-exponential factor for a first order reaction becomes:

$$A = e\beta \left(\frac{d\alpha}{dT}\right)_m Exp\left[e\left(\frac{d\alpha}{dT}\right)_m T_m\right] \quad 3.23$$

In order to solve the reaction rate equation (equation 3.4) without the alpha term, equation 3.11 must be solved for the conversion fraction, which gives:

$$\alpha = 1 - \left((1-n)\left(\frac{1}{1-n} - \frac{kRT^2}{E_a\beta}\right)\right)^{1/1-n} \quad 3.24$$

In the case that the reaction order is greater than unity, equation 3.24 can be substituted into equation 3.4 and simplified to yield:

$$\frac{d\alpha}{dT} = \frac{k}{\beta}\left(1 + \frac{(n-1)kRT^2}{\beta E_a}\right)^{n/1-n} \quad 3.25$$

However, in the case that the reaction order is equal to unity then the limit can be taken of equation 3.25 as the reaction order approaches unity, which gives:

$$\frac{d\alpha}{dT} = \frac{k}{\beta} Exp\left[\frac{-kRT^2}{\beta E_a}\right] \quad 3.26$$

Thus, equations 3.25 and 3.26 can be used to approximate the pyrolytic reaction rate of homogeneous solids (biomass) of a specified reaction order. Furthermore, thermogravimetric analysis (TGA) can be used to obtain the parameters required to calculate the activation energy and pre-exponential factor. However, these values are only rough approximations and rarely yield accurate results. Consequently, these values can be used as a starting point in

determining more accurate parameters by minimizing the sum of the squares function (equation 3.27).

$$SSE = \sum_{i=1}^{n} \left[\left(\frac{d\alpha}{dT}\right)_i^{exp} - \left(\frac{d\alpha}{dT}\right)_i^{sim} \right]^2 \quad 3.27$$

Besides model-fitting kinetics, two common model-free methods used to derive the apparent activation energy, or activation energy as a function of the conversion fraction, are the Kissinger-Akahira-Sunose (KAS) method and the Flynn-Wall-Ozawa (FWO) method [69], [70], [71], [72]. The KAS method is based on the Coats-Redfern [73] approximation and yields acceptable results for apparent activation energies when the conversion fraction is greater than 13% [74]. The KAS method allows for a plot of $\ln(\beta\, T^{-2})$ versus (T^{-1}) at a constant conversion fraction, and is described by equation 3.28 [69], [70], [74], [75].

$$ln\left(\frac{\beta}{T2}\right) = ln\left(\frac{AR}{E_a g(x)}\right) - \frac{E_a}{RT} \quad 3.28$$

The function *g(x)* in equation 3.28 relates to the conversion function, *f(x)*, and relations are given in Table 4. At a constant fractional conversion and over multiple heating rates, a straight line can be fit to equation 3.28 in which the slope of the line corresponds to the apparent activation energy.

The FWO method allows for a plot of $\ln(\beta)$ versus (T^{-1}), is based on Doyle's approximation [76], and is described by equation 3.29.

$$ln(\beta) = ln\left(\frac{0.0048AE_a}{Rg(\alpha)}\right) - 1.0516 - \frac{E_a}{RT} \quad 3.29$$

To avoid errors greater than 5%, equation 3.29 can be used at fractional conversion states greater than 20%, but it can also be used at fractional conversion states greater than 10% if errors of 10% are acceptable [76]. In a manner similar to the KAS method, the apparent activation energy can be calculated by fitting equation 3.29 to a straight line at a constant conversion fraction and multiple heating rates. The slope of equation 3.29 corresponds to the apparent activation energy.

Besides determining kinetic parameters based on the previously mentioned methods, the author intends to fit the rate of switchgrass pyrolysis to the form of equation 3.30.

$$\left(\frac{d\alpha}{dT}\right)_{total} = \gamma_1 \left(\frac{d\alpha}{dT}\right)_{cellulose} + \gamma_2 \left(\frac{d\alpha}{dT}\right)_{hemicellulose} \quad 3.30$$

It is hypothesized that the overall reaction of the biomass during pyrolysis should be explainable by a simple summation of the individual reaction rates of the biomass constituents (in this case modeled by only cellulose and hemicellulose). The reaction rates on the right hand side of equation 3.30 can be explained by equations 3.25 and 3.26, depending upon the reaction order chosen. The activation energies and pre-exponential factors can be estimated for cellulose and hemicellulose from raw biomass by determining the correct peak values, using the model-fitting method previously described, and minimizing the objective function (equation 3.27) to estimate the kinetic parameters. The activation energies, pre-exponential factors, and gamma factors for cellulose and hemicellulose can be obtained by minimizing the sum-squared-errors of the total reaction rate (equation 3.31).

$$SSE = \sum \left[\left(\frac{d\alpha}{dT}\right)_{total} - \left(\frac{d\alpha}{dT}\right)_{switchgrass}\right]^2 \quad 3.31$$

3.4 Results and Discussion

3.4.1 Avicel Kinetics

The pyrolysis of the Avicel obtained from Sigma-Aldrich at various heating rates between 5 - 50 °C showed a distinct correlation among the shapes of the DTG curves (Figure 14); however, the peak reaction rates and corresponding temperatures differed for almost every case (Table 5). The peak reaction rate and temperature for Avicel pyrolysis at 5 °C min^{-1} is 0.0334 $°C^{-1}$ and 327 °C compared to 0.0237 $°C^{-1}$ and 362 °C for Avicel pyrolysis at 50 °C min^{-1}. Although there were noticeable shifts in peak temperature (ΔT) and reaction rate ($\Delta d\alpha/dT$) between the lowest and highest heating rates used, the total area of the DTG curves were estimated using Simpson's rule and remained at unity for all cases. This indicated no errors in the calculation of the DTG curve, as the alpha function is a normalization of the mass loss curve, and integration of its first derivative should inevitably lead to unity. One can visually interpret the integral of the DTG curve leading to unity by observing the trends over the various heating rates (Figure 14). The first DTG curve shown at a heating rate of 5 °C min^{-1} has a taller and narrower peak compared to peaks of higher heating rates. This is logical, since a curve with a smaller peak would have to be wider to have a comparable area to a curve with a taller peak.

The model-fitting method was used to estimate the activation energies and pre-exponential factors for Avicel pyrolysis at various heating rates, assuming they were a 1^{st}, 2^{nd}, or 3^{rd} order reaction. The initial kinetic parameters were initially estimated by equations 3.19, 3.20, 3.22, and 3.23 and then recalculated by using equation 3.27. The initial estimates of the

parameters can be seen in Table 6, and the calculated values using equation 3.27 can be seen in Table 7. The mean values for the activation energies using the model-fitting method, assuming an order of reaction of 1, 2, and 3, are 248.5 ± 19.1 kJ mol^{-1}, 362.9 ± 25.4 kJ mol^{-1}, and 464.9 ± 27.6 kJ mol^{-1}, respectively; and the mean values for the pre-exponential factors are (2.4 ± 3.3)x10^{22} min^{-1}, (9.7 ± 18)x10^{32} min^{-1}, and (8.6 ± 15)x10^{41} min^{-1}, respectively. Since the standard deviations for all of the activation energies were between 5 – 10% of the means, one could argue a single value approach for determining this parameter may be less effective than correlating the values to determine a functional relationship between them. Although there appears to be a slight polynomial trend to the data for the activation energies, linear fits show strong correlations with R^2 values greater than 0.87 for all cases of reaction orders (Figure 15). In this case, it appears that the single mean value would be less effective, as Figure 15 indicates an obvious decrease in activation energy with increasing heating rate. However, due to the intervals of the heating rates (almost all equal), and the rate at which the activation energy decreases over heating rate, the mean value determined most likely does not represent a random sample in the population. Furthermore, Antal et al. (1998) has shown a variety of cellulose producing multiple results for kinetic parameters [43]. More specifically, it has been shown that Avicel (PH 105) pyrolysis at a heating rate of 1 and 65 °C min^{-1} yields activation energies of 244 and 234 kJ mol^{-1} [43]. Cellulose filter paper has also been pyrolyzed at 5 °C min^{-1} and an activation energy of 227 kJ mol^{-1} was determined [22]. Even though the reported

values for Avicel activation energy (268 – 213 kJ mol^{-1}) have a larger span than previous literature, these values are still within agreement.

The FWO method was used to create a plot of T^{-1} versus *ln*(β) over a fractional conversion range of 10 – 80% (Figure 16). Straight lines were fit to the sets of data corresponding to fractional conversion states and fit parameters were recorded (Table 8). It was determined that the range of apparent activation energies (ΔE_a) for the pyrolysis of Avicel ranged from 225.7 – 206.3 kJ mol^{-1} over a fractional conversion range of 10 – 80% (Table 8). The mean value for the apparent activation energy using the FWO method is 213.8 ± 6.6 kJ mol^{-1} (Table 8). Similar to the model-fitting method, a plot of apparent activation energy versus fractional conversion revealed a decreasing trend in activation energy that would indicate the single mean value is not indicative of a random sample from the population (Figure 17). However, this trend discontinued after a fractional conversion state of 70%, after which the apparent activation energy began to increase. It is thought that the decrease in activation energy followed by the increase is due to the depolymerization of Avicel during pyrolysis followed by the subsequent repolymerization reactions which form bio-char. Therefore, a logarithmic fit was determined, only over the fraction conversion range of 10 – 70%, yielding an R^2 value of 0.9836 and the following equation:

$$E_a = -10.898\, ln(\alpha) + 202.028 \qquad 3.32$$

The apparent activation energy can now be estimated well within 95% confidence intervals using equation 3.32. It should be noted that the activation energy range in the FWO method

was reduced by approximately 73% compared to that of the model-fitting method. The higher and lower bounds of activation energies of the FWO method were reduced by 42 and 7 kJ mol^{-1}, respectively, compared to the model-fitting method. Overall, the FWO method has effectively lowered the magnitude of the apparent activation energies and shortened the range for which they can be estimated.

The KAS method was used to determine the apparent activation energies of pyrolyzed Avicel at various fractional conversion states by fitting straight lines to a plot of T^{-1} versus $ln(\beta/T^2)$ (Figure 18). The apparent activation energies determined from the KAS method for Avicel pyrolysis ranged from 215.8 – 195.9 kJ mol^{-1} over a fractional conversion range of 10 – 80% (Table 9). The mean value for the apparent activation energy using the KAS method is 203.6 ± 6.7 kJ mol^{-1} (Table 9). A plot of apparent activation energy versus heating rate shows a decreasing trend in the ordinate (Figure 19) for a fractional conversion rate of less than 70%, similar to the trend observed for the FWO method. However, also similar to the results of the FWO method, apparent activation energies begin to increase for fractional conversion values above 70%, most likely due to the formation of char. Therefore, a logarithmic fit was determined only for 10% ≤ α ≤ 70% to explain the relationship between apparent activation energy and heating rate, yielding an R^2 value of 0.9841, and described by the following equation:

$$E_a = -11.1359\, ln(\alpha) + 191.603 \qquad 3.33$$

Using equation 3.33, the apparent activation energy can be estimated with a 95% confidence interval over a 10 – 70% fractional conversion range. The range, or span, of activation energies (ΔE_a) observed for both the FWO and the KAS method were both approximately 20 kJ mol^{-1}. Also, it appeared that ΔE_a for the FWO method had merely decreased by 10 kJ mol^{-1}; thus, the highest and lowest activation energies observed for the KAS method were approximately 10 kJ mol^{-1} less than those observed for the FWO method.

Ultimately, there was a notable decrease in both ΔE_a and the values of the activation energies when comparing the model-fitting and the model-free methods. However, when comparing the two model-free methods, there only seemed to be a difference among the values of the activation energies and not necessarily their range. Another advantage of using a model-free method, as opposed to the model-fitting method, is the ability to observe the approximate fractional conversion state, in both cases greater than 70%, at which char formation occurs. When using a model-free method, these fractional conversion states can also be linked to temperature to further indicate the state of repolymerization.

3.4.2 Switchgrass Kinetics

Since hemicellulose and cellulose can constitute upwards of 60 weight percent (Table 2) of switchgrass, it is important to distinguish these peaks, especially when calculating kinetic parameters using a model-fitting method (equation 3.30). The DTG profile for pyrolyzed switchgrass at a heating rate of 50 °C min^{-1} shows distinct peaks for hemicellulose and cellulose (Figure 20). The peak reaction rates and peak temperatures for the hemicellulose and cellulose

peaks are given in Table 10. Trends were observed for peak reaction rate and peak temperature versus heating rate for both hemicellulose and cellulose peaks during switchgrass pyrolysis (Figure 21). Both hemicellulose and cellulose peak temperature increased over heating rate; but only cellulose peak reaction rate appeared to indicate any significant reduction with a rising heating rate, compared to hemicellulose peak reaction rate, which remained stagnant (Figure 21). A simple logarithmic relationship was determined to explain the connection between peak temperature and heating rate for both the hemicellulose and cellulose peak temperature profiles. It was determined that the change in peak temperature with heating rate for hemicellulose and cellulose could be explained by equations 3.33 and 3.34, respectively.

$$T_m = 13.853\ ln(\beta) + 261.04 \quad 3.33$$

$$T_m = 13.959\ ln(\beta) + 317.27 \quad 3.34$$

Equations 3.33 and 3.34 yielded R^2 values of 0.9853 and 0.9831, respectively. The terms in front of the logarithm in equations 3.33 and 3.34 were averaged to create a new equation to determine the relationship between peak temperature and heating rate. The following equation was used to fit experimental data and yielded R^2 values of 0.9849 and 0.9828 for hemicellulose and cellulose peak temperatures:

$$T_m = 13.906\ ln(\beta) + T_{bio} \quad 3.35$$

The T_{bio} term in equation 3.35 is different for hemicellulose and cellulose and relates to the temperature as β approaches unity. For hemicellulose and cellulose, T_{bio} values are 261.04

°C and 317.27 °C (the same intercept values from equations 3.33 and 3.34), respectively. Since the goodness of fit from equation 3.35 is comparable to equations 3.33 and 3.34 it is considered a better choice when using a single thermogravimetric analyzer for research. Multiple sample peaks would require multiple relationships to explain peak temperature and heating rate; however, equation 3.35 produces comparable results while only varying the intercept. This indicates that thermal lag within the TGA is systematic, not random, and that temperature shifts seen over different heating rates can potentially be corrected. The DTG profiles of switchgrass pyrolysis over all heating rates (Figure 22) give a visual approximation of how peak temperature and peak reaction rates change with heating rate. By observing the DTG profiles of switchgrass pyrolysis (Figure 22), it can be seen that the peak reaction rates for hemicellulose (Table 10) and the unchanging peak reaction rate trend for hemicellulose (Figure 21) all correspond to one another.

The FWO method was used to create a plot of T^{-1} versus *ln*(β) for switchgrass pyrolysis over a fractional conversion range of 10 – 80% (Figure 23). Straight lines were fit to the sets of data corresponding to fractional conversion states and fit parameters were recorded (Table 11). It was determined that the range of apparent activation energies (ΔE_a) for the pyrolysis of switchgrass ranged from 198.5 – 248.6 kJ mol^{-1} over a fractional conversion range of 10 – 80% (Table 11). The mean value for the apparent activation energy using the FWO method is 227.7 ± 14.6 kJ mol^{-1} (Table 11). A plot of apparent activation energy (calculated from the FWO method) versus fraction conversion for switchgrass pyrolysis revealed a trend that appeared to

increase to a maximum value then decrease (Figure 24). The following modified exponential was fit to the experimental data, which yielded an R^2 value of 0.8811:

$$E_a = 242.0035\, Exp\left[-\left(\frac{\alpha - 0.5272}{0.9043}\right)^2\right] \quad 3.36$$

Following the general trend of the data and considering the number of observations recorded, this may be considered an optimal route for a general data trend. Observation of Figure 24 shows two distinct outliers at fractional conversion states of 40 – 45%, which could be attributed to the initial energy required to breakdown hemicellulose and cellulose. After β-(1→4) bonds are broken in the xylans, this excess energy is no longer required and drops around a fractional conversion rate of 50%, which leaves the apparent activation energy needed to break glycosidic bonds between glucose units. However, one phenomenon not *clearly* shown, as seen from Avicel pyrolysis, is the sharp increase in apparent activation energy around a fractional conversion rate of 70% to indicate char formation. However, there is a noticeable trend in which E_a starts below the fitted exponential for $\alpha < 70\%$ and becomes higher than the fitted exponential for $\alpha > 70\%$ (figure 18), but this small deviation is still well within the 95% confidence intervals. At a fractional conversion state of 85%, the apparent activation energy of switchgrass (determined by the FWO method) is 251.4 kJ mol^{-1}, which yielded an R^2 value of 0.8824 (Table 11 and Figure 24). Since the goodness of fit is not considered optimal, but also not considered substandard, this dramatic increase in E_a could be due to repolymerization reactions that cause char formation, or it may not be correlated to

fractional conversion. In either case, the mean weight percent value of bio-char formed from biomass pyrolysis can be defined by:

$$W_{char} = \frac{1}{n}\sum_{i}\frac{m_{final,i} - m_{ash}}{m_{initial}} \qquad 3.37$$

After experimental results yielded an average ash value of 3.9 ± 0.1%, equation 3.37 was used to determine the mean char value of switchgrass to be 20.5 ± 1.3%. Given that Avicel contained an inorganic fraction no greater than 0.1 weight percent, the mean value of Avicel was determined (using equation 3.37) to be 10.3 ± 4.2%. The difference of the highest char value of Avicel and the lowest char value of switchgrass may be an indication of the percent char formed from hemicellulose. In the worst case scenario, it would most likely be safe to assume that about a quarter of the total char formed, or 4.7% of the initial sample weight, from switchgrass pyrolysis can be attributed to hemicellulose deconstruction.

The KAS method was used to determine the apparent activation energies of pyrolyzed switchgrass at various fractional conversion states by fitting straight lines to a plot of T^{-1} versus $ln(\beta/T^2)$ (Figure 25). The apparent activation energies determined from the KAS method for switchgrass pyrolysis spanned from 189.5 – 238.6 kJ mol^{-1} over a fractional conversion range of 10 – 80% (Table 12). The mean value for the apparent activation energy of switchgrass using the KAS method is 217.8 ± 14.3 kJ mol^{-1} (Table 12). A plot of apparent activation energy (obtained using the KAS method) versus fractional conversion was fit to a modified exponential (Figure 26) and yielded an R^2 value of 0.9086 and the following relationship:

$$E_a = 231.3930\ Exp\left[-\left(\frac{\alpha - 0.5222}{0.9105}\right)^2\right] \quad 3.38$$

By observing the plot of activation energy versus fractional conversion (Figure 26), based on the KAS method, one can still examine similar outliers found between a fractional conversion rate of 40 – 45%, the same as when based on the FWO method. When examining the DTG profiles of switchgrass pyrolysis for 40% ≤ α ≤ 45%, it is clear that this fractional conversion range always occurs at the point in which the cellulose reaction rate becomes greater than that of hemicellulose, or the local minimum (Figure 27). Since there is such a dramatic increase in the energy required to continue cellulose pyrolysis at this local minimum, it suggests a decrease in previously available energy. This indicates that the hemicellulose reaction must be exothermic in the experimental temperature range, and it was also concluded by Yang et al. (2007) [77].

Using the KAS method under a fractional conversion state of 85%, the apparent activation energy of switchgrass was determined to be 204.5 kJ mol^{-1} (Table 12). However, using the KAS method to determine E_a at α = 85% yielded an R^2 value of 0.8728, which is neither optimal nor substandard. As with E_a at α = 85% calculated using the FWO method, it is uncertain whether or not this increase in energy is due to reactions related to char formation. However, a noticeable trend exists in which E_a begins to decrease around α = 55% and subsequently deviates above the exponential fit for α > 70%.

Using the FWO and KAS methods to determine the apparent activation energy between 40% ≤ α ≤ 45%, it was concluded that the hemicellulose degradation of switchgrass pyrolysis is

an exothermic reaction that contributes to the overall breakdown in glycosidic bonds in cellulose. Based on results that indicate that char formation of Avicel may begin at a fractional conversion stage as early as 70% and established by trends of apparent activation energy for switchgrass pyrolysis (Figure 24 and Figure 26), it was also recognized that char forming reactions of switchgrass pyrolysis most likely occur for $\alpha \geq 70\%$. Both sets of apparent activation energies of switchgrass pyrolysis, obtained by using the FWO and KAS methods, are valid only for $10\% \leq \alpha \leq 80\%$.

In order to estimate kinetic parameters from equations 3.19, 3.20, 3.22, and 3.23, the peak reaction rates and peak temperatures for switchgrass hemicellulose and cellulose pyrolysis were determined (Table 13). Estimation of switchgrass cellulose and hemicellulose kinetic parameters based on the aforementioned equations is given in Table 14 and Table 15, respectively. The mean values for the apparent activation energy of switchgrass cellulose assuming a reaction order of one, two, and three are 87.6 ± 6.0 kJ mol^{-1}, 128.9 ± 8.8 kJ mol^{-1}, and 167.4 ± 11.4 kJ mol^{-1} (Table 14), respectively. The mean values for the apparent activation energy of switchgrass hemicellulose assuming a reaction order of one, two, and three are 50.8 ± 1.7 kJ mol^{-1}, 74.8 ± 2.6 kJ mol^{-1}, and 97.2 ± 3.3 kJ mol^{-1} (Table 15), respectively. The reaction rate of switchgrass pyrolysis for heating rates of 5 and 50 °C min^{-1} were fit to equations 3.25 and 3.26 using the kinetic parameters estimated for the cellulose peaks (Figure 28 and Figure 29); however, these fits were not optimized by minimizing the sum squared of the errors. The R^2 values for the reaction rate fits at a heating rate of 5 °C min^{-1} (Figure 28) assuming a

reaction order of one, two and three are 0.6952, 0.5244, and 0.4091, respectively. Since distinction between cellulose and hemicellulose peaks becomes less pronounced with increased heating rate (Figure 22), a single peak fit to the DTG profile at a heating rate of 50 °C min^{-1} yielded R^2 values higher than those corresponding to the DTG profile at a heating rate of 5 °C min^{-1}. The R^2 values for the reaction rate fits at a heating rate of 50 °C min^{-1} (Figure 29) assuming a reaction order of one, two and three are 0.8745, 0.7413, and 0.6192, respectively.

The range of apparent activation energy (ΔE_a) for switchgrass cellulose and hemicellulose, assuming a reaction order of one, are 75.3 – 96.3 kJ mol^{-1} and 47.6 – 57.0 kJ mol^{-1} (Table 14 and Table 15), respectively. In the case that the reaction order is one, two, and three, ΔE_a for switchgrass hemicellulose is approximately one quarter the value of the ΔE_a for switchgrass cellulose. The range of apparent activation energy, as a function of reaction order, for switchgrass cellulose and hemicellulose were fit to linear curves (Figure 30) and their respective relationships are given by:

$$\Delta E_a = 9587.1n + 11558 \quad 3.39$$

$$\Delta E_a = 2487.5n + 2998.8 \quad 3.40$$

The respective R^2 values for equations 3.39 and 3.40 are both 0.9996. Both the slope and the intercept of the hemicellulose fit (equation 3.40) are approximately one quarter the value of the corresponding cellulose fit constants.

Optimizing the kinetic parameters for switchgrass pyrolysis using equation 3.31 yielded mean values for the activation energy of switchgrass cellulose and hemicellulose of 148.9 ± 19.6 kJ mol^{-1} and 114.0 ± 4.5 kJ mol^{-1}, respectively (Table 16). The ΔE_a for the switchgrass cellulose after optimization was almost seven times greater than that of switchgrass hemicellulose after optimization. This difference is greater than that of the ΔE_a for the un-optimized parameters since the ΔE_a differed by a magnitude of four between switchgrass cellulose and hemicellulose. The mean values for the pre-exponential factors of switchgrass cellulose and hemicellulose, after optimization, were 1.7 ± 3.1 x 10^{13} min^{-1} and 3.4 ± 3.2 x 10^{10} min^{-1}, respectively (Table 16). The mean values for the gamma factors for switchgrass cellulose and hemicellulose, after optimization, were 0.5605 ± .0497 and 0.3458 ± 0.0334, respectively (Table 16). All R^2 values reported for the optimized parameters were above 0.95 (Table 16). A plot of activation energy and pre-exponential factor, after optimization, versus heating rate indicates a decrease in activation energy and pre-exponential factor for switchgrass cellulose over the abscissa (Figure 31). However, no clear trend is visible from Figure 31 for the optimized parameters of switchgrass hemicellulose versus heating rate.

The optimized parameters for switchgrass pyrolysis (Table 16) were used to plot the simulated rate of switchgrass pyrolysis (equation 3.30) alongside the experimental data (Figure 32). It is important to note that previous rate fits were made which yielded low R^2 values (Figure 32). The disadvantage of the previous rate model for fitting switchgrass pyrolysis is that it does not account for multiple peaks in the DTG profile. However, since both the

hemicellulose and cellulose peaks could be distinguished from the DTG curve, it allowed a more inclusive fit (based on equation 3.30). Yet, observation of Figure 32 reveals experimental data outside of the fit which is approximately below 250 °C and above 400 °C. It is most likely that the reacted portion below 250 °C is a combination of the pyrolysis of extractives and lignin, while the portion at 400 °C is the pyrolysis of the remaining lignin in the sample. A *current* drawback to model-fitting methods is that one cannot precisely predict to which component of the biomass the activation energy corresponds.

Although using the newer model-fitting method which includes the breakdown of both hemicellulose and cellulose to predict reaction rates in switchgrass has undoubtedly increased the magnitude of the coefficient of determination, and has the general appearance of an improved fit; the addition of the second reaction term and the gamma terms can begin to congest the optimization of the kinetic parameters. In order to obtain values for kinetic parameters which are as true as feasible, it is imperative to ensure the objective function contains a minimal number of variables. Brief examination of gamma for switchgrass cellulose and hemicellulose (Table 16) reveals that there seems to be no alarming deviation in these variables between heating rates. It is theorized that these variables are not changeable, but are most likely constant for all heating rates.

The mean values for γ_1 and γ_2 which were previously determined through optimization are 0.5605 and 0.3458, respectively. These gamma values were assumed constant to optimize a new set of kinetic parameters, using equation 3.31, for switchgrass cellulose and hemicellulose (Table 17). The mean values for the apparent activation energy of switchgrass

cellulose and hemicellulose, assuming constant gamma values, are 158.2 ± 9.2 kJ mol^{-1} and 115.5 ± 4.3 kJ mol^{-1}, respectively (Table 17). The mean value for the activation energy of switchgrass cellulose increased by approximately 10 kJ mol^{-1} compared to when gamma values were not held constant, and the ΔE_a also decreased by 50%, comparatively. Activation energy values for switchgrass hemicellulose remained stable after optimization with constant gamma values. The R^2 values corresponding to the kinetic parameters obtained assuming constant gamma values were all above 0.95 and did not significantly differ from the original R^2 values (Table 17). The new kinetic parameters (Table 17), assuming constant gamma values, were plotted, using equation 3.30 and a 95% confidence interval, against experimental data for all heating rates (Figure 33). The plots for the kinetic parameters assuming constant gammas appear exceptionally similar to those in which the gamma values were allowed to vary. The paramount differences observed were the increase in the mean, the decrease of the standard deviation, and the reduction of the range of the activation energy for switchgrass cellulose, assuming constant gamma values.

Thermogravimetric analysis was also performed on untreated, washed, and extractives-free switchgrass, over all locations, using a constant heating rate of 10 °C min^{-1} during experiments. The two-peak model-fitting method was utilized to determine kinetic parameters for switchgrass cellulose and hemicellulose (Tables 18 and 19) assuming constant gamma factors, which were previously estimated (Table 16). The mean values for the activation energies of untreated, washed, and extractives-free switchgrass cellulose are 150.5 ± 14.2 kJ

mol^{-1}, 194.3 ± 5.7 kJ mol^{-1}, and 192.8 ± 9.8 kJ mol^{-1}, respectively. While the mean values for the activation energies of untreated, washed, and extractives-free switchgrass hemicellulose are 105 ± 12.5 kJ mol^{-1}, 139.9 ± 6.2 kJ mol^{-1}, and 144.9 ± 5.2 kJ mol^{-1}, respectively. The activation energy for both switchgrass cellulose and hemicellulose increased after treatments by approximately 40 kJ mol^{-1}. A Plot of activation energy for switchgrass cellulose versus treatment versus AAEM content (Figure 34) displays a correlation between the reduction in overall alkali and alkaline earth metals and an increase in activation energy. A similar plot of activation energy for switchgrass hemicellulose versus treatment versus AAEM content (Figure 35) demonstrates an equivalent correlation between the decrease in mineral content and increase in activation energy. The appreciation in activation energy during the reduction of alkali and alkaline earth metals indicate the minerals act as a catalyst during pyrolysis, and it is also known that the energy is quantifiable through use of the two-peak model-fitting method. To visually ensure the quality of the kinetic parameters obtained using the two-peak model-fitting method, the experimental data for untreated, washed, and extractives-free switchgrass was fit to equation 3.30 using 95% confidence intervals (Figures 36, 37, and 38) and all R^2 values were greater than 0.96.

3.5 Conclusions

Observation of the DTG profile of Avicel PH-101 and switchgrass showed differing values for both the peak reaction rates and the peak temperatures for varying temperatures, even though their apparent shapes appeared to be similar. A linear relationship was formulated between the activation energy of Avicel, determined by the model-fitting method, versus

heating rate; while exponential trends were observed for the apparent activation energy of Avicel, determined by the FWO and KAS methods, versus heating rate. Based on data trends observed from using the FWO and KAS methods, it has been postulated that the most likely commencement of char reactions for Avicel begins at $\alpha \geq 70\%$. The activation energy values determined for Avicel are in agreement with literature, and it is the author's conviction that the true value for the activation energy of Avicel PH-101 is no less than 200 kJ mol^{-1} based on the given data.

The DTG profile of switchgrass pyrolysis indicated that all peak reaction rates and peak temperatures shifted over heating rate except for the switchgrass hemicellulose peak reaction rate, which remained fairly constant over all heating rates. The shift in the peak temperature over heating rate for both the switchgrass cellulose and hemicellulose was rather systematic and could be explained by logarithmic relationships that yielded R^2 values greater than 0.98. The fix error attributed to the thermal lag was ultimately explained by a single logarithmic equation. Modified exponentials were fit to the apparent activation energies of switchgrass, determined from the FWO and KAS methods, versus heating rate over a fractional conversion rate of 10 – 80%. It was determined that for $0.40 \leq \alpha \leq 0.45$, the reaction rate of the switchgrass cellulose becomes greater than that of the switchgrass hemicellulose. Since the switchgrass hemicellulose reaction is exothermic, this critical fractional conversion state requires a sudden increase in apparent activation energy in order for the reaction to proceed. This phenomenon was also observed from plots of fractional conversion versus apparent activation energy. A two-peak model-fitting method was used to optimize the kinetic

parameters and given the experimental data it was proposed that the gamma terms do not vary over heating rate. Under this assumption, optimization of kinetic parameters yielded activation energies of switchgrass cellulose and hemicellulose to be 158.2 ± 9.2 kJ mol^{-1} and 115.5 ± 4.3 kJ mol^{-1}, respectively. Assuming constant gamma factors, the two-peak model-fitting method yielded activation energies of washed and extractives-free switchgrass cellulose and hemicellulose to be approximately 40 kJ mol^{-1} larger than that of untreated switchgrass cellulose and hemicellulose. It was concluded that alkali and alkaline earth metals present in switchgrass catalyze pyrolytic reactions and decrease activation energy of both cellulose and hemicellulose. The two-peak model-fitting method is valuable for determining the kinetic parameters of switchgrass and explaining the variability between activation energy due to the presence of alkali and alkaline earth metals.

CHAPTER 4

CONCLUSIONS AND FUTURE WORK

4.1 General Conclusions

Statistical analysis has shown that variation exists among pyrolytic products of the same cultivar of cave-in-rock switchgrass, harvested at the four different locations in Michigan. All cellulose contents of the switchgrass samples were similar, except for the Cass County switchgrass, which was comparatively greater. Since the Cass County switchgrass sample also contained the lowest AAEM content, it also led to the initial hypothesis that the Cass County switchgrass sample would produce the largest comparable quantity of anhydrosugars. However, the Grand Valley switchgrass sample produced the largest amount of levoglucosan and the smallest amount of acids during fast pyrolysis, even though it contains a higher AAEM content than the Cass County switchgrass sample. It is evident that AAEM content cannot be the only factor that can influence whether there is depolymerization or ring scission on the cellulose polymer during pyrolysis. It was also observed that washed and extractives-free switchgrass samples can contain as little as half of the original AAEM content of the untreated biomass. There was an observable drop in the production of acids and an increase in the formation of aldehydes post treatment; however, there was no evidence supporting an increase in anhydrosugar production, which would be expected for an equivalent biomass with a lower AAEM content. It is theorized that this phenomenon may have occurred due to a competing reaction during pyrolysis or the abrasive nature of the treatment methods which may have altered cellulose structures, such as crystallinity. Yet, there is also support in the DTG profiles indicating early onset temperatures for cellulose pyrolysis in samples with higher AAEM contents, signifying catalysis. However, although washed and extractives-free switchgrass

contained lower amounts of alkali and alkaline earth metals, the treated samples did not produce higher amounts of six carbon sugars upon pyrolysis.

Using a single peak model-fitting kinetics method, it was determined that the mean value of the activation energy of Avicel PH-101 for heating rates varying from 5 – 50 °C is 248.5 ± 19.1 kJ mol^{-1}. The use of model-free kinetics methods, such as the FWO and KAS methods, yielded much lower mean values for the activation energy of microcrystalline cellulose, which were 213.8 ± 6.6 kJ mol^{-1} and 203.6 ± 6.7 kJ mol^{-1}, respectively. Also, statistics revealed that valid apparent activation energies for Avicel PH-101 only occur within a fractional conversion range of 10 – 80% for the FWO and KAS methods. Furthermore, by means of the model-free plots it was discerned that char formation from Avicel PH-101 begins for fractional conversion states greater than 70%.

Mean values for the apparent activation energy of switchgrass were determined, using the model-free FWO and KAS methods, to be 227.7 ± 14.6 kJ mol^{-1} and 217.8 ± 14.3 kJ mol^{-1}, respectively. It was concluded that the fractional conversion range for acceptable apparent activation energy for switchgrass pyrolysis, using the FWO and KAS methods, is 10 – 80%. Moreover, a critical state was observed for $0.40 \leq \alpha \leq 0.45$ in which the switchgrass cellulose reaction rate becomes larger than that of the switchgrass hemicellulose. Given that hemicellulose pyrolysis is exothermic, this critical state requires a sudden increase in apparent activation energy in order for switchgrass pyrolysis to persist, which was observed from plots of fractional conversion versus apparent activation energy. Additionally, a two peak model-fitting method was utilized in order to help describe switchgrass pyrolysis as a function of

temperature. It was determined that the gamma terms in the proposed model are not a function of time or temperature and the mean values for the activation energy of switchgrass cellulose and hemicellulose, assuming constant gamma, were determined to be 158.2 ± 9.2 kJ mol^{-1} and 115.5 ± 4.3 kJ mol^{-1}, respectively. Furthermore, the overall mineral content of the switchgrass was seen to have contributed to approximately a 40 kJ mol^{-1} reduction in the activation energy of both the cellulose and hemicellulose, indicating that the alkali and alkaline earth metals within the switchgrass catalyze pyrolytic reactions. The two-peak model-fitting method can, therefore, be beneficial for estimating kinetic parameters and help determining the variability between activation energy.

4.2 Suggestions for Future Work

It has been shown that AAEM content cannot be the only variable affecting depolymerization or ring scission of the cellulose chain during fast pyrolysis, however, this work could not verify any other specific source. Since the treatment techniques used for the removal of alkali and alkaline earth metals may have fragmented cellulose microfibrils into amorphous cellulose, it is proposed that the degree of cellulose crystallinity be examined in forthcoming studies that are similar. Scanning electron microscopy may be used to investigate switchgrass topology and to visually compare any major affects treatments have on the structure of cell walls. Also, seeing that treated switchgrass samples produced smaller quantities of anhydrosugars, even though they theoretically ought to favor the production of six carbon saccharides, than untreated samples; it is recommended that nuclear magnetic resonance be utilized in future experiments to assist in the determination of bonding structures.

Sustained research is necessary in order to advance the methods used to characterize pyrolysis kinetics of switchgrass. Literature has shown that cellulose has a range of activation energies, even though it is a homopolymer, most likely due to the degree of polymerization. Therefore, it is important to design laboratory techniques that allow for the thermogravimetric analysis of the individual native constituents of switchgrass, such as cellulose, hemicellulose, and lignin. Such methods would eliminate multitudes of error attributed to using commercially purchased samples and would ultimately result in more accurate estimations of kinetic parameters.

APPENDIX

Figure 7. Locations of switchgrass plots around Michigan. Numbers 1, 2, 3, 4 represent Frankenmuth (43.3317 °N, 83.7381 °W), Roger City (45.4214 °N, 83.8183 °W), Cass County (41.9215 °N, 86.0221 °W), and Grand Valley (42.9722 °N, 85.9536 °W), respectively.

Soil Property		Frankenmuth	Roger City	Cass County	Grand Valley
Soil pH		6.1	6.5	7.1	6.8
Phosphorus (ppm)		38.0	25.0	222.0	119.5
Potassium (ppm)		178.0	36.0	176.0	255.5
Magnesium (ppm)		140.0	259.0	107.0	407.5
Calcium (ppm)		1003.0	1165.0	1463.0	2033.5
Total CEC (meq/100g)		9.0	8.1	8.7	14.8
% Base Saturation	K	6.9	2.0	5.2	4.6
	Mg	17.6	26.5	10.3	23.9
	Ca	75.5	71.5	84.5	71.6

Table 1. Soil properties of switchgrass plots located in Michigan. CEC is the largest quantity of cations the soil is able to hold and available for exchange with the soil solution. Percent base saturation indicates the percentage of exchange cites that are occupied by the given cation.

Biomass Composition	Frankenmuth	Roger City	Cass County	Grand Valley
ADF	41.0	40.6	51.3	40.4
NDF	73.2	72.3	81.6	72.5
ADL	4.8	5.7	8.9	5.5
% Cellulose	36.2	34.9	42.4	34.9
% Hemicellulose	32.2	31.7	30.3	32.1
% Ash	4.85	4.74	3.53	5.47
% Calcium	0.49	0.44	0.24	0.38
% Phosphorus	0.07	0.12	0.05	0.13
% Magnesium	0.23	0.14	0.11	0.15
% Potassium	0.51	0.64	0.32	0.45
% Sodium	0.013	0.012	0.013	0.014
PPM Iron	115	121	66	131
% Chloride Ion	0.12	0.07	0.05	0.08
Total % AAEM	1.44	1.43	0.79	1.22

Table 2. Biomass composition for switchgrass grown at Frankenmuth, Roger City, Cass County, and Grand Valley. Total AAEM is defined as the total alkali and alkaline earth metals content.

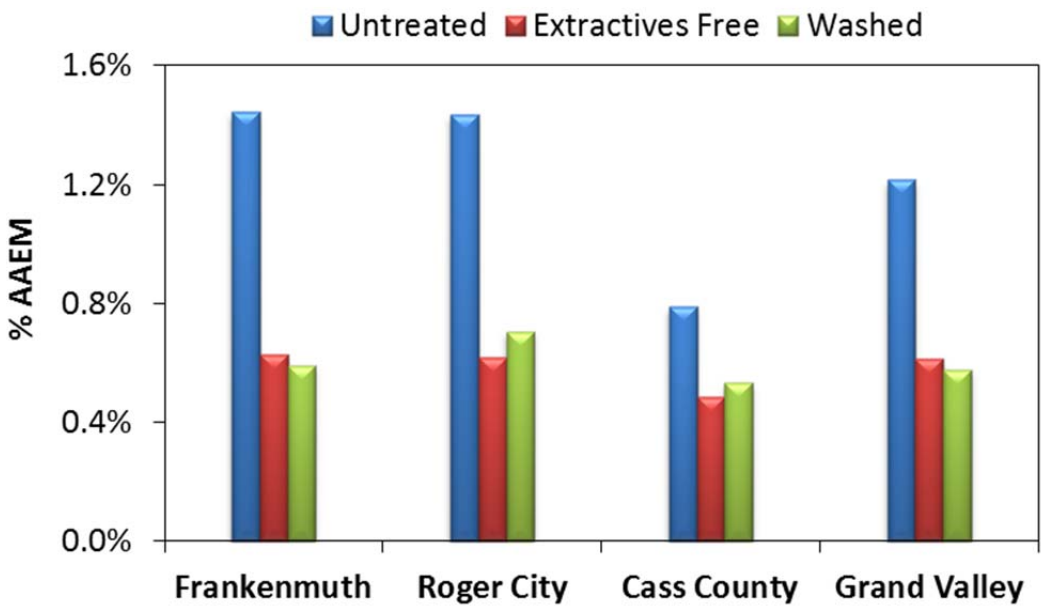

Figure 8. Total weight percent of alkali and alkaline earth metals (AAEM) for untreated, washed, and extractives-free switchgrass grown at different locations.

Group	Compound	Group	Compound
Acid	Formic Acid	Ketone	Cyclohexanone
Acid	Acetic Acid	Ketone	4-hydroxy-5,6-dihydro-(2H)-pyran-2-one
Acid	Pyruvic Acid	Ketone	2-Butanone
Aldehyde	Glycoaldehyde	Ketone	5-hydroxymethyl-2-tetrahydrofuraldehyde-3-one
Aldehyde	Betanedial	Ketone	2H-Pyran-3(4H)-one, dihydro-4-(hydroxymethyl)tetrahydropyran-3-one
Aldehyde	2-Furaldehyde, 5-methyl	Ketone	
Aldehyde	Butanal	Ketone	2-Pentanone
Ester	Acetic Anhydride	Phenolic	Toluene
Ester	Ethyl cyanoformate	Phenolic	p-Benzenediol
Ester	Methyl pyruvate	Phenolic	Phenol
Ester	Acetol acetate	Phenolic	Guaiacol
Ester	4-hydroxymethyl-1,4-butyrolactone	Phenolic	p-Cresol
Ester	Methyl Acetate	Phenolic	Creosol
Furan	(5H)-furan-2-one	Phenolic	4-Vinylphenol
Furan	Furfural	Phenolic	4-Vinylguaiacol
Furan	Furfuryl alcohol	Phenolic	Syringol
Furan	2(5H)-Furanone	Phenolic	trans-Isoeugenol
Furan	Cyclotene	Phenolic	Vanillin
Furan	HMF	Phenolic	2,6-dimethoxy-4-vinylphenol
Ketone	Diacetyl	Phenolic	Methoxyeugenol
Ketone	Acetol	Saccharide	3,4-Anhydro-D-galactosan
Ketone	Butanone	Saccharide	Levoglucosan

Table 3. Classification of principal compounds produced during switchgrass pyrolysis.

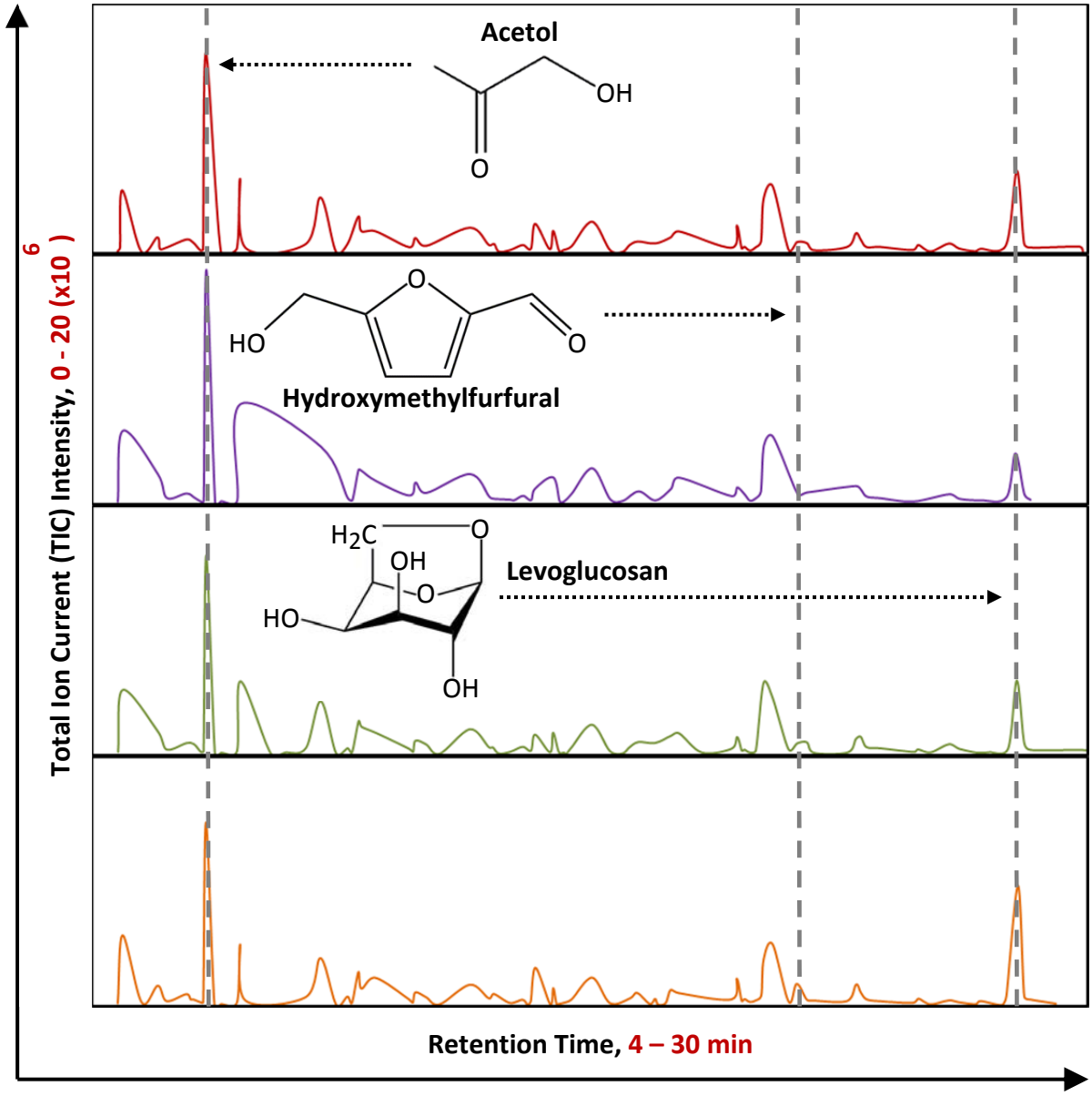

Figure 9. Stack plot of ion chromatograms for untreated switchgrass over differing locations. Solid colored lines represent data from Frankenmuth (maroon), Roger City (purple), Cass County (green), and Grand Valley (orange). Highlighted peaks indicate a noticeable variance in specified compound over location. All graph axes were scaled equivalently and their corresponding limits can be seen above.

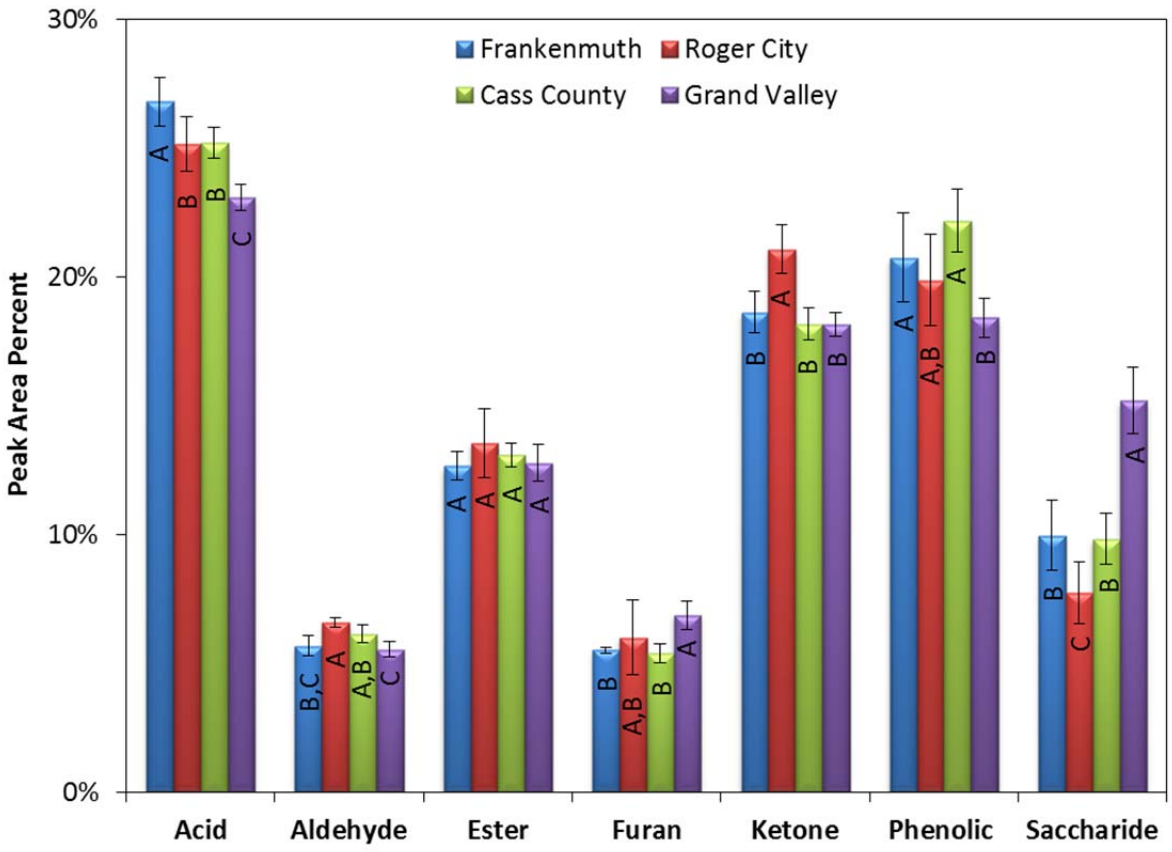

Figure 10. Mean differences between groups of pyrolytic compounds for untreated switchgrass between locations. Locations with the same letter for a given group represent similar means for the corresponding group of compounds. Comparisons were made using a 95% confidence interval ($\alpha = 0.05$) and error bars are reported as ± 1 standard deviation.

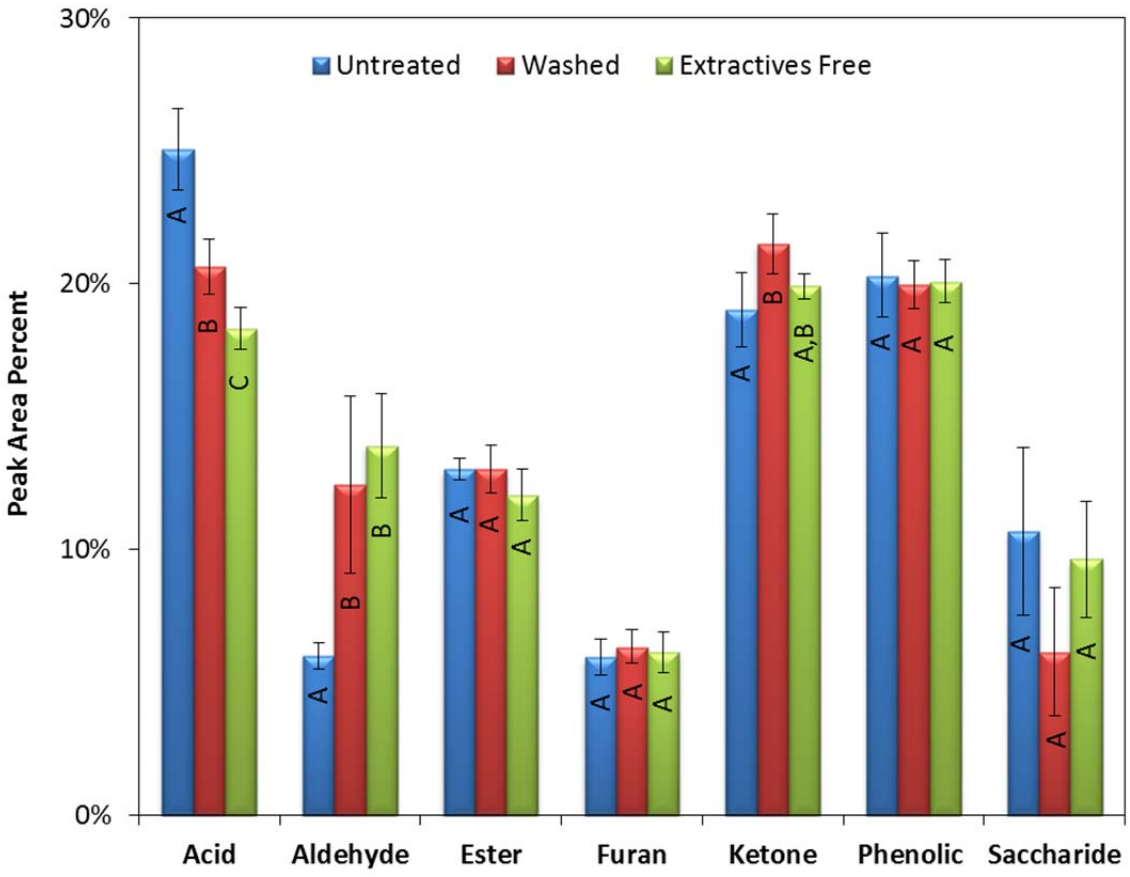

Figure 11. Mean differences between groups of pyrolytic compounds for untreated, washed, and extractives-free switchgrass. Groups of compounds were averaged over all locations. Treatments with the same letter for a given group represent similar means for the corresponding group of compounds. Comparisons were made using a 95% confidence interval ($\alpha = 0.05$) and error bars are reported as ± 1 standard deviation.

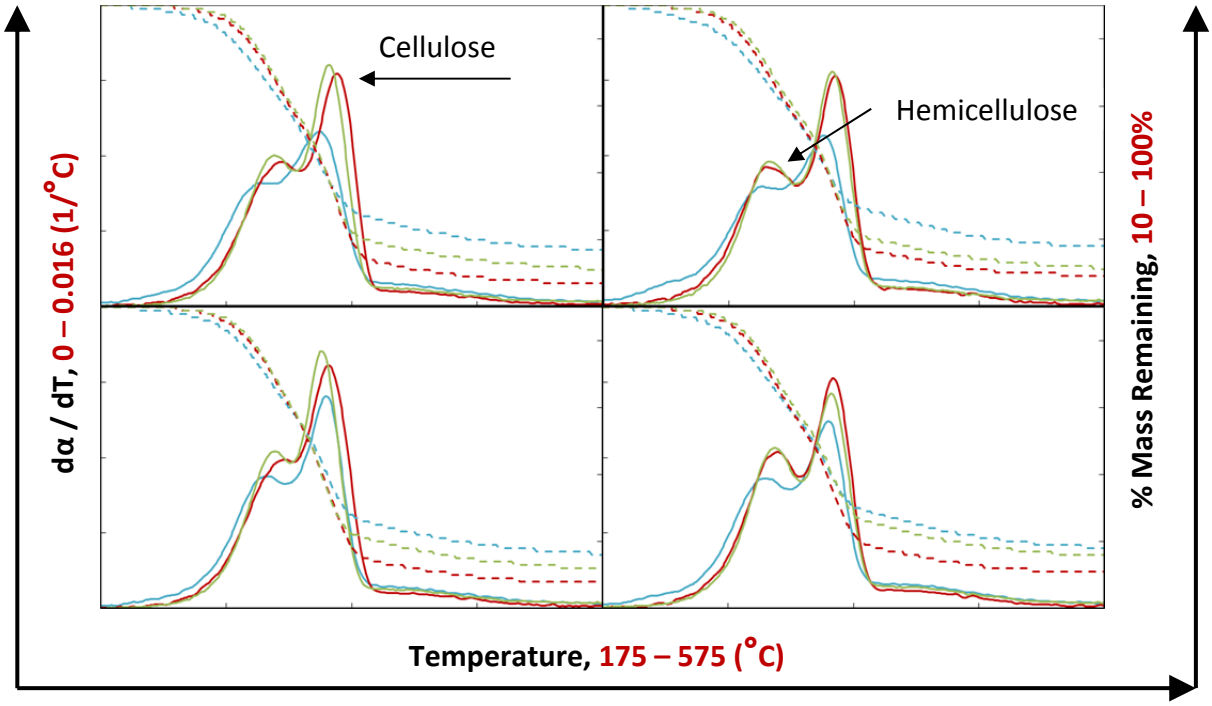

Figure 12. Thermogravimetric (TG) curve and first derivative of extent of reaction (DTG) curve. DTG curves are shown on the left y-axis and TG curves are shown on the right y-axis. Graphs represent curves for Frankenmuth (top left), Roger City (top right), Cass County (bottom left), and Grand Valley (bottom right). Colors represent untreated (blue), washed (red), and extractives free (green) switchgrass samples. All graph axes were scaled equivalently and their limits are given above.

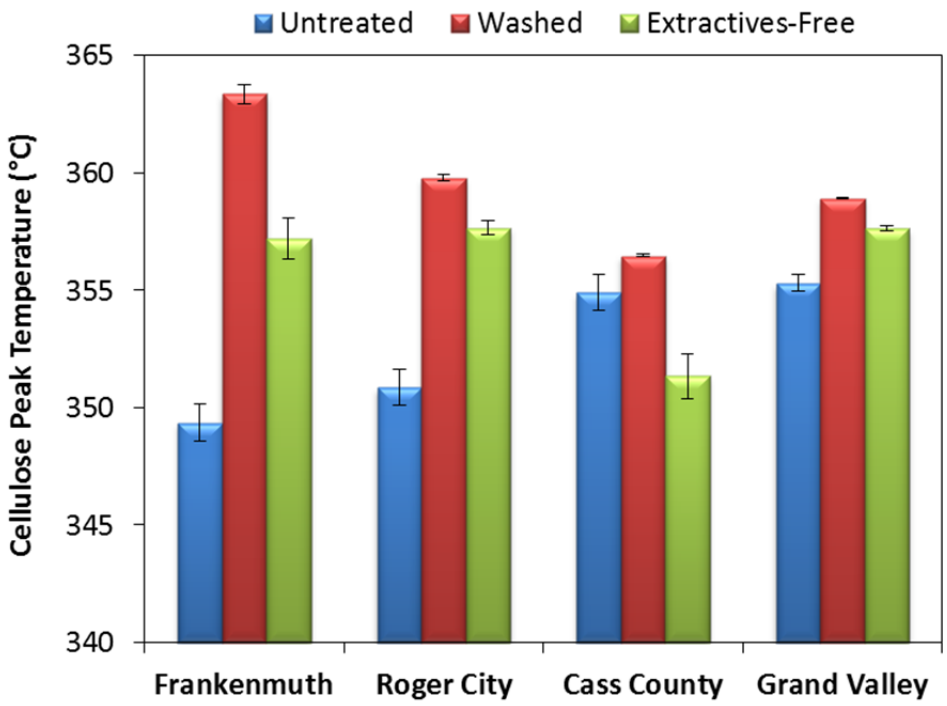

Figure 13. Cellulose peak temperature over Frankenmuth, Roger City, Cass County, and Grand Valley switchgrass for untreated (blue), washed (red), and extractives-free (green) samples.

Order of Reaction	*f(x)*	*g(x)*
1	$(1-\alpha)$	$-ln(1-\alpha)$
2	$(1-\alpha)^2$	$\frac{1}{(1-\alpha)}-1$
3	$(1-\alpha)^3$	$\frac{1}{2(1-\alpha)^2}-\frac{1}{2}$

Table 4. The *g(x)* functions related to the conversion functions and order of reactions.

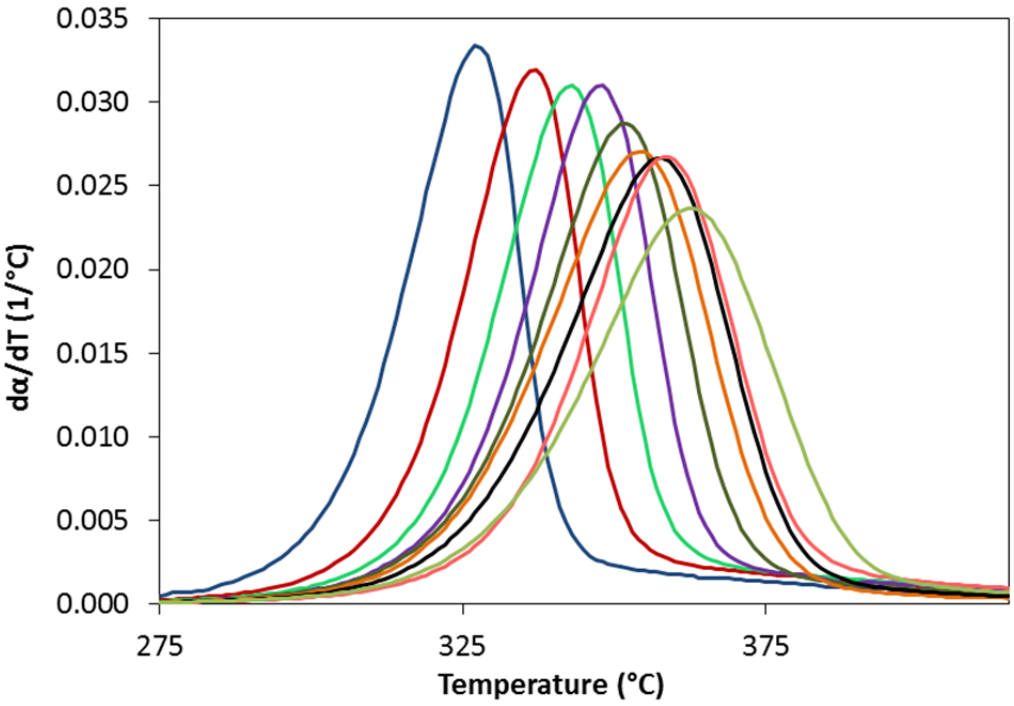

Figure 14. DTG profiles of pyrolyzed Avicel (PH-101) at various heating rates. The line colors represent the heating rates as follows: dark blue (5 °C min^{-1}), maroon (10 °C min^{-1}), teal (15 °C min^{-1}), purple (20 °C min^{-1}), dark green (25 °C min^{-1}), orange (30 °C min^{-1}), black (35 °C min^{-1}), pink (40 °C min^{-1}), light green (50 °C min^{-1}).

β (°C min^{-1})	$d\alpha/dT_{max}$ (1 °C^{-1})	T_{max} (°C)
5	0.03337	327.3
10	0.03195	336.7
15	0.03097	342.8
20	0.03099	347.9
25	0.02873	351.6
30	0.02706	354.4
35	0.02669	357.7
40	0.02678	358.6
50	0.02368	362.2

Table 5. Peak reaction rates and peak temperatures for Avicel pyrolysis at different heating rate

	1st Order		2nd Order		3rd Order	
β (°C min^{-1})	E_a (kJ mol^{-1})	A (min^{-1})	E_a (kJ mol^{-1})	A (min^{-1})	E_a (kJ mol^{-1})	A (min^{-1})
5	240.5	8.2E+21	353.9	3.8E+32	459.7	3.0E+42
10	237.9	3.9E+21	350.0	9.3E+31	454.7	4.1E+41
15	235.6	2.1E+21	346.6	3.3E+31	450.3	9.5E+40
20	240.0	4.8E+21	353.1	9.3E+31	458.7	3.5E+41
25	224.8	9.3E+20	330.8	1.0E+31	429.7	2.2E+40
30	214.1	1.9E+19	315.0	2.4E+28	409.2	7.0E+36
35	213.4	1.4E+19	314.1	1.4E+28	408.0	3.3E+36
40	215.9	2.6E+19	317.7	3.4E+28	412.7	9.9E+36
50	192.7	2.0E+17	283.5	2.6E+25	368.3	8.5E+32
Mean	223.9	2.2E+21	329.4	6.7E+31	427.9	4.3E+41
Std Dev	16.2	2.9E+21	23.9	1.2E+32	31.1	9.9E+41

Table 6. Kinetic parameters estimated using equations 3.19, 3.20, 3.22, and 3.23 from the model-fitting method.

	1st Order		2nd Order		3rd Order	
β (°C min^{-1})	E_a (kJ mol^{-1})	A (min^{-1})	E_a (kJ mol^{-1})	A (min^{-1})	E_a (kJ mol^{-1})	A (min^{-1})
5	268.0	9.5E+22	388.5	5.5E+33	488.5	4.6E+42
10	264.9	4.1E+22	383.7	1.2E+33	487.5	1.5E+42
15	266.0	4.4E+22	381.7	5.4E+32	488.8	1.1E+42
20	265.4	3.4E+22	388.6	1.5E+33	487.6	5.3E+41
25	248.5	1.1E+21	365.4	1.3E+31	473.1	2.2E+40
30	235.5	8.0E+19	347.5	3.4E+29	450.9	2.4E+38
35	236.4	8.9E+19	346.5	2.3E+29	448.1	1.1E+38
40	239.0	1.5E+20	350.7	4.8E+29	450.8	1.5E+38
50	213.0	8.8E+17	313.8	3.3E+26	408.6	3.5E+34
Mean	248.5	2.4E+22	362.9	9.7E+32	464.9	8.6E+41
Std Dev	19.1	3.3E+22	25.4	1.8E+33	27.6	1.5E+42

Table 7. Kinetic parameters estimated using equation 3.27 from the model-fitting method.

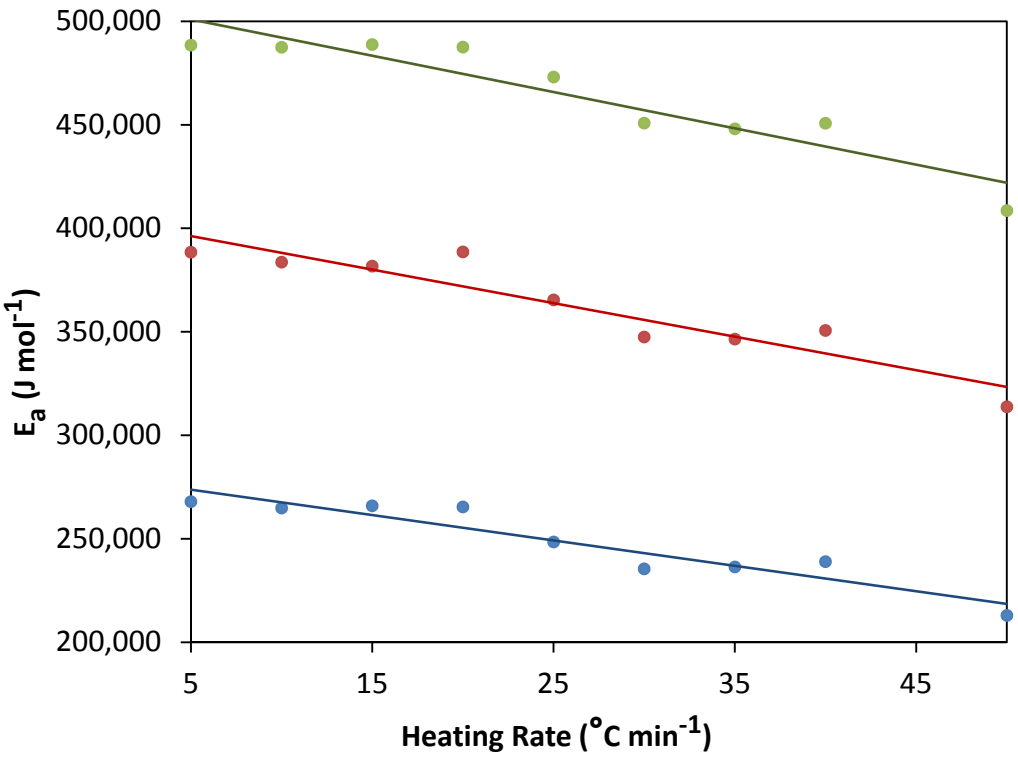

Figure 15. Activation energy, calculated from equation 3.27, versus heating rate for Avicel. The following colors correspond to the assumed reaction orders: blue (1st order), red (2nd order), green (3rd order). Markers indicate calculated activation energies, while solid lines represent fitted values.

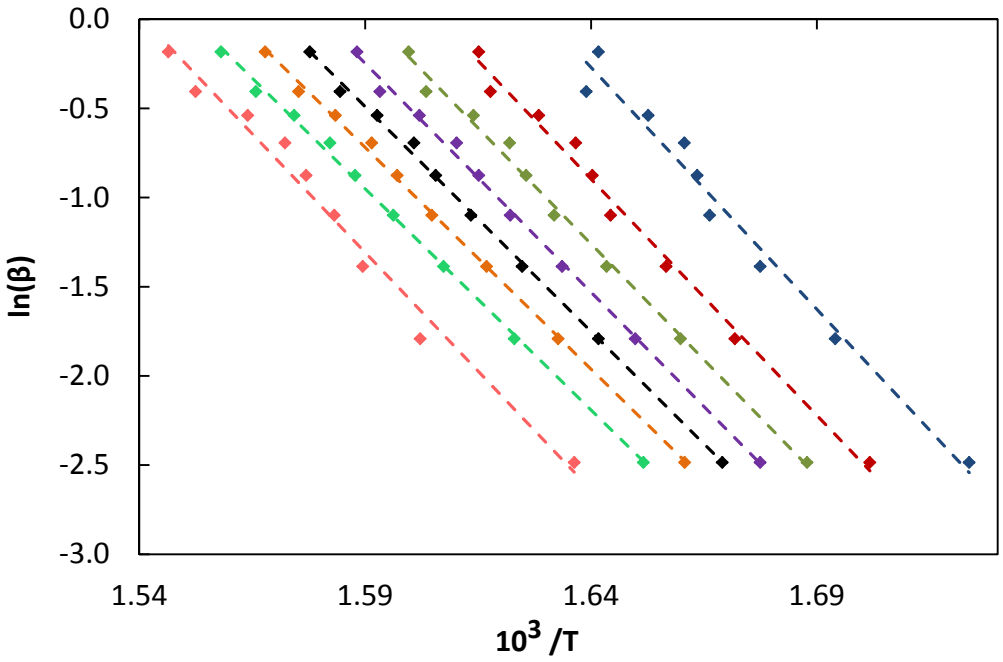

Figure 16. Plot of T^{-1} vs. *ln*(β) over the fractional conversion range of 10 – 80% for Avicel pyrolysis. Colors represent the following fractional conversion states: blue (10%), red (20%), green (30%), purple (40%), black (50%), orange (60%), teal (70%), pink (80%). Dashed lines indicate fitted values and markers indicate experimental values.

α (%)	E_a (J mol^{-1})	E_a (kJ mol^{-1})	m	y_0	R^2
10	225,695	225.7	-27.15	44.25	0.9769
15	223,306	223.3	-26.86	43.41	0.9818
20	220,524	220.5	-26.52	42.60	0.9898
25	217,000	217.0	-26.10	41.72	0.9924
30	216,031	216.0	-25.98	41.35	0.9939
35	212,816	212.8	-25.60	40.58	0.9956
40	213,324	213.3	-25.66	40.55	0.9969
45	211,104	211.1	-25.39	40.00	0.9974
50	209,586	209.6	-25.21	39.59	0.9979
55	207,535	207.5	-24.96	39.08	0.9982
60	206,661	206.7	-24.86	38.80	0.9982
65	206,399	206.4	-24.83	38.64	0.9981
70	206,260	206.3	-24.81	38.49	0.9979
75	208,873	208.9	-25.12	38.86	0.9969
80	221,350	221.4	-26.62	41.02	0.9810
Mean	213,764	213.8	-25.71	40.60	
Std Dev	6,555	6.6	0.79	1.80	

Table 8. Apparent activation energies and fitted values for Avicel pyrolysis calculated using the FWO method. Equation 3.29 was used to fit temperature versus heating rate for α = .10 - .90 (.05 intervals). The *m* value represents the slope of the line in equation 3.29, and E_a was calculated accordingly. The y_0 value is a combination of all the other terms on the right hand side of equation 3.29. After error estimation, R^2 determination, and observing the overall trend of apparent activation energy as a function of inverse temperature, it was determined that the activation energies obtained from the FWO method are only valid over the fractional conversion range of 10 – 80%.

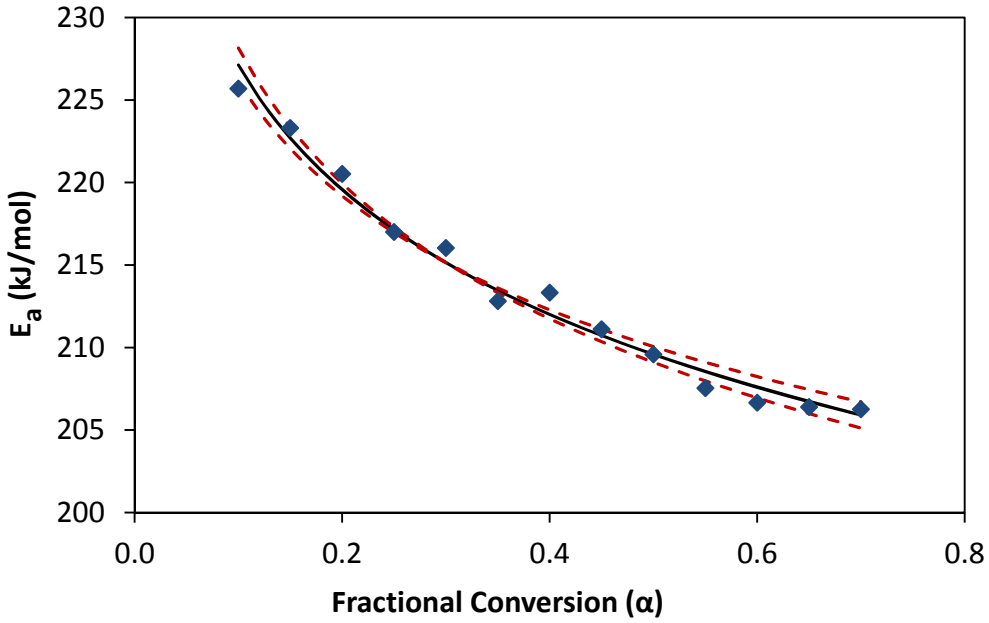

Figure 17. Plot of apparent activation energy (calculated from the FWO method) versus fractional conversion fit to a logarithmic curve with a 95% confidence interval. The solid black line represents the fitted values, while the dashed red lines represent the confidence bounds. Fitted values are only valid for the fractional conversion range of 10 – 70%.

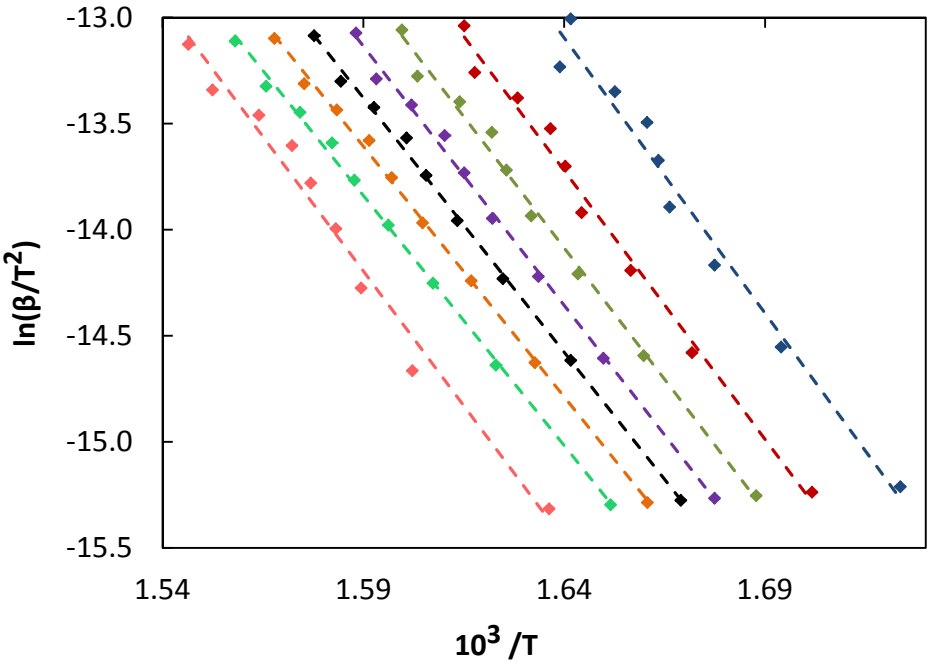

Figure 18. Plot of T^{-1} vs $ln(\beta/T^2)$ over the fractional conversion range of 10 – 80% for Avicel pyrolysis. Colors represent the following fractional conversion states: blue (10%), red (20%), green (30%), purple (40%), black (50%), orange (60%), teal (70%), pink (80%). Dashed lines indicate fitted values and markers indicate experimental values.

α (%)	E_a (J mol^{-1})	E_a (J mol^{-1})	m	y_0	R^2
10	215,797	215.8	-25.96	29.47	0.9749
15	213,326	213.3	-25.66	28.62	0.9801
20	210,487	210.5	-25.32	27.80	0.9888
25	206,917	206.9	-24.89	26.90	0.9917
30	205,905	205.9	-24.77	26.53	0.9933
35	202,656	202.7	-24.38	25.75	0.9952
40	203,131	203.1	-24.43	25.71	0.9966
45	200,881	200.9	-24.16	25.15	0.9971
50	199,335	199.3	-23.98	24.74	0.9977
55	197,255	197.3	-23.73	24.22	0.9979
60	196,353	196.4	-23.62	23.94	0.9980
65	196,061	196.1	-23.58	23.78	0.9979
70	195,891	195.9	-23.56	23.62	0.9976
75	198,467	198.5	-23.87	23.98	0.9965
80	210,892	210.9	-25.37	26.14	0.9792
Mean	203,557	203.6	-24.48	25.76	
Std Dev	6,667	6.7	0.80	1.83	

Table 9. Apparent activation energies and fitted values determined using the KAS method for Avicel pyrolysis. Equation 3.28 was used to fit temperature versus heating rate for α = .10 - .90 (.05 intervals). The *m* value represents the slope of the line in equation 3.28, and E_a was calculated accordingly. The y_0 value represents the other term on the right hand side of equation 3.28 After error estimation, R^2 determination, and observing the overall trend of apparent activation energy as a function of inverse temperature, it was determined that the activation energies obtained from the KAS method are only valid over the fractional conversion range of 10 – 80%.

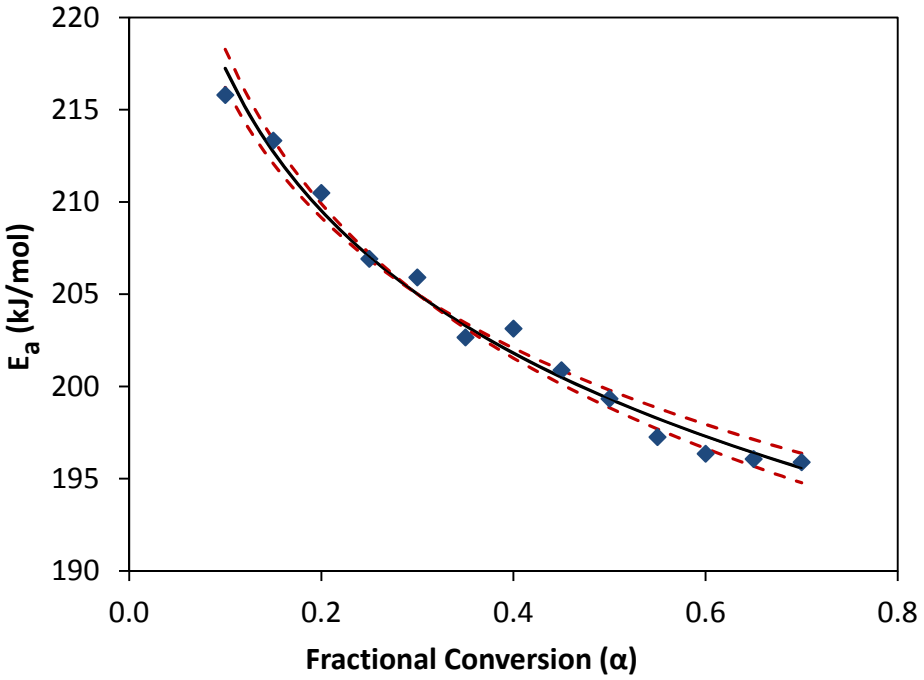

Figure 19. Plot of apparent activation energy (calculated from the KAS method) versus fractional conversion fit to a logarithmic curve with a 95% confidence interval. The solid black line represents the fitted values, while the dashed red lines represent the confidence bounds. Fitted values are only valid for the fractional conversion range of 10 – 70%.

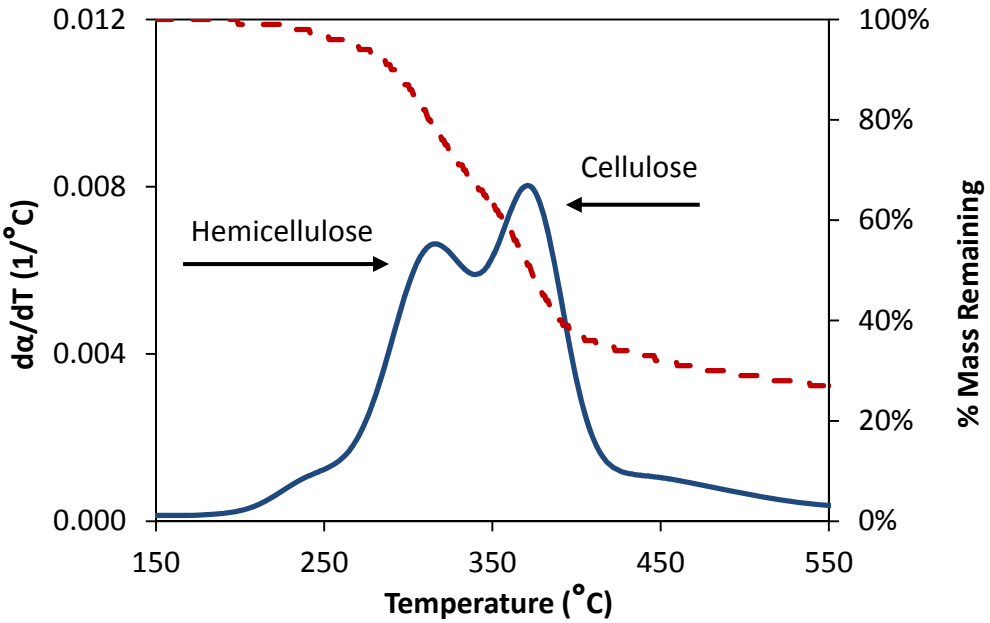

Figure 20. DTG/TG curve of pyrolyzed switchgrass at 50 °C min^{-1}. Solid blue line represents the DTG curve with the primary axis on the left. Dashed red line represents the TG curve, or weight loss curve, with the primary axis on the right.

	Cellulose		Hemicellulose	
β (°C min^{-1})	$(d\alpha/dT)_m$	T_m (°C)	$(d\alpha/dT)_m$	T_m (°C)
5	0.01130	340.7	0.00680	284.1
10	0.01042	346.6	0.00671	293.2
15	0.01004	354.8	0.00681	296.9
20	0.00988	360.7	0.00695	300.6
25	0.00980	363.6	0.00694	307.2
30	0.00985	365.3	0.00670	309.5
35	0.00937	366.5	0.00670	310.3
40	0.00878	368.5	0.00665	311.3
50	0.00803	371.1	0.00663	315.7

Table 10. Max reaction rates and max temperatures for hemicellulose and cellulose peaks during switchgrass pyrolysis.

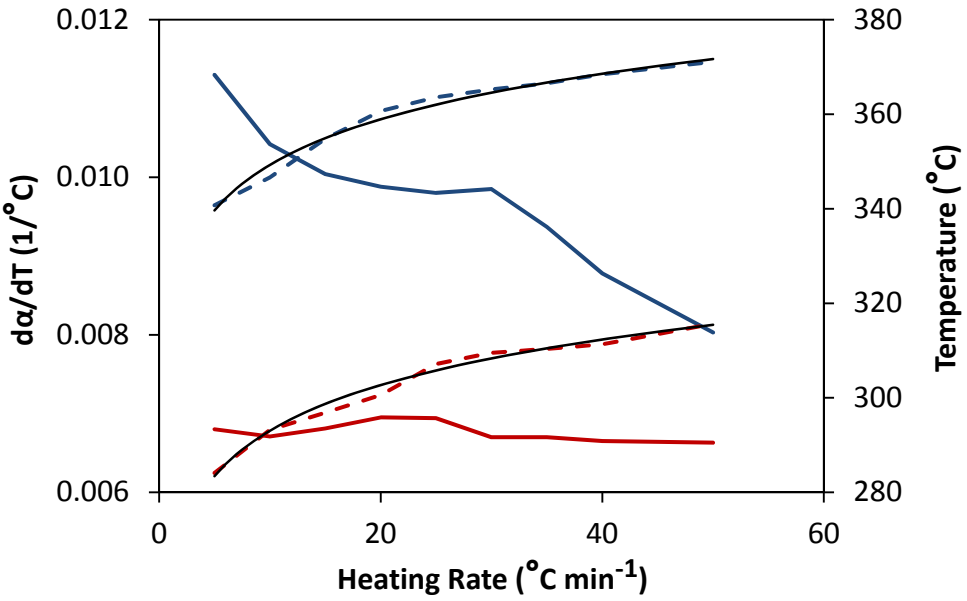

Figure 21. Max reaction rate and max temperature versus heating rate for switchgrass pyrolysis. Blue lines represent values of cellulose peaks and red lines represent values of hemicellulose peaks. Solid lines correspond to reaction rate (the left vertical axis) and dashed lines correspond to temperature (the right vertical axis). Solid black lines indicate fitted values.

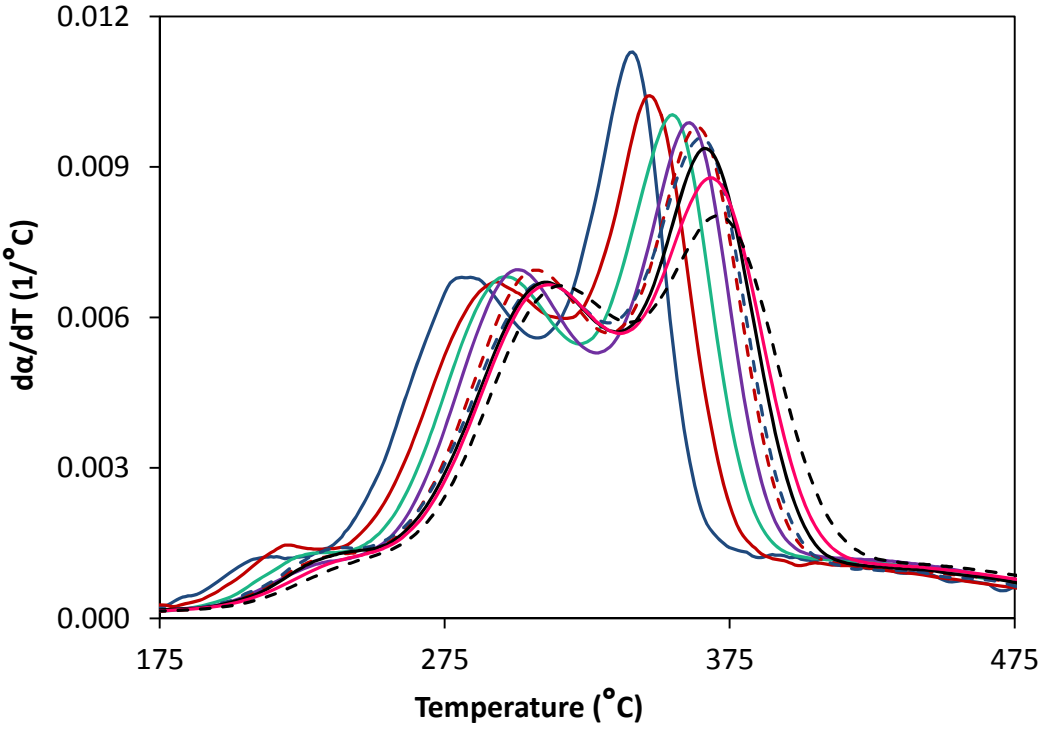

Figure 22. DTG curve of pyrolyzed switchgrass at various heating rates. The line colors represent the heating rates as follows: dark blue (5 °C min^{-1}), maroon (10 °C min^{-1}), teal (15 °C min^{-1}), purple (20 °C min^{-1}), dashed red (25 °C min^{-1}), dashed blue (30 °C min^{-1}), black (35 °C min^{-1}), pink (40 °C min^{-1}), dashed black (50 °C min^{-1}).

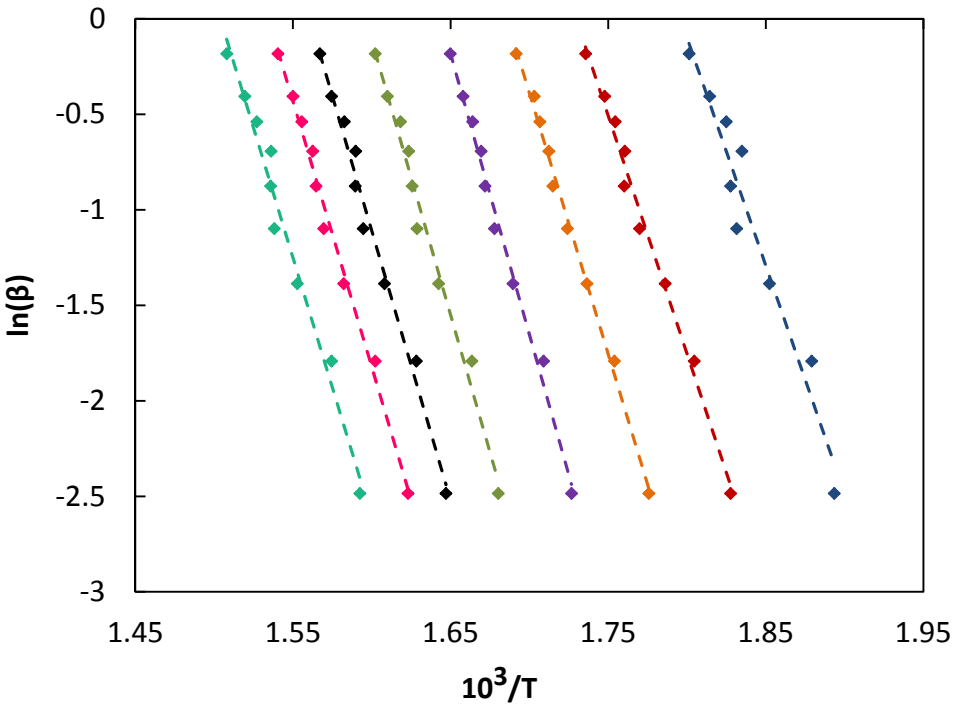

Figure 23. Plot of T^{-1} versus *ln*(β) over the fractional conversion range of 10 – 80% for switchgrass pyrolysis. Colors represent the following fractional conversion states: dark blue (10%), red (20%), orange (30%), purple (40%), green (50%), black (60%), pink (70%), teal (80%). Dashed lines indicate fitted values and markers indicate experimental values.

α (%)	E_a (J mol^{-1})	E_a (kJ mol^{-1})	m	y_0	R^2
10	198,481	198.5	-23.87	42.87	0.9480
15	204,766	204.8	-24.63	43.22	0.9680
20	207,453	207.5	-24.95	43.16	0.9893
25	218,694	218.7	-26.30	44.93	0.9962
30	227,340	227.3	-27.34	46.10	0.9949
35	232,892	232.9	-28.01	46.67	0.9949
40	244,241	244.2	-29.38	48.29	0.9911
45	248,601	248.6	-29.90	48.40	0.9831
50	239,236	239.2	-28.78	45.93	0.9830
55	240,756	240.8	-28.96	45.67	0.9770
60	234,710	234.7	-28.23	44.06	0.9848
65	232,253	232.3	-27.94	43.20	0.9848
70	231,399	231.4	-27.83	42.71	0.9908
75	228,730	228.7	-27.51	41.84	0.9860
80	226,192	226.2	-27.21	40.92	0.9769
85	251,415	251.4	-30.24	44.70	0.8824
Mean	227,716	227.7	-27.39	44.53	
Std Dev	14,635	14.6	1.76	2.26	

Table 11. Apparent activation energies and fitted values for switchgrass pyrolysis calculated using the FWO method. Equation 3.29 was used to fit temperature versus heating rate for α = .10 - .90 (.05 intervals). The m value represents the slope of the line in equation 3.29, and E_a was calculated accordingly. The y_0 value is a combination of all the other terms on the right hand side of equation 3.29. After error estimation, R^2 determination, and observing the overall trend of apparent activation energy as a function of inverse temperature, it was determined that the activation energies obtained from the FWO method are only valid over the fractional conversion range of 10 – 80%. Mean and standard deviation values were determined over a fractional conversion range of 10 – 80%.

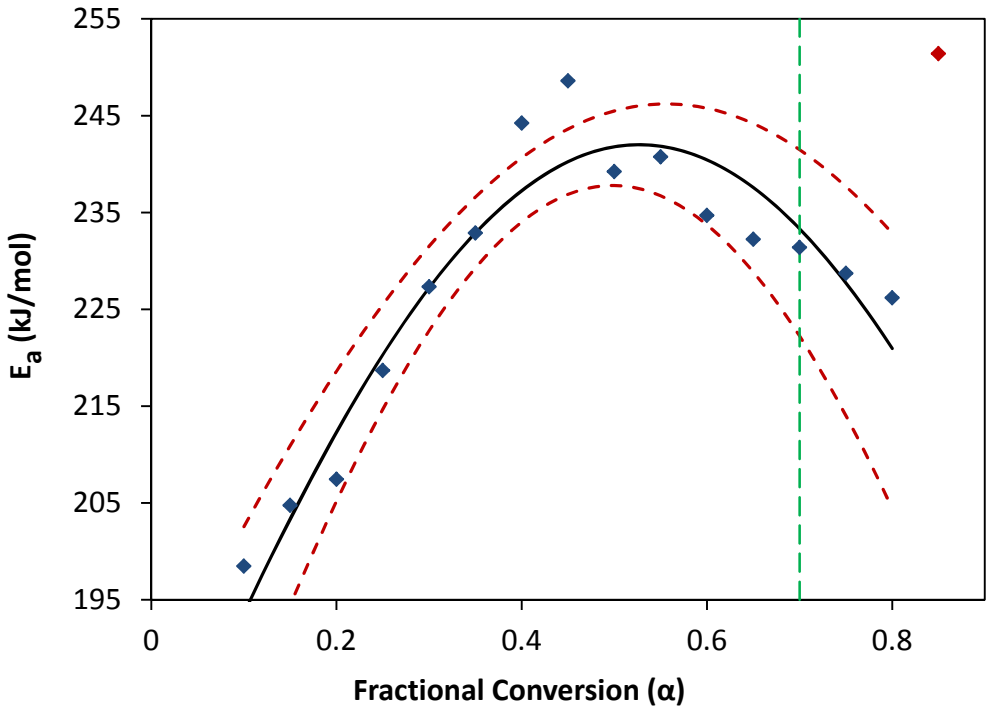

Figure 24. Plot of apparent activation energy (calculated from the FWO method) versus fractional conversion fit to a modified exponential with a 95% confidence interval. The solid black line represents the fitted values, while the dashed red lines represent the confidence bounds. The dashed green line is a boundary for a fractional conversion state of 70%. Blue markers represent experimental data that are fitted and red markers indicated unfitted data that correspond to char formation. Fitted values are only valid for the fractional conversion range of 10 – 80%.

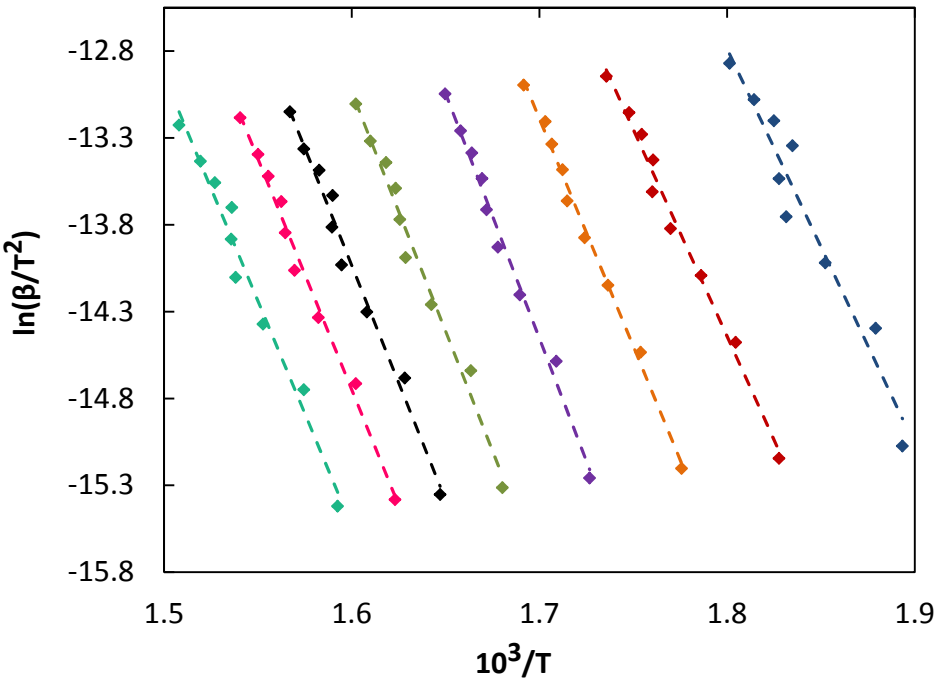

Figure 25. Plot of T^{-1} versus $ln(\beta/T^2)$ over the fractional conversion range of 10 – 80% for switchgrass pyrolysis. Colors represent the following fractional conversion states: dark blue (10%), red (20%), orange (30%), purple (40%), green (50%), black (60%), pink (70%), teal (80%). Dashed lines indicate fitted values and markers indicate experimental values.

α (%)	E_a (J mol^{-1})	E_a (kJ mol^{-1})	m	y_0	R^2
10	189,489	189.5	-22.79	28.29	0.9432
15	195,564	195.6	-23.52	28.58	0.9651
20	198,122	198.1	-23.83	28.50	0.9882
25	209,234	209.2	-25.17	30.24	0.9958
30	217,749	217.7	-26.19	31.38	0.9944
35	223,185	223.2	-26.84	31.94	0.9944
40	234,393	234.4	-28.19	33.52	0.9903
45	238,601	238.6	-28.70	33.60	0.9817
50	229,107	229.1	-27.56	31.11	0.9815
55	230,510	230.5	-27.73	30.82	0.9750
60	224,363	224.4	-26.99	29.19	0.9834
65	221,817	221.8	-26.68	28.32	0.9834
70	220,887	220.9	-26.57	27.81	0.9900
75	218,128	218.1	-26.24	26.93	0.9846
80	215,471	215.5	-25.92	25.98	0.9746
85	240,461	240.5	-28.92	29.72	0.8728
Mean	217,775	217.8	-26.19	29.75	
Std Dev	14,286	14.3	1.72	2.28	

Table 12. Apparent activation energies and fitted values determined using the KAS method for switchgrass pyrolysis. Equation 3.28 was used to fit temperature versus heating rate for α = .10 - .90 (.05 intervals). The m value represents the slope of the line in equation 3.28, and E_a was calculated accordingly. The y_0 value represents the other term on the right hand side of equation 3.28 After error estimation, R^2 determination, and observing the overall trend of apparent activation energy as a function of inverse temperature, it was determined that the activation energies obtained from the KAS method are only valid over the fractional conversion range of 10 – 80%. Mean and standard deviation values were determined over a fractional conversion range of 10 – 80%.

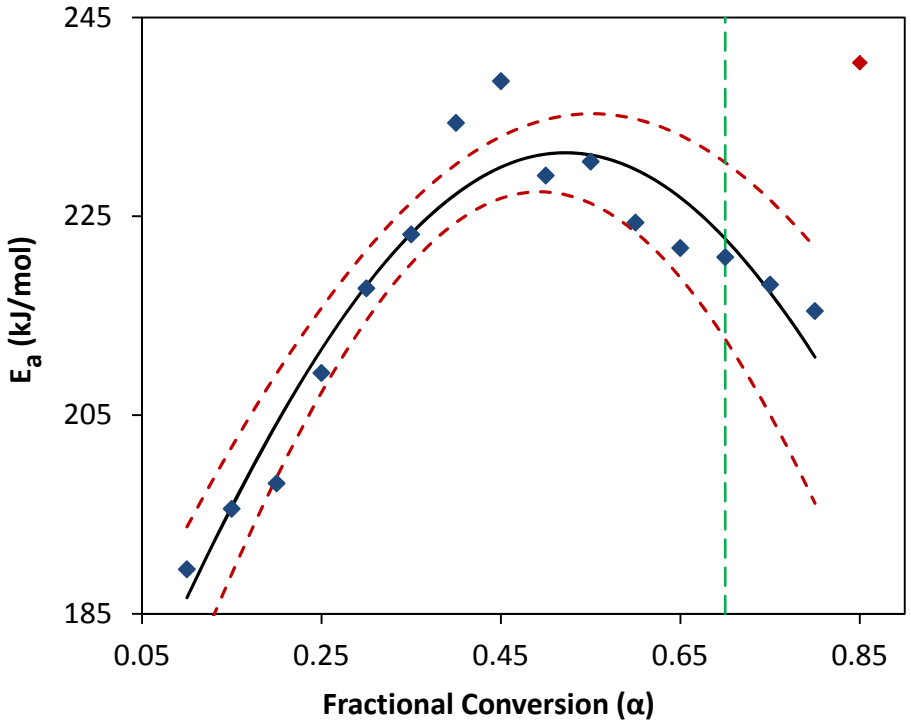

Figure 26. Plot of apparent activation energy (calculated from the KAS method) versus fractional conversion fit to a modified exponential with a 95% confidence interval. The solid black line represents the fitted values, while the dashed red lines represent the confidence bounds. The dashed green line is a boundary for a fractional conversion state of 70%. Blue markers represent experimental data that are fitted and red markers indicated unfitted data that correspond to char formation. Fitted values are only valid for the fractional conversion range of 10 – 80%.

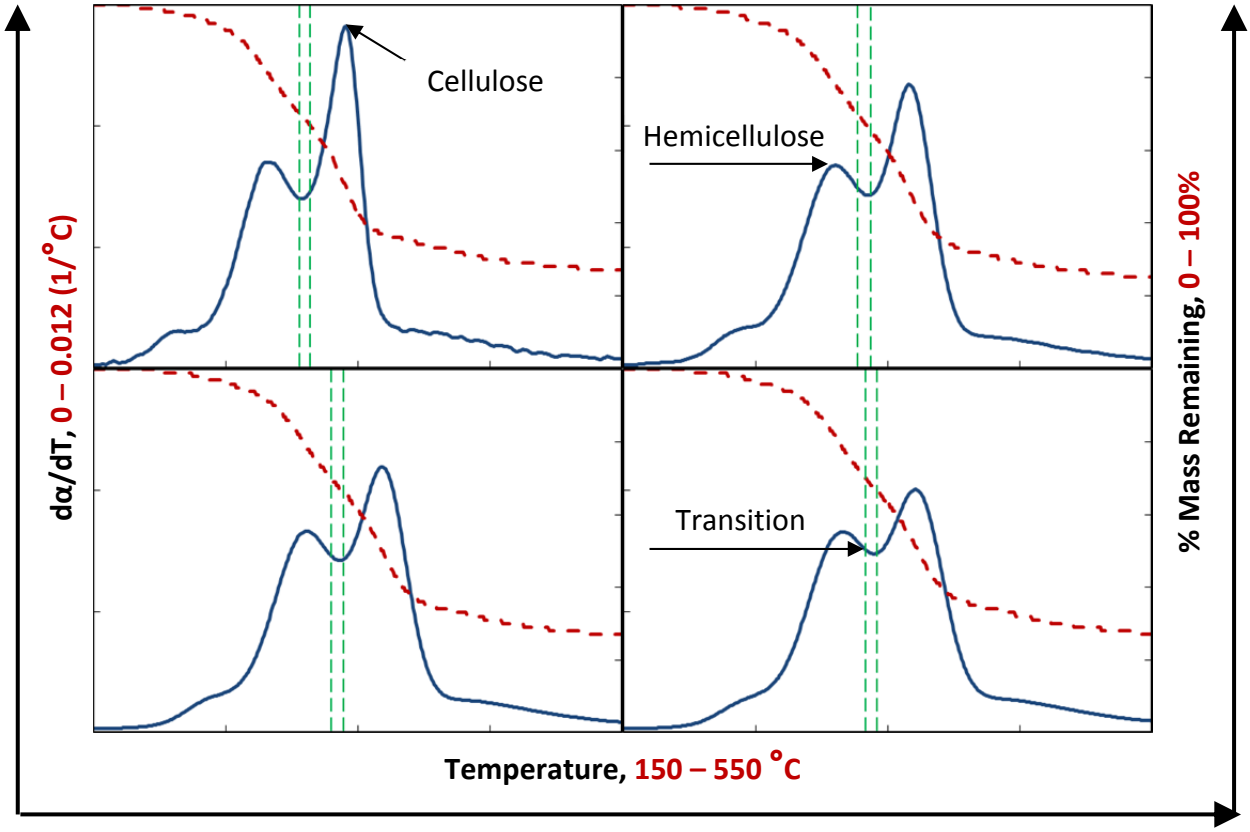

Figure 27. DTG/TG profiles of switchgrass pyrolysis for heating rates of 5 °C min^{-1} (top left), 35 °C min^{-1} (top right), 40 °C min^{-1} (bottom left), and 50 °C min^{-1} (bottom right). Solid blue lines indicate DTG curves and correspond to the left vertical axis, while dashed red lines indicate TG curves and correspond to the right vertical axis. Dashed green lines are boundary lines indicating fractional conversion states of 40 and 45%. All graph axes were scaled equivalently and their limits are given above.

	Cellulose		Hemicellulose	
β ($^{\circ}C\ min^{-1}$)	$(d\alpha/dT)_m$ ($^{\circ}C^{-1}$)	T_m ($^{\circ}C$)	$(d\alpha/dT)_m$ ($^{\circ}C^{-1}$)	T_m ($^{\circ}C$)
5	0.0113	340.74	0.0068	284.09
10	0.0104	346.63	0.0067	293.21
15	0.0100	354.79	0.0068	296.87
20	0.0099	360.68	0.0070	300.60
25	0.0098	363.60	0.0069	307.16
30	0.0099	365.26	0.0067	309.54
35	0.0094	366.54	0.0067	310.33
40	0.0088	368.45	0.0067	311.31
50	0.0080	371.09	0.0066	315.67

Table 13. Peak reaction rates and peak temperatures for cellulose and hemicellulose during switchgrass pyrolysis.

	1st Order		2nd Order		3rd Order	
β (°C min^{-1})	E_a (J mol^{-1})	A (min^{-1})	E_a (J mol^{-1})	A (min^{-1})	E_a (J mol^{-1})	A (min^{-1})
5	96,335	2.5E+07	141,759	2.7E+11	184,151	1.4E+15
10	90,766	1.3E+07	133,564	7.9E+10	173,505	2.5E+14
15	89,526	1.8E+07	131,739	1.3E+11	171,134	4.8E+14
20	89,702	1.4E+07	131,999	7.0E+10	171,471	1.8E+14
25	89,755	1.6E+07	132,077	7.3E+10	171,573	1.7E+14
30	88,314	1.3E+07	129,955	5.0E+10	168,817	9.8E+13
35	86,696	1.1E+07	127,574	3.7E+10	165,724	6.4E+13
40	81,796	4.4E+06	120,365	8.9E+09	156,358	9.9E+12
50	75,301	1.4E+06	110,806	1.6E+09	143,942	1.0E+12
Mean	87,577	1.3E+07	128,871	8.0E+10	167,408	3.0E+14
Std Dev	5,973	6.9E+06	8,789	8.1E+10	11,417	4.5E+14
Min E_a	75,301		110,806		143,942	
Max E_a	96,335		141,759		184,151	
ΔE_a	21,035		30,953		40,209	

Table 14. Kinetic parameters for switchgrass cellulose pyrolysis estimated by using equations 3.19, 3.20, 3.22, and 3.23. The range of apparent activation energy (E_{max} - E_{min}) is represented by ΔE_a.

	1st Order		2nd Order		3rd Order	
β (°C min^{-1})	E_a (J mol^{-1})	A (min^{-1})	E_a (J mol^{-1})	β (°C min^{-1})	E_a (J mol^{-1})	A (min^{-1})
5	47,572	2.8E+03	70,003	5.3E+05	90,937	6.5E+07
10	48,679	6.0E+03	71,631	1.2E+06	93,052	1.6E+08
15	50,010	1.1E+04	73,591	2.3E+06	95,597	3.2E+08
20	51,703	2.0E+04	76,083	4.9E+06	98,834	7.6E+08
25	53,030	2.8E+04	78,034	7.3E+06	101,369	1.2E+09
30	51,396	2.2E+04	75,630	4.9E+06	98,246	6.8E+08
35	51,600	2.6E+04	75,930	5.9E+06	98,637	8.2E+08
40	51,418	2.9E+04	75,662	6.5E+06	98,288	9.1E+08
50	52,049	3.7E+04	76,590	8.3E+06	99,494	1.2E+09
Mean	50,828	2.0E+04	74,795	4.6E+06	97,162	6.8E+08
Std Dev	1,741	1.2E+04	2,563	2.7E+06	3,329	4.1E+08
Min E_a	47,572		70,003		90,937	
Max E_a	53,030		78,034		101,369	
ΔE_a	5,458		8,031		10,433	

Table 15. Kinetic parameters for switchgrass hemicellulose pyrolysis estimated by using equations 3.19, 3.20, 3.22, and 3.23. The range of apparent activation energy (E_{max} - E_{min}) is represented by ΔE_a.

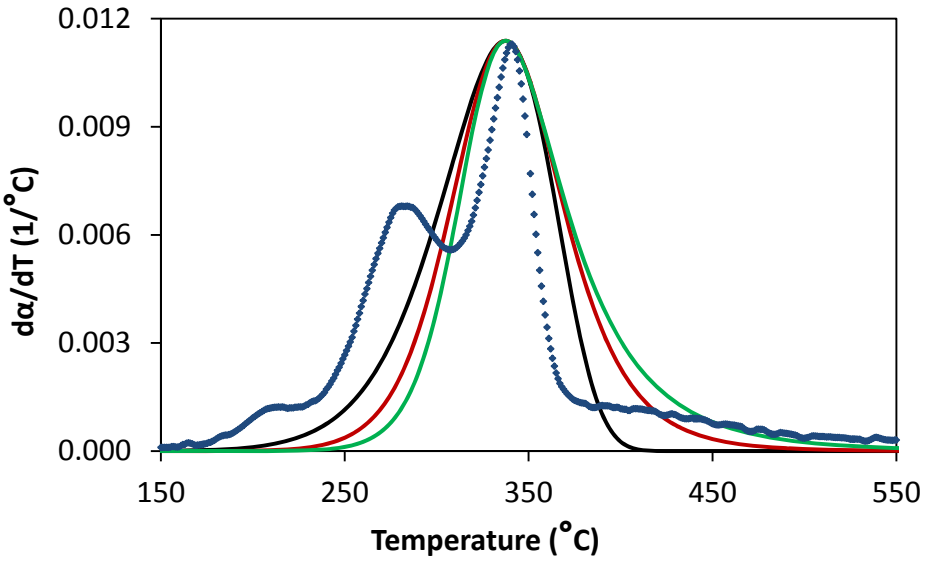

Figure 28. DTG profile of switchgrass pyrolysis at a heating rate of 5 °C min^{-1} fit to equations 3.25 and 3.26 using kinetic parameters estimated for the cellulose peak. Blue markers indicate experimental data. Solid lines indicate fitted values and colors represent the following reaction orders: black (n = 1), red (n = 2), green (n = 3).

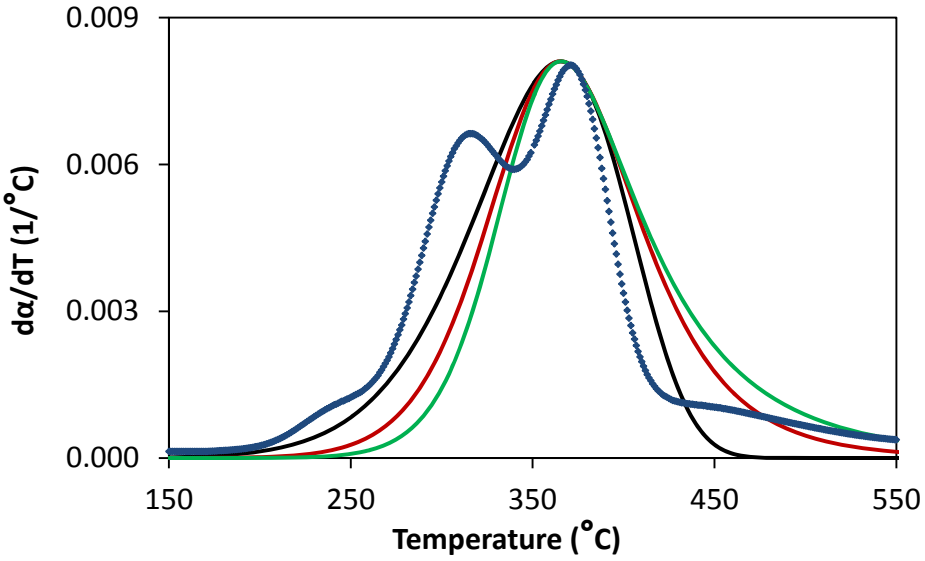

Figure 29. DTG profile of switchgrass pyrolysis at a heating rate of 50 °C min^{-1} fit to equations 3.25 and 3.26 using kinetic parameters estimated for the cellulose peak. Blue markers indicate experimental data. Solid lines indicate fitted values and colors represent the following reaction orders: black (n = 1), red (n = 2), green (n = 3).

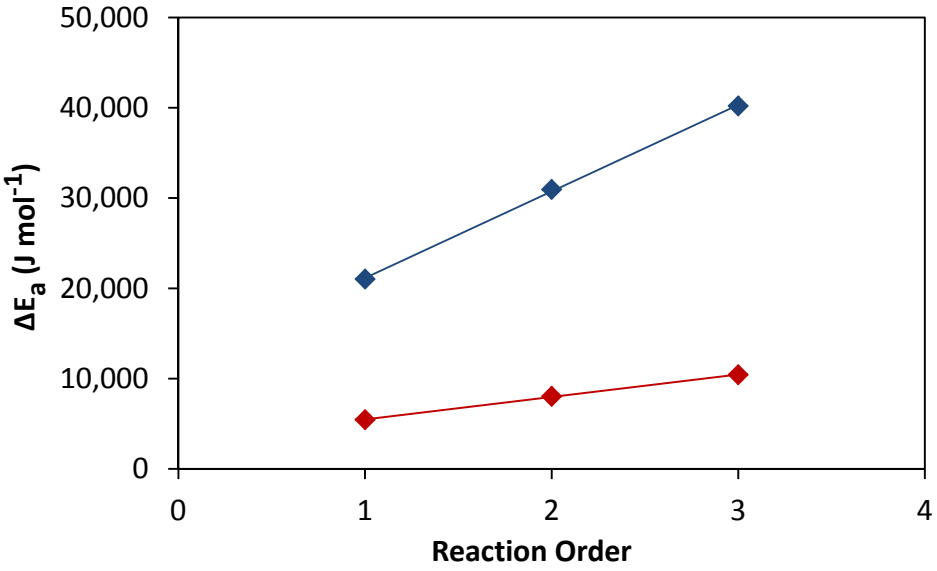

Figure 30. Range of apparent activation energy versus reaction order for switchgrass cellulose and hemicellulose pyrolysis. Markers indicate experimental values for the range of apparent activation energy and solid lines indicate linear fits. Blue colors correspond to switchgrass cellulose and red colors correspond to switchgrass hemicellulose.

	Cellulose		Hemicellulose				
β ($^{\circ}$C min^{-1})	E_a (kJ mol^{-1})	A (min^{-1})	E_a (kJ mol^{-1})	A (min^{-1})	γ_1	γ_2	R^2
5	170.9	9.7E+13	117.6	2.7E+10	0.5209	0.3541	0.9557
10	155.2	5.4E+12	109.5	6.3E+09	0.5424	0.3517	0.9601
15	160.7	1.6E+13	114.3	2.1E+10	0.5273	0.3613	0.9566
20	162.0	2.0E+13	120.5	8.6E+10	0.5255	0.3634	0.9574
25	156.0	6.7E+12	117.4	4.5E+10	0.5451	0.3620	0.9654
30	147.6	1.5E+12	110.0	1.1E+10	0.5683	0.3527	0.9686
35	147.0	1.4E+12	109.8	1.1E+10	0.5597	0.3597	0.9663
40	136.8	2.0E+11	108.8	9.7E+09	0.5722	0.3499	0.9646
50	103.6	3.8E+08	118.0	8.7E+10	0.6834	0.2579	0.9644
Mean	148.9	1.7E+13	114.0	3.4E+10	0.5605	0.3458	
Std Dev	19.6	3.1E+13	4.5	3.2E+10	0.0497	0.0334	
Min E_a	103.6		108.8				
Max E_a	170.9		120.5				
ΔE_a	67.3		11.7				

Table 16. Kinetic parameters for switchgrass cellulose and hemicellulose pyrolysis, assuming 1st order reactions for all cases, determined using equation 3.31. The values of γ_1 and γ_2 were assumed to be 0.5, before optimization. Initial values of all other kinetic parameters were assumed to be values from Tables 14 and 15, before optimization.

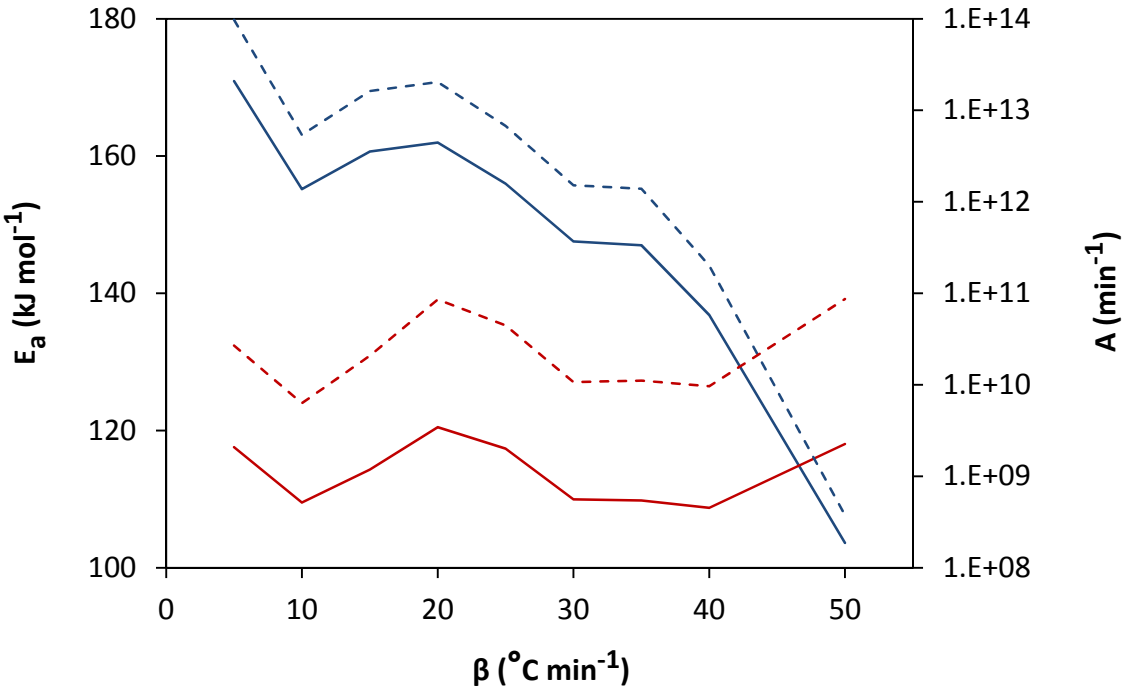

Figure 31. Activation energy and pre-exponential factor versus heating rate for switchgrass. All reactions are assumed to be first order. Blue lines indicate values for cellulose and red lines indicate values for hemicellulose. Solid lines correspond to activation energy (the right vertical axis) and dashed lines correspond to pre-exponential factor (the left vertical axis).

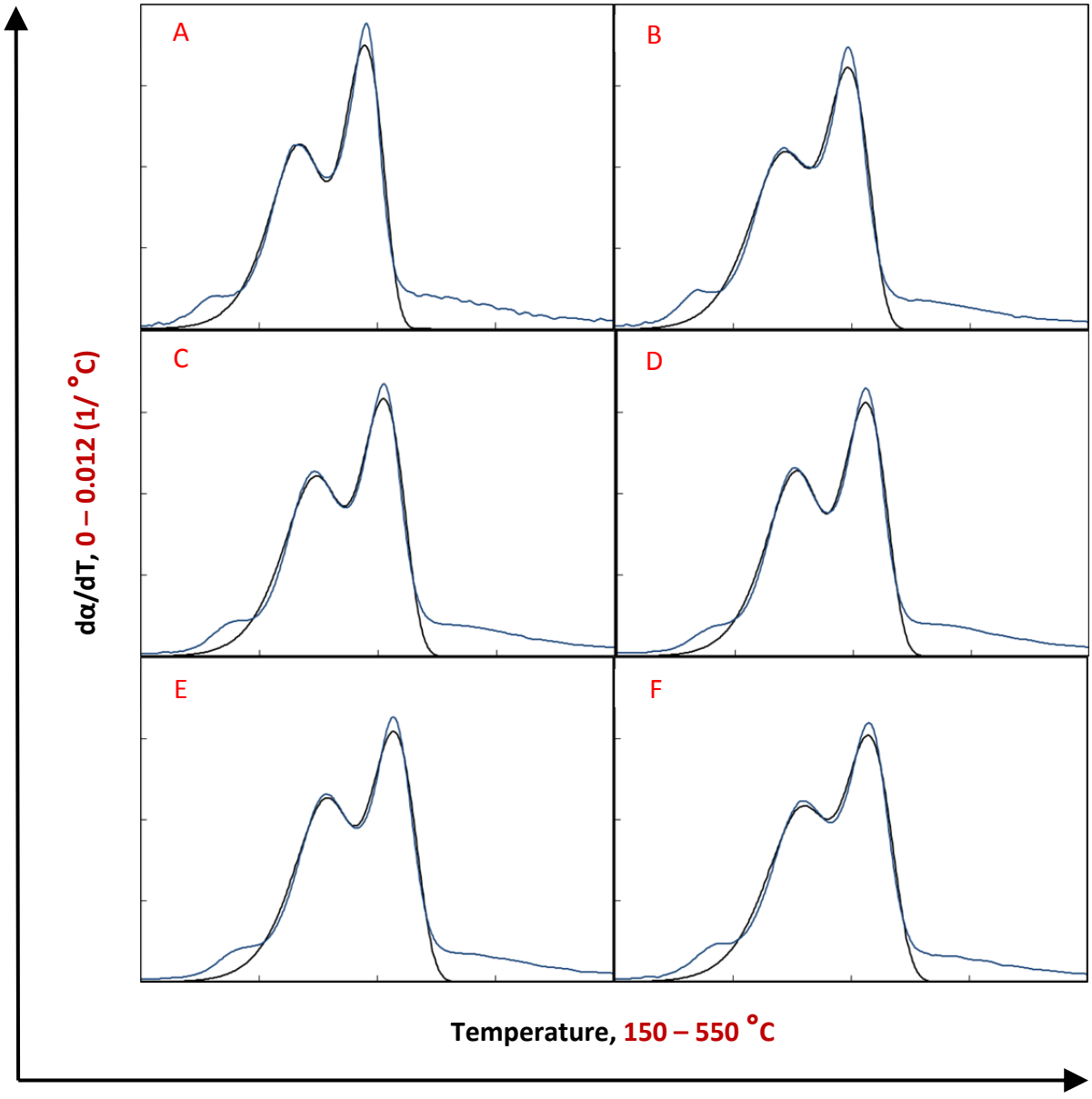

Figure 32. DTG profile of switchgrass pyrolysis fit to equation 3.30 using parameters given in Table 16. Blue markers indicate experimental values and solid black lines represent fitted values. Red letters indicate heating rate conditions and are as follows: 5 °C min^{-1} (A), 10 °C min^{-1} (B), 15 °C min^{-1} (C), 20 °C min^{-1} (D), 25 °C min^{-1} (E), 30 °C min^{-1} (F), 35 °C min^{-1} (G), 40 °C min^{-1} (H), 50 °C min^{-1} (I). All graph axes were scaled equivalently and their limits are given above.

Figure 32 (cont'd). DTG profile of switchgrass pyrolysis fit to equation 3.30 using parameters given in Table 16. Blue markers indicate experimental values and solid black lines represent fitted values. Red letters indicate heating rate conditions and are as follows: 5 °C min^{-1} (A), 10 °C min^{-1} (B), 15 °C min^{-1} (C), 20 °C min^{-1} (D), 25 °C min^{-1} (E), 30 °C min^{-1} (F), 35 °C min^{-1} (G), 40 °C min^{-1} (H), 50 °C min^{-1} (I). All graph axes were scaled equivalently and their limits are given above.

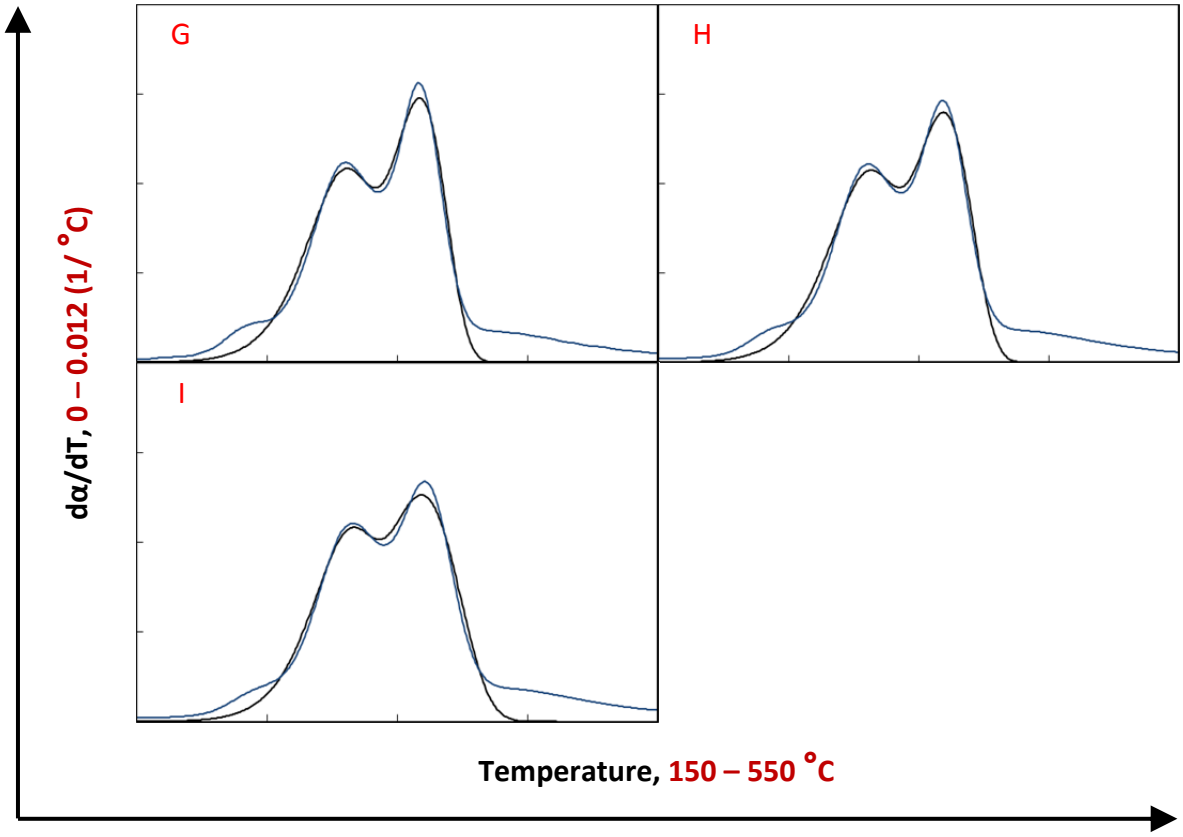

	Cellulose		Hemicellulose			
β ($^{\circ}$C min^{-1})	E_a (kJ mol^{-1})	A (min^{-1})	E_a (kJ mol^{-1})	A (min^{-1})	R^2 (γ_{avg})	R^2 (γ_{opt})
5	170.9	9.7E+13	117.6	2.7E+10	0.9531	0.9557
10	162.1	2.1E+13	109.9	6.5E+09	0.9598	0.9600
15	162.5	2.3E+13	115.9	3.0E+10	0.9564	0.9566
20	162.5	2.3E+13	123.4	1.6E+11	0.9571	0.9574
25	162.4	2.4E+13	120.8	9.0E+10	0.9641	0.9654
30	160.6	1.9E+13	113.2	2.0E+10	0.9662	0.9686
35	156.8	9.2E+12	115.0	3.2E+10	0.9638	0.9663
40	148.8	2.0E+12	113.6	2.5E+10	0.9614	0.9646
50	137.4	2.3E+11	110.0	1.2E+10	0.9576	0.9644
Mean	158.2	2.4E+13	115.5	4.5E+10		
Std Dev	9.2	2.7E+13	4.3	4.6E+10		
ΔE_a	33.5		13.5			

Table 17. Optimized kinetic parameters for switchgrass cellulose and hemicellulose assuming constant γ values equal to the mean γ values for cellulose and hemicellulose (table 16). R^2 (γ_{avg}) values represent the coefficient of determination from the fit of equation 3.30 to experimental data, using the parameters given in the table and assuming the mean γ value for cellulose and the mean γ value for hemicellulose (Table 16) over all heating rates. R^2 (γ_{opt}) values represent the coefficient of determination from the fit of equation 3.30 to experimental data using all optimized parameters at a given heating rate (Table 16).

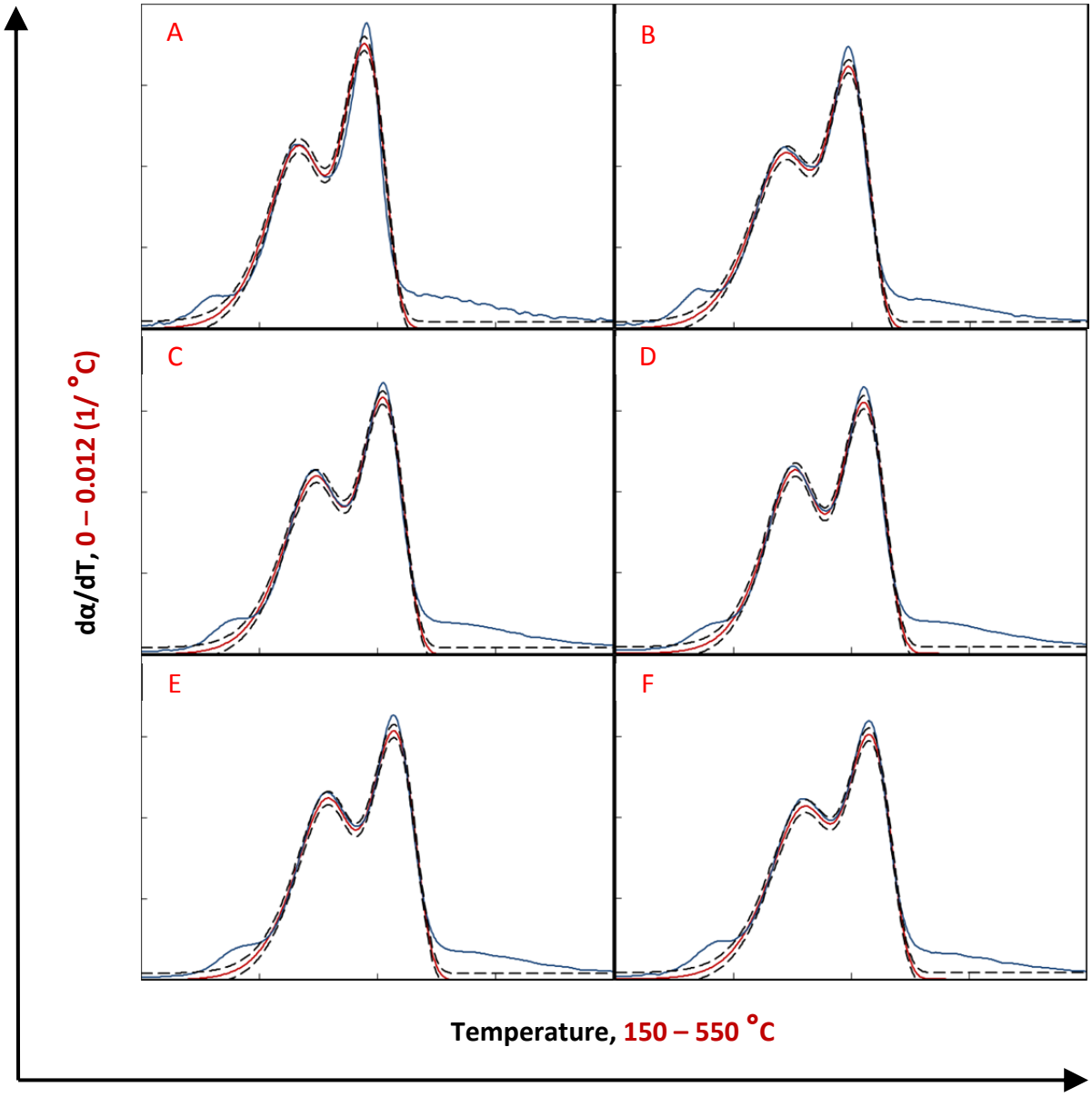

Figure 33. DTG profile of switchgrass pyrolysis optimized using equation 3.31 and mean gamma values (constant) from Table 16. Blue lines indicate experimental values and solid red lines represent fitted values. Dashed black lines represent lower and upper bounds for 95% confidence intervals. Red letters indicate heating rate conditions and are as follows: 5 °C min^{-1} (A), 10 °C min^{-1} (B), 15 °C min^{-1} (C), 20 °C min^{-1} (D), 25 °C min^{-1} (E), 30 °C min^{-1} (F), 35 °C min^{-1} (G), 40 °C min^{-1} (H), 50 °C min^{-1} (I). All graph axes were scaled equivalently and their limits are given above.

Figure 33 (cont'd). DTG profile of switchgrass pyrolysis optimized using equation 3.31 and mean gamma values (constant) from Table 16. Blue lines indicate experimental values and solid red lines represent fitted values. Dashed black lines represent lower and upper bounds for 95% confidence intervals. Red letters indicate heating rate conditions and are as follows: 5 °C min^{-1} (A), 10 °C min^{-1} (B), 15 °C min^{-1} (C), 20 °C min^{-1} (D), 25 °C min^{-1} (E), 30 °C min^{-1} (F), 35 °C min^{-1} (G), 40 °C min^{-1} (H), 50 °C min^{-1} (I). All graph axes were scaled equivalently and their limits are given above.

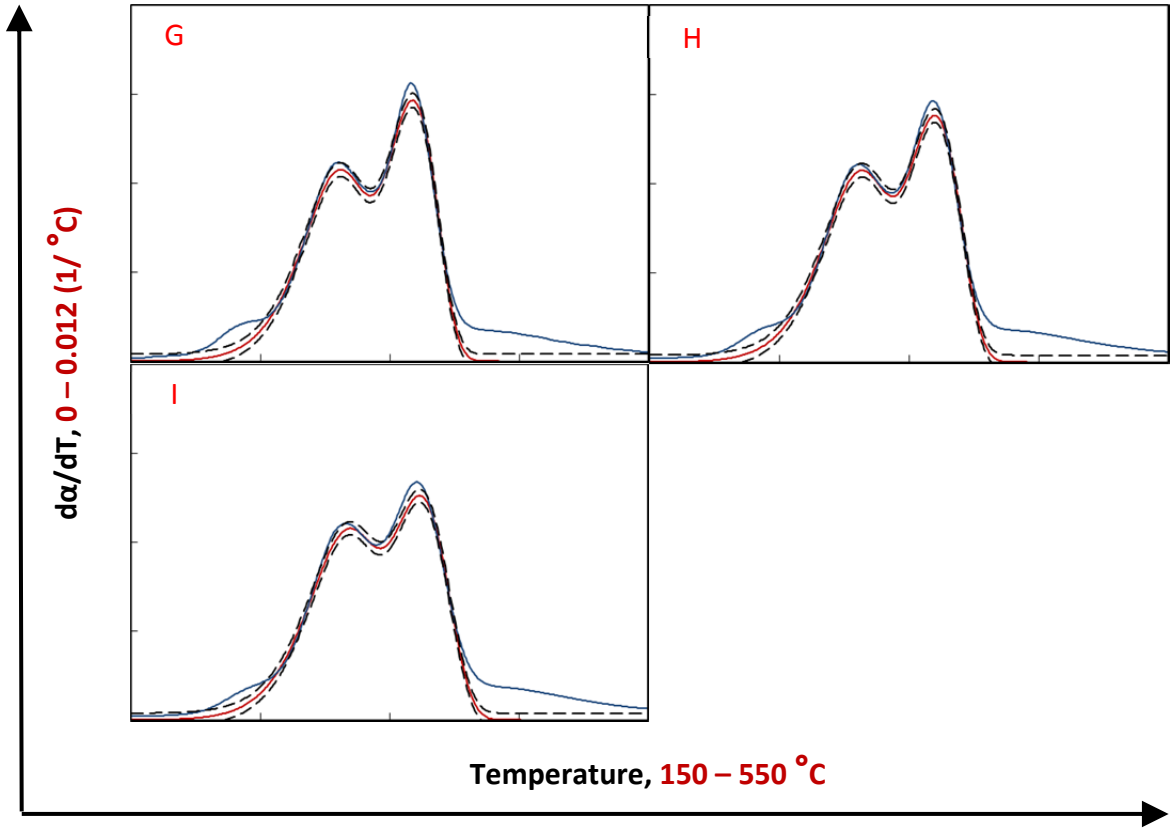

Location	Untreated E ($J\ mol^{-1}$)	Washed E ($J\ mol^{-1}$)	E.F. E ($J\ mol^{-1}$)	Untreated A (min^{-1})	Washed A (min^{-1})	E.F. A (min^{-1})	γ_1	γ_2
Frankenmuth	143,225	196,280	201,571	4.15E+11	7.29E+15	2.84E+16	0.5605	0.3458
Roger City	135,284	188,410	194,663	8.70E+10	1.91E+15	7.14E+15	0.5605	0.3458
Cass County	173,271	202,798	198,531	1.35E+14	3.42E+16	2.12E+16	0.5605	0.3458
Grand Valley	150,193	189,689	176,403	1.45E+12	2.57E+15	2.05E+14	0.5605	0.3458
Mean	150,493	194,294	192,792	3.42E+13	1.15E+16	1.43E+16	0.5605	0.3458
Std Dev	14,169	5,747	9,774	5.81E+13	1.33E+16	1.12E+16	0.0000	0.0000

Table 18. Kinetic parameters for switchgrass cellulose peaks of untreated, washed, and extractives-free (E.F.) samples, determined through optimization of equation 3.31. Gamma factors were assumed constant using values expressed in Table 16. A constant heating rate of $\beta = 10\ °C\ min^{-1}$ was utilized during experiments.

Location	Untreated E (J mol^{-1})	Washed E (J mol^{-1})	E.F. E (J mol^{-1})	Untreated A (min^{-1})	Washed A (min^{-1})	E.F. A (min^{-1})	γ_1	γ_2
Frankenmuth	99,292	137,510	146,052	4.75E+08	9.35E+11	6.54E+12	0.5605	0.3458
Roger City	87,735	140,804	144,371	4.19E+07	2.64E+12	5.43E+12	0.5605	0.3458
Cass County	120,247	132,153	137,246	3.84E+10	2.96E+11	1.04E+12	0.5605	0.3458
Grand Valley	112,848	149,324	151,776	8.89E+09	1.35E+13	2.34E+13	0.5605	0.3458
Mean	105,031	139,947	144,861	1.20E+10	4.34E+12	9.10E+12	0.5605	0.3458
Std Dev	12,497	6,232	5,183	1.57E+10	5.35E+12	8.50E+12	0.0000	0.0000

Table 19. Kinetic parameters for switchgrass hemicellulose peaks of untreated, washed, and extractives-free (E.F.) samples, determined through optimization of equation 3.31. Gamma factors were assumed constant using values expressed in Table 16. A constant heating rate of $\beta = 10$ °C min^{-1} was utilized during experiments.

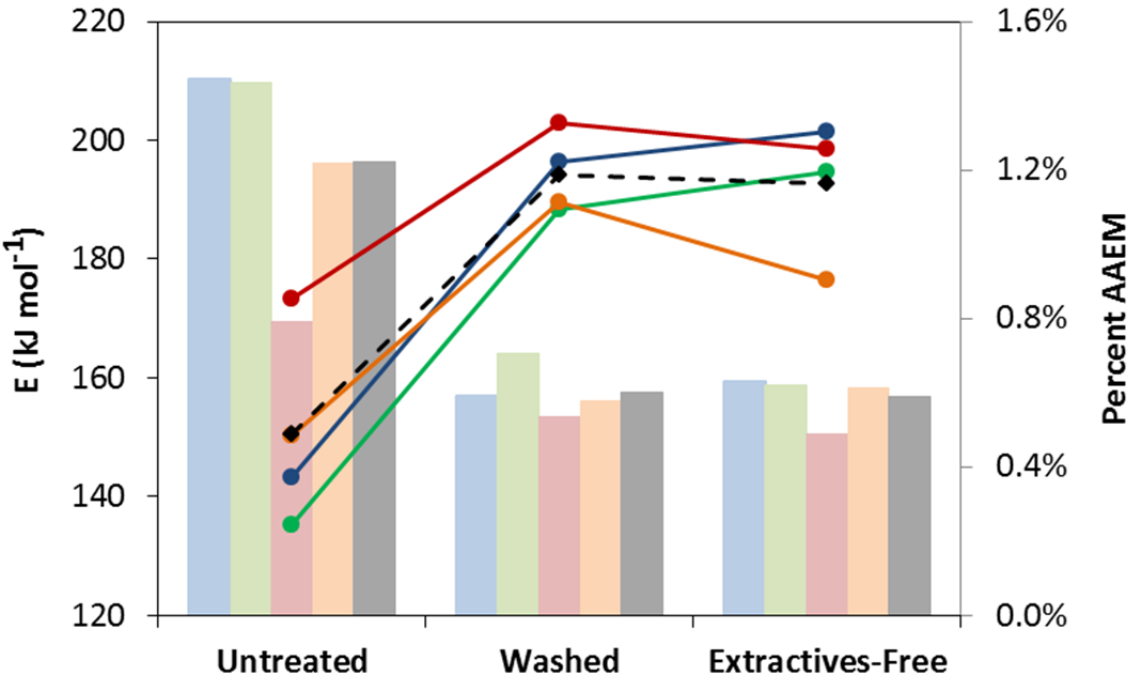

Figure 34. Activation energy for switchgrass cellulose pyrolysis given untreated, washed, and extractives-free samples over different locations (values obtained from Table 18). Colors are represented as Frankenmuth (blue), Roger City (green), Cass County (red), Grand valley (orange), and the average value (dotted-black). Lines do not represent numerical values, and are present only to indicate a trend between activation energy and treatment.

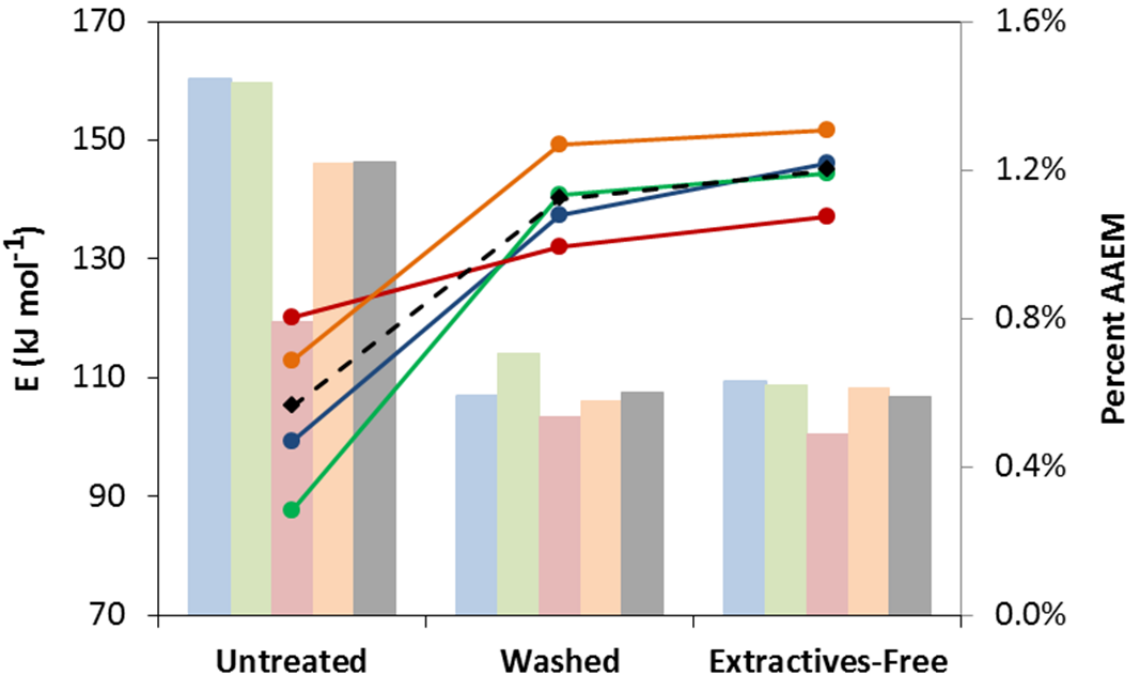

Figure 35. Activation energy for switchgrass hemicellulose pyrolysis given untreated, washed, and extractives-free samples over different locations (values obtained from Table 18). Colors are represented as Frankenmuth (blue), Roger City (green), Cass County (red), Grand valley (orange), and the average value (dotted-black). Lines do not represent numerical values, and are present only to indicate a trend between activation energy and treatment.

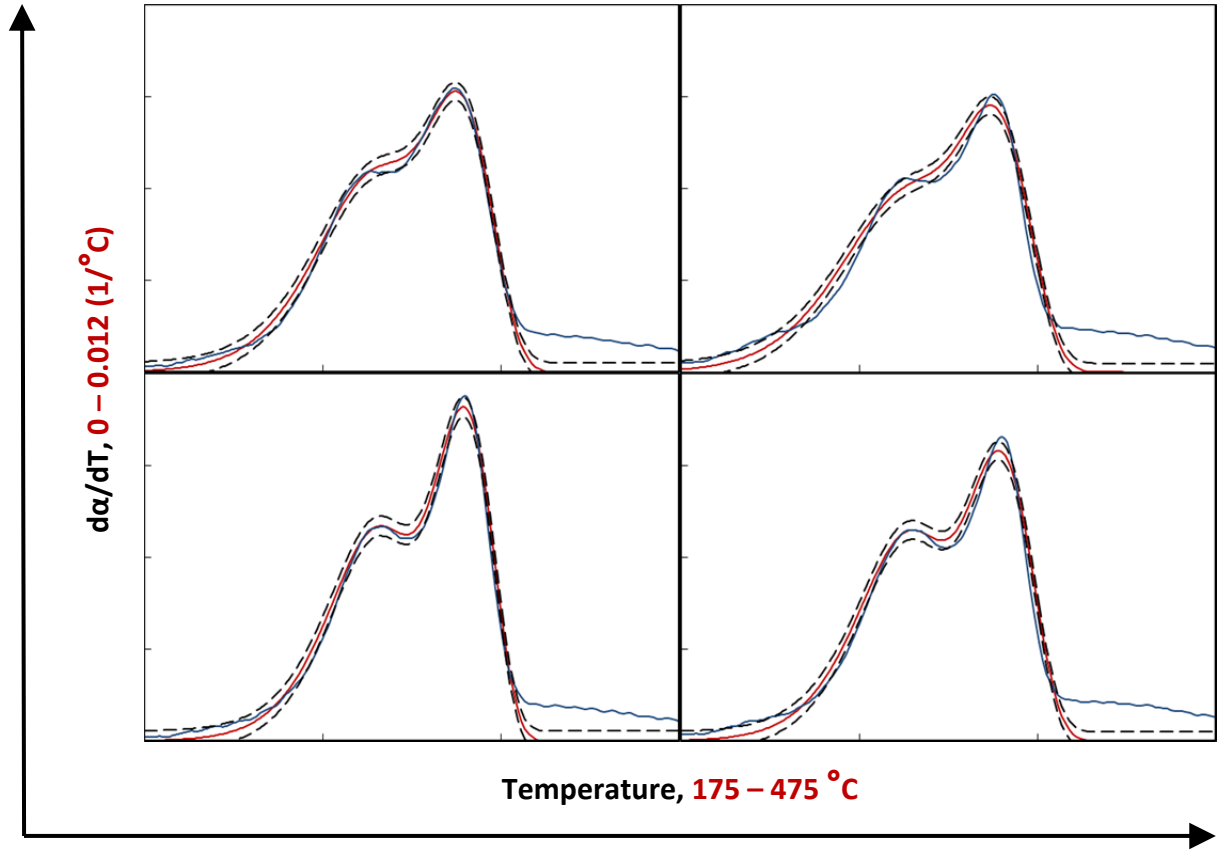

Figure 36. DTG profile of untreated switchgrass samples from Frankenmuth (top left), Roger City (top right), Cass County (bottom left), and Grand Valley (bottom right) plots. Kinetic parameters were optimized using equation 3.31 and mean gamma values (constant) from Table 16. Blue lines indicate experimental values and solid red lines represent fitted values to equation 3.30. Dashed black lines represent lower and upper bounds for 95% confidence intervals. R^2 values for Frankenmuth, Roger City, Cass County, and Grand Valley fits are 0.9805, 0.9653, 0.9825, and 0.9728, respectively. All graph axes were scaled equivalently and their limits are given above.

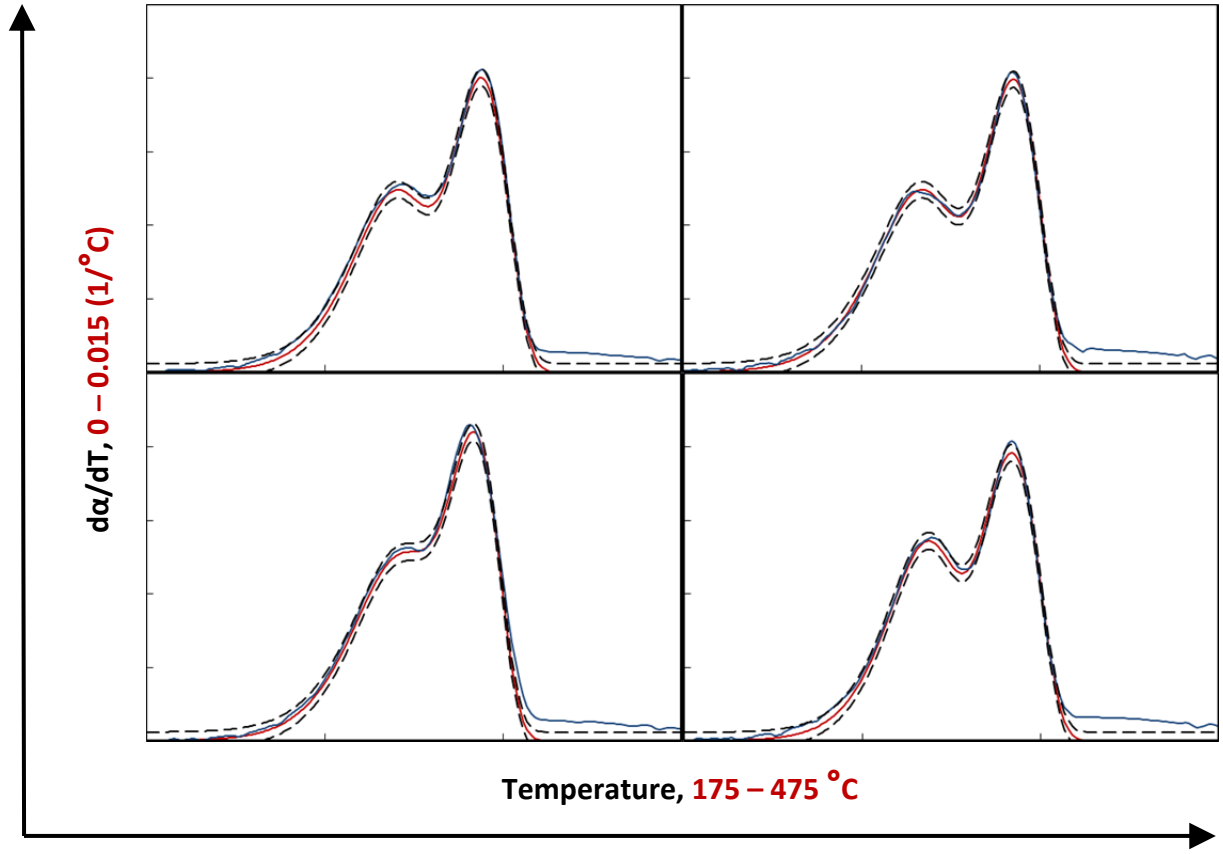

Figure 37. DTG profile of washed switchgrass samples from Frankenmuth (top left), Roger City (top right), Cass County (bottom left), and Grand Valley (bottom right) plots. Kinetic parameters were optimized using equation 3.31 and mean gamma values (constant) from Table 16. Blue lines indicate experimental values and solid red lines represent fitted values to equation 3.30. Dashed black lines represent lower and upper bounds for 95% confidence intervals. R^2 values for Frankenmuth, Roger City, Cass County, and Grand Valley fits are 0.9926, 0.9905, 0.9924, and 0.9912, respectively. All graph axes were scaled equivalently and their limits are given above.

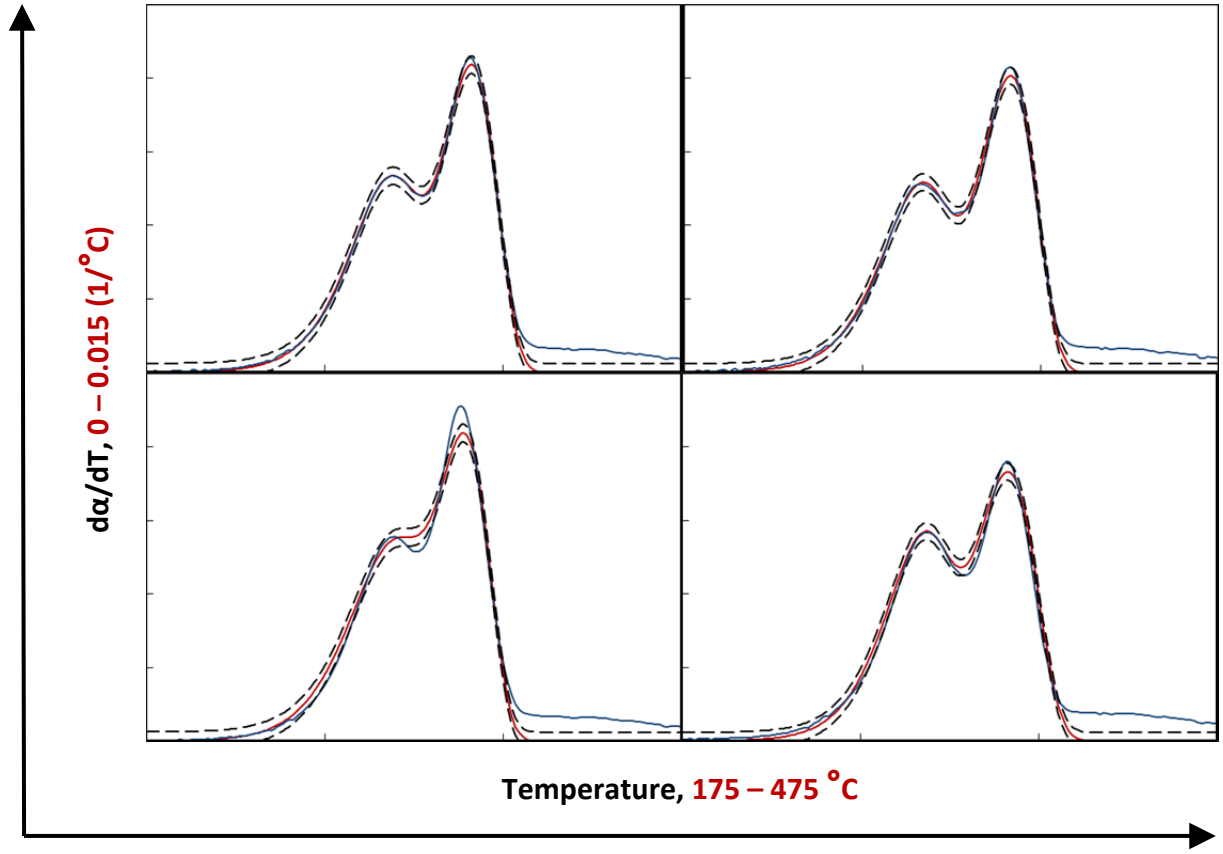

Figure 38. DTG profile of extractives-free switchgrass samples from Frankenmuth (top left), Roger City (top right), Cass County (bottom left), and Grand Valley (bottom right) plots. Kinetic parameters were optimized using equation 3.31 and mean gamma values (constant) from Table 16. Blue lines indicate experimental values and solid red lines represent fitted values to equation 3.30. Dashed black lines represent lower and upper bounds for 95% confidence intervals. R^2 values for Frankenmuth, Roger City, Cass County, and Grand Valley fits are 0.9915, 0.9898, 0.9862, and 0.9840, respectively. All graph axes were scaled equivalently and their limits are given above.

BIBLIOGRAPHY

BIBLIOGRAPHY

[1] J.-K. Weng and C. Chapple, "The origin and evolution of lignin biosynthesis.," *The New phytologist*, vol. 187, no. 2, pp. 273–85, Jul. 2010.

[2] W. Boerjan, J. Ralph, and M. Baucher, "Lignin biosynthesis.," *Annual review of plant biology*, vol. 54, pp. 519–46, Jan. 2003.

[3] C. Dong, Z. Zhang, Q. Lu, and Y. Yang, "Characteristics and mechanism study of analytical fast pyrolysis of poplar wood," *Energy Conversion and Management*, vol. 57, pp. 49–59, May 2012.

[4] B. J. (Leads) Perlack, R.D. and Stokes, "U.S. Billion-Ton Update: Biomass Supply for a Bioenergy and Bioproducts Industry," Oak Ridge, TN, 2011.

[5] Energy Information Administration (EIA), "How dependent are we on foreign oil?," 2013. [Online]. Available: http://www.eia.gov/energy_in_brief/article/foreign_oil_dependence.cfm.

[6] A. A. Boateng, K. HICKS, and K. VOGEL, "Pyrolysis of switchgrass (Panicum virgatum) harvested at several stages of maturity," *Journal of Analytical and Applied Pyrolysis*, vol. 75, no. 2, pp. 55–64, Mar. 2006.

[7] P. R. Adler, M. A. Sanderson, A. A. Boateng, P. J. Weimer, and H.-J. G. Jung, "Biomass Yield and Biofuel Quality of Switchgrass Harvested in Fall or Spring.pdf," *Agronomy Journal*, vol. 98, no. November-December, pp. 1518–1525, 2006.

[8] M. a Sanderson and P. R. Adler, "Perennial forages as second generation bioenergy crops.," *International journal of molecular sciences*, vol. 9, no. 5, pp. 768–88, May 2008.

[9] M. A. Sanderson, P. R. Adler, A. A. Boateng, M. D. Casler, and G. Sarath, "Switchgrass as a biofuels feedstock in the USA," *Canadian Journal of Plant Science*, 2006.

[10] M. R. Schmer, M. a. Liebig, K. P. Vogel, and R. B. Mitchell, "Field-scale soil property changes under switchgrass managed for bioenergy," *GCB Bioenergy*, vol. 3, no. 6, pp. 439–448, Dec. 2011.

[11] A. Zumkehr and J. E. Campbell, "Historical U.S. Cropland Areas and the Potential for Bioenergy Production on Abandoned Croplands," *Environmental Science & Technology*, vol. 47, pp. 3840–3847, 2013.

[12] D. M. Wilson, E. A. Heaton, M. Liebman, and K. J. Moore, “Intraseasonal Changes in Switchgrass Nitrogen Distribution Compared with Corn,” *Agronomy Journal*, vol. 105, no. 2, pp. 285–294, 2013.

[13] K. P. Vogel, B. S. Dien, H. G. Jung, M. D. Casler, S. D. Masterson, and R. B. Mitchell, “Quantifying Actual and Theoretical Ethanol Yields for Switchgrass Strains Using NIRS Analyses,” *BioEnergy Research*, vol. 4, no. 2, pp. 96–110, Aug. 2010.

[14] S. Mclaughlin and L. Adamskszos, “Development of switchgrass (Panicum virgatum) as a bioenergy feedstock in the United States,” *Biomass and Bioenergy*, vol. 28, no. 6, pp. 515–535, Jun. 2005.

[15] P. R. Patwardhan, J. a Satrio, R. C. Brown, and B. H. Shanks, “Influence of inorganic salts on the primary pyrolysis products of cellulose.,” *Bioresource technology*, vol. 101, no. 12, pp. 4646–55, Jun. 2010.

[16] I.-Y. Eom, J.-Y. Kim, T.-S. Kim, S.-M. Lee, D. Choi, I.-G. Choi, and J.-W. Choi, “Effect of essential inorganic metals on primary thermal degradation of lignocellulosic biomass.,” *Bioresource technology*, vol. 104, pp. 687–94, Jan. 2012.

[17] G. R. Ponder, G. N. Richards, and T. T. Stevenson, “Influence of linkage position and orientation in pyrolysis of polysaccharides: A study of several glucans,” *Journal of Analytical and Applied Pyrolysis*, vol. 22, no. 3, pp. 217–229, Mar. 1992.

[18] I.-Y. Eom, K.-H. Kim, J.-Y. Kim, S.-M. Lee, H.-M. Yeo, I.-G. Choi, and J.-W. Choi, “Characterization of primary thermal degradation features of lignocellulosic biomass after removal of inorganic metals by diverse solvents,” *Bioresource technology*, vol. 102, no. 3, pp. 3437–44, Feb. 2011.

[19] A. Saddawi, J. M. Jones, and A. Williams, “Influence of alkali metals on the kinetics of the thermal decomposition of biomass,” *Fuel Processing Technology*, vol. 104, pp. 189–197, Dec. 2012.

[20] D. Nowakowski, J. Jones, R. Brydson, and a Ross, “Potassium catalysis in the pyrolysis behaviour of short rotation willow coppice,” *Fuel*, vol. 86, no. 15, pp. 2389–2402, Oct. 2007.

[21] R. Fahmi, a. V. Bridgwater, L. I. Darvell, J. M. Jones, N. Yates, S. Thain, and I. S. Donnison, “The effect of alkali metals on combustion and pyrolysis of Lolium and Festuca grasses, switchgrass and willow,” *Fuel*, vol. 86, no. 10–11, pp. 1560–1569, Jul. 2007.

[22] Y. F. Huang, W. H. Kuan, P. T. Chiueh, and S. L. Lo, “A sequential method to analyze the kinetics of biomass pyrolysis.,” *Bioresource technology*, vol. 102, no. 19, pp. 9241–6, Oct. 2011.

[23] D. Shen, R. Xiao, S. Gu, and K. Luo, “The pyrolytic behavior of cellulose in lignocellulosic biomass: a review,” *RSC Advances*, vol. 1, no. 9, p. 1641, 2011.

[24] S. Pérez and D. Samain, *Structure and engineering of celluloses.*, vol. 64, no. 10. 2010, pp. 25–116.

[25] Q. Lu, X. Yang, C. Dong, Z. Zhang, X. Zhang, and X. Zhu, “Influence of pyrolysis temperature and time on the cellulose fast pyrolysis products: Analytical Py-GC/MS study,” *Journal of Analytical and Applied Pyrolysis*, vol. 92, no. 2, pp. 430–438, Nov. 2011.

[26] R. Alén, E. Kuoppala, and P. Oesch, “Formation of the main degradation compound groups from wood and its components during pyrolysis,” *Journal of Analytical and Applied Pyrolysis*, vol. 36, no. 2, pp. 137–148, Jun. 1996.

[27] F. Shafizadeh and Y. L. Fu, “Pyrolysis of Cellulose,” *Carboyhydrate Research*, vol. 29, pp. 113–122, 1973.

[28] D. K. Shen, S. Gu, and a. V. Bridgwater, “The thermal performance of the polysaccharides extracted from hardwood: Cellulose and hemicellulose,” *Carbohydrate Polymers*, vol. 82, no. 1, pp. 39–45, Aug. 2010.

[29] S. Wang, X. Guo, K. Wang, and Z. Luo, “Influence of the interaction of components on the pyrolysis behavior of biomass,” *Journal of Analytical and Applied Pyrolysis*, vol. 91, no. 1, pp. 183–189, May 2011.

[30] A. Ebringerova, “Structural Diversity and Application Potential of Hemicelluloses,” no. 333, pp. 1–12, 2006.

[31] R. Samuel, M. Foston, N. Jiang, L. Allison, and A. J. Ragauskas, “Structural changes in switchgrass lignin and hemicelluloses during pretreatments by NMR analysis,” *Polymer Degradation and Stability*, vol. 96, no. 11, pp. 2002–2009, Nov. 2011.

[32] S. Kumar and R. B. Gupta, “Biocrude Production from Switchgrass Using Subcritical Water,” *Energy & Fuels*, vol. 23, no. 10, pp. 5151–5159, Oct. 2009.

[33] a. V. Bridgwater, “Review of fast pyrolysis of biomass and product upgrading,” *Biomass and Bioenergy*, vol. 38, pp. 68–94, Mar. 2011.

[34] D. Mohan, C. U. Pittman,, and P. H. Steele, “Pyrolysis of Wood/Biomass for Bio-oil: A Critical Review,” *Energy & Fuels*, vol. 20, no. 3, pp. 848–889, May 2006.

[35] J. G. Rogers and J. G. Brammer, “Estimation of the production cost of fast pyrolysis bio-oil,” *Biomass and Bioenergy*, vol. 36, no. 0, pp. 208–217, Jan. 2012.

[36] G. W. Huber, S. Iborra, and A. Corma, “Synthesis of transportation fuels from biomass: chemistry, catalysts, and engineering.,” *Chemical reviews*, vol. 106, no. 9, pp. 4044–98, Sep. 2006.

[37] R. J. Evans and T. a. Milne, “Molecular characterization of the pyrolysis of biomass,” *Energy & Fuels*, vol. 1, no. 2, pp. 123–137, Mar. 1987.

[38] D. K. Shen and S. Gu, “The mechanism for thermal decomposition of cellulose and its main products.,” *Bioresource technology*, vol. 100, no. 24, pp. 6496–504, Dec. 2009.

[39] C. W. Klampfl, G. Breuer, C. Schwarzinger, and B. Ktil, “Investigations on the Effect of Metal Ions on the Products Obtained From the Pyrolysis of Cellulose,” *Chemical Technology*, 2005.

[40] N. Shimada, H. Kawamoto, and S. Saka, “Different action of alkali/alkaline earth metal chlorides on cellulose pyrolysis,” *Journal of Analytical and Applied Pyrolysis*, vol. 81, no. 1, pp. 80–87, Jan. 2008.

[41] S. Wang, Y. Liao, Q. Liu, Z. Luo, and K. Cen, “Experimental study of the influence of acid wash on cellulose pyrolysis,” *Frontiers of Chemical Engineering in China*, vol. 1, no. 1, pp. 35–39, Feb. 2007.

[42] D. Vamvuka and S. Sfakiotakis, “Effects of heating rate and water leaching of perennial energy crops on pyrolysis characteristics and kinetics,” *Renewable Energy*, vol. 36, no. 9, pp. 2433–2439, Sep. 2011.

[43] M. J. Antal and E. Jakab, “Cellulose Pyrolysis Kinetics : Revisited,” vol. 5885, no. 97, pp. 1267–1275, 1998.

[44] C. E. Greenhalf, D. J. Nowakowski, a. V. Bridgwater, J. Titiloye, N. Yates, a. Riche, and I. Shield, “Thermochemical characterisation of straws and high yielding perennial grasses,” *Industrial Crops and Products*, vol. 36, no. 1, pp. 449–459, Mar. 2012.

[45] H. Haykiri-Acma, S. Yaman, and S. Kucukbayrak, “Comparison of the thermal reactivities of isolated lignin and holocellulose during pyrolysis,” *Fuel Processing Technology*, vol. 91, no. 7, pp. 759–764, Jul. 2010.

[46] O. Ioannidou, C. G. Jung, and a. Zabaniotou, “A thermogravimetric model to predict yield product distribution in pyrolysis of agricultural biomass,” *Catalysis Today*, vol. 167, no. 1, pp. 129–134, Jun. 2011.

[47] V. Leroy, D. Cancellieri, and E. Leoni, “Thermal degradation of ligno-cellulosic fuels: DSC and TGA studies,” *Thermochimica Acta*, vol. 451, no. 1–2, pp. 131–138, Dec. 2006.

[48] K. Norinaga, T. Shoji, S. Kudo, and J. Hayashi, “Detailed chemical kinetic modelling of vapour-phase cracking of multi-component molecular mixtures derived from the fast pyrolysis of cellulose,” *Fuel*, vol. 103, pp. 141–150, Sep. 2011.

[49] J. Peng, G. Chen, Z. Fan, Q. Lin, and D. Wang, “Different Methods for Evaluating Pinewood Sawdust Pyrolysis Kinetics by Thermogravimetry Mass Spectrum Analysis.pdf,” *Biobased Materials and Bioenergy*, vol. 5, no. 3, pp. 324–330, 2011.

[50] H. Zhao, H. Yan, C. Zhang, B. Sun, Y. Zhang, S. Dong, Y. Xue, and S. Qin, “Thermogravimetry study of pyrolytic characteristics and kinetics of the giant wetland plant Phragmites australis,” *Journal of Thermal Analysis and Calorimetry*, vol. 110, no. 2, pp. 611–617, Nov. 2011.

[51] L. Cabrales and N. Abidi, “On the thermal degradation of cellulose in cotton fibers,” *Journal of Thermal Analysis and Calorimetry*, vol. 102, no. 2, pp. 485–491, Jun. 2010.

[52] M. G. Grønli, G. Várhegyi, and C. Di Blasi, “Thermogravimetric Analysis and Devolatilization Kinetics of Wood,” *Industrial & Engineering Chemistry Research*, vol. 41, no. 17, pp. 4201–4208, Aug. 2002.

[53] J. Cai, W. Wu, R. Liu, and G. W. Huber, “A distributed activation energy model for the pyrolysis of lignocellulosic biomass,” *Green Chemistry*, vol. 15, no. 5, p. 1331, 2013.

[54] H. C. Yoon, P. Pozivil, and A. Steinfeld, “Thermogravimetric Pyrolysis and Gasification of Lignocellulosic Biomass and Kinetic Summative Law for Parallel Reactions with Cellulose, Xylan, and Lignin,” *Energy & Fuels*, vol. 26, no. 1, pp. 357–364, Jan. 2012.

[55] Z. Sebestyén, E. Jakab, Z. May, B. Sipos, and K. Réczey, “Thermal behavior of native, washed and steam exploded lignocellulosic biomass samples,” *Journal of Analytical and Applied Pyrolysis*, vol. 101, pp. 61–71, May 2013.

[56] G.-L. Guo, W.-H. Chen, W.-H. Chen, L.-C. Men, and W.-S. Hwang, “Characterization of dilute acid pretreatment of silvergrass for ethanol production.,” *Bioresource technology*, vol. 99, no. 14, pp. 6046–53, Sep. 2008.

[57] M. J. de la Torre, A. Moral, M. D. Hernández, E. Cabeza, and A. Tijero, “Organosolv lignin for biofuel,” *Industrial Crops and Products*, vol. 45, pp. 58–63, Feb. 2013.

[58] R. J. Garlock, B. Bals, P. Jasrotia, V. Balan, and B. E. Dale, “Influence of variable species composition on the saccharification of AFEX^{TM} pretreated biomass from unmanaged fields in comparison to corn stover,” *Biomass and Bioenergy*, vol. 37, pp. 49–59, Feb. 2012.

[59] V. Balan, C. Sousa, S. P. S. Chundawat, D. Marshall, E. Lansing, L. N. Sharma, C. K. Chambliss, and B. E. Dale, “Enzymatic Digestibility and Pretreatment Degradation Products of AFEX-Treated Hardwoods (Populus nigra),” 2009.

[60] R. J. Garlock, V. Balan, B. E. Dale, V. R. Pallapolu, Y. Y. Lee, Y. Kim, N. S. Mosier, M. R. Ladisch, M. T. Holtzapple, M. Falls, R. Sierra-Ramirez, J. Shi, M. a Ebrik, T. Redmond, B. Yang, C. E. Wyman, B. S. Donohoe, T. B. Vinzant, R. T. Elander, B. Hames, S. Thomas, and R. E. Warner, “Comparative material balances around pretreatment technologies for the conversion of switchgrass to soluble sugars.,” *Bioresource technology*, vol. 102, no. 24, pp. 11063–71, Dec. 2011.

[61] L. Laureano-Perez, F. Teymouri, H. Alizadeh, and B. E. Dale, “Understanding Factors that Limit Enzymatic Hydrolysis of Biomass,” *Applied biochemistry and biotechnology*, vol. 121–124, pp. 1081 – 1099, 2005.

[62] C. Cateto, G. Hu, and A. Ragauskas, “Enzymatic hydrolysis of organosolv Kanlow switchgrass and its impact on cellulose crystallinity and degree of polymerization,” *Energy & Environmental Science*, vol. 4, no. 4, p. 1516, 2011.

[63] P. J. Van Soest and H. K. Goering, “Forage Fiber Analysis (Apparatus, Reagents, Procedures, and Some Applications),” in in *Agriculture Handbook 379, U.S. Department of Agriculture*, no. 379, 1970, pp. 1 – 20.

[64] A. Sluiter, B. Hames, R. Ruiz, C. Scarlata, J. Sluiter, and D. Templeton, “Determination of Ash in Biomass,” 2005.

[65] J. R. Brown, T. R. Peck, S. Brouder, A. Mallarino, D. Whitney, D. D. Warncke, G. Rehm, K. Frank, L. J. Cihacek, M. Watson, D. Beegle, R. Gelderman, S. Combs, J. Dennig, R. Eliason, R. J. Goos, B. Hoskins, M. V. Nathan, and A. Wolf, “Recommended Chemical Soil Test Procedures for the North Central Region,” 2011.

[66] R. Fahmi, a. V. Bridgwater, L. I. Darvell, J. M. Jones, N. Yates, S. Thain, and I. S. Donnison, “The effect of alkali metals on combustion and pyrolysis of Lolium and Festuca grasses, switchgrass and willow,” *Fuel*, vol. 86, no. 10–11, pp. 1560–1569, Jul. 2007.

[67] A. Sluiter, R. Ruiz, C. Scarlata, J. Sluiter, and D. Templeton, “Determination of Extractives in Biomass: Laboratory Analytical Procedure (LAP),” Golden, CO, 2008.

[68] J. Ralph and R. D. Hatfield, “Pyrolysis-GC-MS characterization of forage materials,” *Journal of Agricultural and Food Chemistry*, vol. 39, no. 8, pp. 1426–1437, Aug. 1991.

[69] H. E. Kissinger, “Reaction Kinetics in Differential Thermal Analysis,” *Analytical Chemistry*, no. 1956, pp. 1702 – 1706, 1957.

[70] T. Akahira and T. Sunose, “Res. Report CHIBA Inst. Technol.,” 1971.

[71] J. H. Flynn and L. A. Wall, “General Treatment of the Thermogravimetry of Polymers,” vol. 70, no. 6, pp. 487–523, 1966.

[72] T. Ozawa, “A New Method of Analyzing Thermogravimetric Data,” *Bulletin of the Chemical Society of Japan*, vol. 707, no. 1952, pp. 1881 – 1886, 1965.

[73] A. W. Coats and J. P. Redfern, “Kinetic Parameters from Thermogravimetric Data,” *Nature*, vol. 201, no. 4914, pp. 68 – 69, 1964.

[74] B. Janković, B. Adnađević, and J. Jovanović, “Application of model-fitting and model-free kinetics to the study of non-isothermal dehydration of equilibrium swollen poly (acrylic acid) hydrogel: Thermogravimetric analysis,” *Thermochimica Acta*, vol. 452, no. 2, pp. 106–115, Jan. 2007.

[75] C. Gai, Y. Dong, and T. Zhang, “The kinetic analysis of the pyrolysis of agricultural residue under non-isothermal conditions.,” *Bioresource technology*, vol. 127, pp. 298–305, Jan. 2013.

[76] C. Doyle, “Series Approximations to the Equation of Thermogravimetric Data,” *Nature*, vol. 207, no. 4994, pp. 290 – 291, 1965.

[77] H. Yang, R. Yan, H. Chen, D. Lee, and C. Zheng, “Characteristics of hemicellulose, cellulose and lignin pyrolysis,” *Fuel*, vol. 86, no. 12–13, pp. 1781–1788, Aug. 2007.